

SOME PROPERTIES OF SINGULARITIES IN THE
TOLMAN MODEL

CHARLES HELLABY

1985

SOME PROPERTIES OF SINGULARITIES IN THE TOLMAN MODEL

A thesis submitted to the Department of Physics
in conformity with the requirements for
the degree of Doctor of Philosophy

Queen's University at Kingston
Ontario, Canada

August 1985

Copyright © Charles Hellaby 1985

Contents

Abstract	iv
Acknowledgements	v
Statement of Originality	vi
List of Figures	vii
List of Tables	viii
1 INTRODUCTION	1
2 THE TOLMAN MODEL	3
2.1 The Origin and the Topology	6
2.2 Singularities	8
3 THE REDSHIFT	11
3.1 The geodesic equations	12
3.2 Expansions of the tangent vectors near Σ_0	13
3.3 Calculation of the tangent vectors	13
3.4 Shell crossing surfaces	16
3.5 General results for the redshift	16
3.6 Discussion	18
4 SURFACE LAYERS AND REGULAR EXTREMA	21
4.1 Surface layers	21
4.2 Regular extrema	23
5 THE CONDITIONS FOR NO SHELL CROSSINGS	25
5.1 Elliptic regions, $f < 0$	25
5.2 Hyperbolic regions, $f > 0$	26

5.3	Parabolic regions, $f = 0$	27
5.4	The origin	27
5.5	Other formulations	28
5.6	Discussion	29
5.7	Figures	31
6	SOME EXAMPLES	33
6.1	A closed hyperbolic model	33
6.2	An open elliptic model	33
6.3	A closed hybrid model	34
6.4	A model with no origin	34
6.5	Figure	35
7	THE E.S.C. SINGULARITY	36
7.1	The light rays	37
7.2	The conformal diagram	41
7.3	The case of general m	42
7.4	The case $m = 3$	44
7.5	The orientation of the crunch surface	45
7.6	Discussion	48
7.7	Note Added at Defence	48
7.8	Figures	50
8	CONCLUSIONS	76
	REFERENCES	78
	Appendix	80

Abstract

There are three kinds of singularity in the Tolman model: the big bang and big crunch are the standard cosmological singularities that begin and end the spacetime; shell crossings, or caustics, are the result of the breakdown of the assumptions of the model, and are not expected to occur in reality; and the ESC singularity, which appears instantaneously at the centre of symmetry at the big crunch in certain models, and can violate current formulations of cosmic censorship.

The thesis consists of three principal investigations of these singularities. Firstly, the redshift from the bang and shell crossing surfaces is determined, secondly, the conditions that guarantee no shell crossings will occur in a model are derived, and lastly, a description of the behaviour of the ESC singularity is attempted.

The redshift from the big bang in the standard model is always infinite, but in inhomogeneous cosmological models infinite blueshifts are also possible. To avoid such divergent energy fluxes, it is required that all realistic cosmological models must not display infinite blueshifts. This requirement is applied to the Tolman model, using the geometrical optics approximation, and assuming that the geodesic tangent vectors may be expanded in power series. It is concluded that the bang time must be simultaneous. The stronger requirement, that only infinite redshifts from the bang may occur, does not lead to a stronger condition on the metric. Further consequences of simultaneity are that no decaying mode fluctuations are possible, and that the only acceptable model which is homogeneous at late times is the Robertson-Walker model.

Regular maxima are a necessary feature of all closed spherically symmetric models, but shell crossings are undesirable for physically realistic situations. The necessary and sufficient conditions which ensure no shell crossings will arise in Tolman models are derived, and it is shown explicitly that a Tolman model (in general, with a surface layer) may contain both elliptic and hyperbolic regions without developing any shell crossings and without the hyperbolic regions recollapsing. This finding is contrary to the hypothesis of Zel'dovich and Grishchuk.

The ESC singularity, reported separately by Eardley and Smarr in a numerical study, and later by Christodoulou in an existence proof, is a single point in standard coordinates, and appears at the centre of symmetry on the crunch surface, yet it emits an infinite set of light rays. If the dust cloud of the Tolman model is joined to a Schwarzschild exterior, then some of those rays can reach future null infinity, and it can be seen for a finite length of time. The conditions under which this singularity occurs are generalised and approximate forms for the rays emerging from it are derived. The paths of the light rays in the vicinity of this singularity are integrated numerically for a particular case, and a conformal diagram is also calculated numerically for this same case. The conditions for existence agree with those of Eardley and Smarr, but the conformal diagram is different in one respect. Some preliminary calculations for more general cases are presented. The calculation of the orientation of the crunch surface at the ESC singularity is found to be heavily dependent on the path chosen to approach that point. Further points of investigation are suggested. Lastly, a reasonable continuity condition is put forward which is not satisfied by models containing an ESC singularity. The condition is that the derivative of the density with respect to the mass at constant time must be zero at the origin.

Acknowledgements

It is a pleasure to thank my supervisor, Dr. Kayll Lake for looking after me academically during these past six years. I have been unusually lucky in this respect, especially considering I had no choice of supervisor when I arrived here at Queen's, because all the other professors in Astronomy had already chosen their students. He expected a lot, but never told me off, even when I really had been dragging my feet, and the nearest he got to hinting I wasn't getting on with things was "Aren't you eager to see what the results will be?" He could never find his references, but, astonishingly, could always give the author, the journal, and the approximate year. He would always take the time to discuss things if at all possible, he was flexible about my extracurricular commitments, he was as forgetful as I am, and generally suited me down to the ground. I hope his memories of his first student will not be too painful.

I wish to express my gratitude to Queen's University for providing generous financial support of my studies during these past six years, which also enabled me to come to Canada and to Kingston, and to enjoy a full and busy life while I was here.

I would like to thank my conscience, Post Doctor Pimbleton (FRP), for keeping my watch in seconds mode, and I would also like to thank Uncle Arno for outfitting his Zenith with a special "Chuckles glitch switch", so that the thing would never do what it should unless he was around.

Thanks finally to the Physics grads and assorted others of the hockey-before-breakfast crowd who taught me to enjoy rising at ungodly hours, rushing around in the bitter cold, and being battered against the boards and the ice, all on an empty stomach. Not much else could get me out of bed so early.

Statement of Originality

The work presented in this thesis is that of the author, and of the author in collaboration with his supervisor, unless otherwise acknowledged. Much, but not all of chapter 2 is introducing known material, some in reworked form, and chapter 4, as stated there, is a review of results that will be needed. The majority of the material of chapters 3, 5, and 6 has appeared in two papers in the *Astrophysical Journal* (Hellaby and Lake 1984, 1985), and this plus much of chapter 7 has been summarised in conference talks.

List of Figures

1	The functions $\phi_1(\eta)$, $\phi_2(\eta)$, and $\phi_2(\eta, \alpha = 2/3)$	31
2	The function $\phi_2(\eta, \alpha)$ for $\alpha = .1, 0$, and $-.3$	31
3	The functions $\phi_4(\eta)$, $\phi_5(\eta)$	32
4	The evolution of the function $R(r, t)$ for example 6(c)	35
5	The conformal diagrams of Eardley and Smarr for parabolic Tolman models with and without an ESC singularity	50
6	Gradient diagram for the radial light ray equation near the ESC singularity, with $m = 2$, in the $s-q$ plane	51
7	Paths of the radial light rays near the ESC singularity, with $m = 2$, in the $s-q$ plane. Three different scales are shown	52
8	Paths of the radial light rays near the ESC singularity, with $m = 2$, in the $r-t$ plane. Three different scales are shown	55
9	The conformal diagram, showing the $u-v$ plane near the ESC singularity <ul style="list-style-type: none"> (a) constant s curves (b) constant q curves (c) constant t curves (d) constant R curves (e) constant ρ curves 	57
10	Gradient diagram for the radial light ray equation near the ESC singularity, for several values of m , in the $s-q$ plane	60
11	Paths of the radial light rays near the ESC singularity, for several values of $m < 3$, in the $s-q$ plane	64
12	Paths of the radial light rays near the ESC singularity, for several values of $m < 3$, in the $r-t$ plane	68
13	The outgoing critical rays on the same scale in the $s-q$ plane for $m < 3$	70
14	The dependence of the critical radius on m	71
15	The dependence of M_{crit}/t_{crit} on m	72
16	Gradient diagram for the radial light ray equation near the ESC singularity, for $m = 3$ and several values of a_1 , in the $s-q$ plane	73

List of Tables

1	Limiting behaviour of the null and timelike vectors near Σ_0 .	17
2	Limiting behaviour of χ_e for comoving emitters, and the resulting redshift from Σ_0 .	18
3	Limiting behaviour of χ_e for geodesic emitters, and the resulting redshift from Σ_0 .	19
4	The conditions for no shell crossings.	30
5	The orientation of the crunch surface at the origin.	47

Chapter 1

INTRODUCTION

The standard big bang model of the universe is based on the Robertson-Walker metric. This metric is derived from Einstein's equations by assuming that the universe is completely homogeneous and isotropic. The metric is written in spherical polar coordinates, and the coordinates are synchronous and comoving. The former means that the time coordinate is the proper time for any observer remaining at constant spatial coordinates, and the latter means that the spatial coordinates are attached to the particles of matter, so that any given particle always remains at constant radial and angular positions. With this choice, the Einstein equations reduce to the Friedmann equations and there is only one undetermined metric function — the scale factor, which depends on time only, and expresses the expansion or contraction of space. These equations relate the scale factor to the density and pressure. The Robertson-Walker model assumes that the matter is a perfect fluid, but the equation of state, giving the relation between the pressure and the density, may be freely chosen. Given this equation, the Friedmann equations may be solved for the scale factor.

While the assumptions of homogeneity and isotropy seem to agree well with observations on the largest scales, and the model has led to several important successes, such as the prediction of the correct helium abundance, and the existence of the cosmic background radiation, it cannot describe any of the universe's smaller scale features. The Tolman metric represents a distribution of pressureless matter (dust) that is characterised by spherical symmetry, but is inhomogeneous in the radial direction. Like the Robertson-Walker model, it is expressed in synchronous, comoving coordinates, but, in order to make the Einstein equations tractable, the pressure is set to zero, thus specifying the equation of state. The resulting equations of motion are closely analogous to the Friedmann equations for a dust Robertson-Walker model, save only that the total time derivatives become partial. The solutions are also very similar, except that the constants of integration become arbitrary functions of the radial coordinate. The function that is solved for is not the scale factor, but the areal radius, the coefficient of the angular terms in the metric. It is a function of both the radial and time coordinates, but, for a given particle, it plays the role of a scale factor.

A restricted form of the metric was first presented by Lemaitre (1933 a and b) in a pair of short papers in *Comptes Rendus*, without an explicit solution for the evolution of the model. Later that year he wrote down the general metric in a large paper in the *Annals of the Brussels Scientific Society* (1933c), discussing this and several other cosmological models. Using a particular choice of coordinates, he provided the full solution for all models with a closed geometry, including a non zero cosmological constant. He also discussed the relation between the relativistic and classical equations, as well as noting the breakdown of the results when shell crossings developed. He then used the model, together with the assumption that clusters of galaxies have been in equilibrium since the static Einstein universe was disturbed, to derive an estimate of the degree of expansion that has

subsequently occurred.

Tolman's paper of the following year (1934) in the Proceedings of the National Academy of Sciences, actually cited Lemaitre's third paper, but derived the model from scratch anyway, also using a non zero cosmological constant. In this paper he does not give a solution of the equations of motion, except in the form of an integral. What he does do is examine the time derivatives of perturbations from known homogeneous cosmologies, and demonstrate that enhancements continue to grow while rarefactions become more pronounced, thus revealing an instability in those models.

The model was discovered a third time by Datt (1938) in Calcutta. Writing in *Zeitschrift für Physik*, he derived the metric, and solved the equations of motion for all models with an open geometry and zero cosmological constant. Unfortunately, his solution is not correct, though his specific examples are. (In that paper he also provides a (correct) solution for Kantowski-Sachs models.)

The most cited paper for the Tolman metric is one by Bondi (1947) in *Monthly Notices*. He refers to Tolman's paper, and to a 1931 paper by Lemaitre, but omits mention of any of Lemaitre's 1933 papers. This may be why the model is now known as the Tolman model, and sometimes as the Tolman-Bondi model¹. Bondi's paper consists of a thorough derivation and review of the model (with zero cosmological constant in the solution, though not in most of his discussion), and includes sections on the comparison with classical equations, the luminosity distance, the redshift, and the apparent horizon. He also discusses an "impenetrable barrier" in the model, which is in fact only a coordinate problem, and corresponds to the regular maximum defined in the next chapter.

The Tolman metric has often been used to model the development of density fluctuations, and even to model specific clusters of galaxies. For epochs later than recombination, and regions of low density, its dust equation of state is quite realistic, so that its lack of rotation is the major deficiency. For early times, or high densities the pressure becomes significant in the real universe, and so the model is a lot less reliable here. In particular, the divergent densities that occur at singularities in the Tolman model cannot be considered realistic when the pressure remains zero. Nevertheless, there are no inhomogeneous models with non zero pressure that are of comparable generality to the Tolman model. Thus the Tolman model is used in this thesis to study some properties of singularities in an inhomogeneous cosmology. Since the differences between singularities in homogeneous models with and without pressure are purely quantitative, it is reasonable to suppose that the properties found in the Tolman model will hold qualitatively for more general equations of state.

Chapter two describes the Tolman model in some detail and also introduces the remaining chapters.

¹Following Krasinski (1997) [*Inhomogeneous Cosmological Models*, Cambridge U P], I recommend calling it the Lemaître-Tolman model.

Chapter 2

THE TOLMAN MODEL

As already mentioned, the Tolman model represents a distribution of pressure free matter (dust) that is spherically symmetric, but inhomogeneous in the radial direction. It is written in synchronous, comoving coordinates, so that $g_{tt} = -1$, and $g_{ti} = 0$ ($i = 1, 2, 3$), and the tangent vector of the particles of matter is $u^\alpha \equiv (1, 0, 0, 0)$, which means that the coordinate time, t , is also the proper time of the particles. The cosmological constant, Λ , will be neglected throughout this thesis. In addition, geometric units such that $G = 1$ and $c = 1$ will be used throughout. Thus the metric is,

$$ds^2 = -dt^2 + \frac{R'^2(r, t)}{1 + f(r)} dr^2 + R^2(r, t) d\Omega^2, \quad (2.1)$$

where $d\Omega^2 = d\theta^2 + \sin^2 \theta d\phi^2$, $' \equiv \partial/\partial r$, and $\dot{} \equiv \partial/\partial t$ will be used below. The evolution of the areal radius, $R(r, t)$, is found from the Einstein equations with $\Lambda = 0$, which give

$$\dot{R}^2 = \frac{F(r)}{R} + f, \quad (2.2)$$

and has the following parametric solutions;

hyperbolic, $f > 0$

$$R = \frac{F}{2f}(\cosh \eta - 1), \quad (\sinh \eta - \eta) = \frac{2f^{3/2}(t - a)}{F}; \quad (2.3)$$

parabolic, $f = 0$

$$R = \left[\frac{9F(t - a)^2}{4} \right]^{1/3}; \quad (2.4)$$

elliptic, $f < 0$

$$R = \frac{F}{2(-f)}(1 - \cos \eta), \quad (\eta - \sin \eta) = \frac{2(-f)^{3/2}(t - a)}{F}. \quad (2.5)$$

There is also a particular solution for the case $F = 0$, $f > 0$,

$$R = f^{1/2}(t - a), \quad (2.6)$$

which is the same as the late time behaviour of all hyperbolic models. This last solution is in fact Minkowski space, and is discussed further below.

The three types of time evolution of these models, given by eqs (2.3) to (2.5), are equivalent to those of the hyperbolic, parabolic and elliptic Robertson-Walker models, and for any given point, a dust Robertson-Walker model with identical evolution can be found. They all emerge from the big bang at $t = a(r)$ with a positive expansion rate, $\dot{R} > 0$, so that the areal radius of the shells of matter at $r = \text{const}$ is increasing. In hyperbolic models, the expansion continues indefinitely, while elliptic models eventually reach a maximum size and then start collapsing, terminating in a big crunch. The parabolic models are the borderline cases, since their expansion asymptotically decreases to zero at infinite time. The time reversed parabolic and hyperbolic cases, obtained by writing $(a - t)$ instead of $(t - a)$, are also valid solutions, though they are no good as cosmological models. Unlike the Robertson-Walker models, the bang does not necessarily occur simultaneously everywhere, neither are the times of the crunch or maximum expansion simultaneous in general. The hyperbolic and elliptic cases can easily be shown to reduce to the parabolic form for $\eta \rightarrow 0$, i.e. as $t \rightarrow a$, so that all three cases have the same behaviour at very early times. Similarly, near the big crunch in elliptic models, when $\eta \rightarrow 2\pi$, the behaviour approaches that of a collapsing parabolic model. It is entirely possible for all three types of evolution to obtain within different regions in the same model.

The density is given by

$$8\pi\rho = \frac{F'}{R'R^2}, \quad (2.7)$$

and the Kretschmann scalar is (e.g. Bondi 1947)

$$K = R^{\alpha\beta\gamma\delta}R_{\alpha\beta\gamma\delta} = \frac{12F^2}{R^6} - \frac{8FF'}{R^5R'} - \frac{3F'^2}{R^4R'^2}, \quad (2.8)$$

where $R_{\alpha\beta\gamma\delta}$ is the Riemann tensor.

The functions, F , f , and a , are all arbitrary functions of the coordinate radius r , which allow a coordinate choice, plus the specification of two physically independent quantities. Nevertheless, they all have a physical meaning. The local time at which $R = 0$ is $a(r)$, and, in the region $t \geq a$, it is the time of the big bang, while for $t \leq a$ it is the time of the big crunch. The function $F(r)$ is twice the effective gravitational mass, M , within coordinate radius r (see Bondi 1947), which can be defined by

$$\frac{2M}{R} = R^\phi_{\theta\phi\theta}$$

(Cahill and McVittie 1970). The third function, $f(r)$, determines both the type of time evolution, and the local geometry. A local value of π can be defined in terms of the rate of change of areal radius, on some constant time slice, with¹

$$\Pi(r) = \frac{\pi(\partial_r g_{\theta\theta})}{\sqrt{g_{rr}}} = \pi\sqrt{1+f(r)}. \quad (2.9)$$

However, the local geometry in an elliptic Tolman model is not necessarily analogous to that of an elliptic Robertson-Walker model. In the latter, where $f = -\varepsilon r^2$, the $\varepsilon = +1$ case has a positively curved spatial geometry, so that its constant t , $\theta = \pi/2$ sections have the geometry of a sphere. A

¹Erratum: The printed version had

$$\Pi(r) = \frac{\pi(\partial_r g_{\theta\theta})^2}{g_{rr}} = \pi[1+f(r)].$$

similar local geometry only occurs in elliptic Tolman models if $f' < 0$ as well as $f < 0$. Similarly, the hyperbolic Tolman models only have a saddle like geometry, similar to the $\varepsilon = -1$ Robertson-Walker models, if $f' > 0$ as well as $f > 0$. Also, $f(r)$ may be regarded as a local energy constant. For hyperbolic and parabolic regions, the expansion rate at late times is given by $\dot{R} = f^{1/2}$, while in elliptic regions, the “mean speed”, defined by dividing the radius, R_{\max} , at maximum expansion by the time from bang to R_{\max} , is just $2(-f)^{1/2}/\pi$. In fact, these three functions cannot be chosen completely arbitrarily. Since F is proportional to the mass, it must be everywhere positive,

$$F \geq 0, \quad (2.10)$$

and the condition

$$f \geq -1, \quad (2.11)$$

must hold for a Lorentzian manifold. Further restrictions on the arbitrary functions will be derived below and in chapter 5.

A scale radius and a scale time can be defined for each particle of the fluid (except where $f = 0$) by

$$p(r) = \frac{F}{(\pm f)}, \quad \text{and} \quad q(r) = \frac{F}{(\pm f)^{3/2}}, \quad (2.12)$$

respectively, where the upper sign is for $f > 0$, and the lower one for $f < 0$. Obviously, they are both positive. In elliptic regions they have a particular meaning, since the value of $R(r, t)$ at maximum expansion ($\eta = \pi$) is just $p(r)$, while the time from bang to crunch is $\pi q(r)$.

For all three cases, the radial derivative of the areal radius is given by,

$$R' = \left(\frac{F'}{F} - \frac{f'}{f} \right) R - \left[a' + \left(\frac{F'}{F} - \frac{3f'}{2f} \right) (t - a) \right] \dot{R}, \quad (2.13)$$

It is quite possible for one model to contain adjacent elliptic and hyperbolic regions. At the boundary, where $f = 0$, it can be seen from the second parts of eqs (2.3) and (2.5) that, for finite $(t - a)$, $\eta \rightarrow 0$ on the boundary and the evolution smoothly approaches the parabolic type from either side. This means that, in the t - r plane, the surfaces of constant η , diverge towards $t = \infty$ here, so on either side of the boundary η is a different parameter. Expanding (2.3) or (2.5) in powers of f , and remembering that $f' \neq 0$ in general, gives, after some manipulation,

$$\frac{R'}{R} = \frac{F'}{3F} - \frac{2a'}{3(t-a)} + \frac{3f'}{10} \left[\frac{2(t-a)^2}{3F^2} \right]^{1/3} + O(f), \quad (2.14)$$

which is valid for sufficiently small f in both $f > 0$, and $f < 0$ regions, and is exact for $f = 0$. For an extended parabolic region, where $f' = 0$, eq (2.14) becomes the derivative of eq (2.4). (It is also possible for f' to be zero only at the point where $f = 0$.) The derivatives of R with respect to t and r can be expressed as series in powers of R , by performing a Taylor expansion on the trigonometric functions in eqs (2.3) and (2.5);

$$\dot{R} = \sqrt{\frac{F}{R}} \sqrt{1 + \frac{fR}{F}}, \quad (2.15)$$

$$R' = \left(\frac{F'}{F} - \frac{f'}{f} \right) R - a' \sqrt{\frac{F}{R}} \sqrt{1 + \frac{fR}{F}} + \left(\frac{F'}{F} - \frac{3f'}{2f} \right) \left(\frac{F}{f} \right) \left[\sum_{i=1}^{\infty} \frac{(2i)!}{(i!)^2 (2i+1)} \left(-\frac{fR}{F} \right)^i \left(1 + \frac{fR}{F} \right)^{i+1} \right], \quad (2.16)$$

and a further expansion is implied wherever powers of $[1 + (fR/F)]$ occur. The above are series in half and whole powers of R , whose coefficients are functions of r only and are thus well behaved near $R = 0$. Equations (2.15) and (2.16) are valid for all f . These expansions will be needed in chapter 3.

For particular choices of the arbitrary functions, the Tolman metric reduces to some other standard metrics. All models with $F = 0$ are flat and empty, as one might expect. Thus the form (2.1) with solution (2.6) can be obtained from Minkowski space,

$$ds^2 = -dT^2 + dR^2 + R^2 d\Omega^2 ,$$

using the transformations (2.6) and

$$T = x(r)t + y(r) ,$$

where

$$x = (1 + f)^{1/2} , \quad y = y_0 - \int \frac{(f'a + 2a'f)}{2(1 + f)^{1/2}} dr .$$

The case when both F and f are zero gives $R = R(r)$ as the solution of (2.2), and is obviously Minkowski space. The Robertson-Walker metric is generated by setting $a = 0$, $F \propto r^3$, and $f \propto \pm r^2$, or more generally, $a = 0$ and $F \propto f^{3/2}$. Any Tolman region in which $F = \text{const}$, has zero density, and is a section of Schwarzschild space. In order to produce the complete Kruskal manifold, however, it is necessary to chose an elliptic model, with $f = -1$ at $r = 0$, say, and rising asymptotically to 0 in both directions. The function a must be monotonically decreasing in either direction from $r = 0$, the simplest choice being

$$a = -\frac{\pi F}{2(-f)^{3/2}} ,$$

and of course F is a constant. This was first done by Novikov (1963), and is described on pp 319-20 of Landau and Lifshitz (1975).

2.1 The Origin and the Topology

An origin occurs at r_0 if $R(r_0, t) = 0$ (i.e. $g_{\theta\theta} = 0$) for all t . Normally at the origin, F and f both go to zero, but this does not necessarily mean that the time evolution is parabolic. Suppose that, near the origin in an elliptic or hyperbolic region, $(t - a)$ remains finite, $F \rightarrow 0$, and

$$f \rightarrow f_0 F^s , \quad s > 0 . \quad (2.17)$$

As long as both functions go smoothly to zero at the same point, this will be a valid approximation. Then η will remain finite and non zero along any spacelike slice that does not include the bang or crunch, provided

$$s = 2/3 . \quad (2.18)$$

This constitutes a regular origin, because the density remains finite and the type of time evolution does not change as $F \rightarrow 0$.

Now suppose $s > 2/3$. Then, for constant $(t - a)$, $\eta \rightarrow 0$ as $F \rightarrow 0$, so the time evolution does become parabolic at the origin, and η obeys

$$\eta \sim F^{(s/2-1/3)} ,$$

while R obeys

$$R \sim F^{1/3} ,$$

as expected. The density is finite here and the behaviour is entirely equivalent to $f = 0$ elsewhere.

For the case $s < 2/3$, η diverges as $F \rightarrow 0$, giving instantaneous evolution, so that, in elliptic models, the bang and crunch surfaces touch here, while in hyperbolic models the late time behaviour is reached immediately. The volume expansion rate, $\Theta = \nabla_\alpha u^\alpha$, of a volume element centered on $r = 0$ is, for very early times (small η),

$$\Theta^2 = \frac{9\dot{R}^2}{R^2} = 9 \left(\frac{2}{3(t-a)} \right)^{4/3} \left[\left(\frac{2}{(t-a)} \right)^{2/3} + f_0 F^{s-2/3} \right]. \quad (2.19)$$

Approaching $F = 0$ along constant η , with $s < 2/3$, $(t-a)$ goes to zero, so all terms in eq (2.19) diverge. At later times in the hyperbolic model however, i.e. for η large and for all² $t-a > 0$, the expansion rate becomes

$$\Theta^2 = \frac{9}{f_0(t-a)^2} \left[\frac{F^{1-3s/2}}{f_0^{1/2}(t-a)} + f_0 \right], \quad (2.20)$$

so Θ remains finite right up to the origin. (This last expression is not valid for $s > 2/3$ because large η is never attained.) The behaviour is equivalent to $f \rightarrow \infty$ elsewhere in hyperbolic models. However, R now goes as eq (2.6) near the origin, so the density goes to zero here. In elliptic models f must not be less than -1 , so $F = 0$ is the only point where the time from bang to crunch can be zero. Along a constant η curve, R goes as F^{1-s} , and of course the density diverges. It is even possible to have $s = 0$ so that f is finite as F goes to zero. In elliptic models the bang and crunch touch here also, and there is an effective origin. For hyperbolic models $s = 0$ has quite a different meaning. At such a point the areal radius R is finite, indicating there is no origin here. Since the density is finite but the mass is zero, the only possible interior is Minkowski space, eq (2.6). One cannot have F going negative, because, even if the negative mass is ignored, eq (2.2) then gives an imaginary value for \dot{R} for small R .

Inspection of eq (2.13) shows that problems with R' going negative could be encountered with $s \neq 2/3$, or with a or a' divergent. This will be considered in detail in chapter 5, and certain conditions at the origin will be disallowed.

If the time of the big bang, $a(r)$, is a decreasing function of r , so that the outer shells of matter emerge first, and the origin emerges last, then there is initially a singular origin to the space, of finite but decreasing mass. Similarly, the crunch surface can form a singular origin of growing mass. If the model consists of a hyperbolic region surrounding an elliptic region, then at late times the origin develops a singularity whose mass asymptotically approaches a maximum value.

The terms 'elliptic', 'parabolic', and 'hyperbolic' are here defined to indicate only the local type of time evolution (i.e. $f < 0$, $f = 0$, and $f > 0$, respectively). The terms 'open' and 'closed' refer only to the topological properties of the model, so that, for spherically symmetric metrics, closed models have two values of r where $R = 0$, while open models have only one (or conceivably none).

If a model is closed, it must necessarily have a region where $F' < 0$ and $R' < 0$ near the second origin, unless the radial coordinate is badly behaved, as it is in the closed Robertson-Walker model with the usual coordinates (see eq (3.2)). The density will be well behaved everywhere only if $R' = 0$ and $F' = 0$ are coincident, which means that $R' = 0$ must remain at fixed r . This point was made clear by Zel'dovich and Grishchuk (1984). Any point where R' passes through zero, but where the density remains positive and finite, is a regular extremum, and not a shell crossing as described below. Regular extrema will be discussed further in chapter 4.

²Erratum: The printed version had $t > 0$.

2.2 Singularities

There is no accepted definition of a singularity in General Relativity (Tipler, Clarke, and Ellis 1979) but, loosely speaking, a singularity is a point or locus of points where the Einstein equations break down, and which is often associated with divergences in quantities like the density and the Kretschmann scalar. Therefore, since nothing can be said about singular points themselves, the study of a singularity is actually the study of the limiting behaviour as the singular point is approached.

There are two hypersurfaces where the density and the Kretschmann scalar, given by eqs (2.7) and (2.8), diverge; the loci of $R = 0$, and of $R' = 0$. All Tolman models have a big bang singularity, or a big crunch singularity, or both, and these surfaces will be designated by Σ_0 . They occur at $\eta = 0$ in all models, and also at $\eta = 2\pi$ in elliptic models, and are characterised by $R = 0$. For the region $t \geq a$, $\eta = 0$ is the bang, while for $t \leq a$, it is the crunch. These surfaces can be shown to be spacelike everywhere by considering the $\eta = \text{const}$ surfaces. For the hyperbolic case, these surfaces have an (unnormalised) normal vector,

$$n_\alpha \propto \left(\frac{2f^{3/2}}{F}, \left[(\sinh \eta - \eta) \left(\frac{3f'}{2f} - \frac{F'}{F} \right) - \frac{2f^{3/2}a'}{F} \right], 0, 0 \right), \quad (2.21)$$

so that the contraction of n_α is

$$n^\alpha n_\alpha \propto -f + \frac{(1+f) \left[(\sinh \eta - \eta) \left(\frac{3f'}{2f} - \frac{F'}{F} \right) - \frac{2f^{3/2}a'}{F} \right]^2}{(\cosh \eta - 1)^2 \left[\frac{F'}{F}(1 - \phi_4) + \frac{f'}{f} \left(\frac{3}{2}\phi_4 - 1 \right) - \frac{2f^{3/2}a'}{F}\phi_5 \right]^2}. \quad (2.22)$$

Clearly, this is negative for $\eta \rightarrow 0$, so that the surface is spacelike. A similar argument applies for the elliptic case, taking both $\eta \rightarrow 0$, and $\eta \rightarrow 2\pi$, while for the parabolic case the surfaces of constant $(t - a)$ must be used. It would not help to consider surfaces of constant R , since $R = 0$ along the origin, which is timelike, as well as on the bang and collapse surfaces.

If our universe really does contain singularities, the big bang must be one of the most certain to exist (Hawking and Ellis 1968, 1973), at least in classical relativity. In the standard model, the big bang is a spacelike hypersurface, and it is connected to later observers by timelike geodesics, but it is not visible since its redshift is infinite. However, in inhomogeneous models, the bang is not necessarily simultaneous, so the redshift is not necessarily infinite. In fact, infinite blueshifts can occur along radial rays in the Tolman model (e.g. Dyer 1979; Szekeres 1980). The divergent energy fluxes implied by these infinite blueshifts are physically unacceptable. Therefore in this work all realistic inhomogeneous cosmological models are required to exhibit no infinite blueshifts from the big bang. The stronger requirement, that only infinite redshifts be generated, would ensure that the bang is completely invisible. In chapter 3, a general result for the redshift structure of the bang surface in Tolman models is derived, and the consequences of applying the above requirements are investigated.

The second type of divergence is the shell crossing, $R' = 0$, so called because the spherical shells of matter appear to be trying to pass through each other here. These surfaces will be designated by Σ_1 . Though some authors (e.g. Bonnor 1974, Szekeres 1980) treat these surfaces as if they were part of the big bang or big crunch, shell crossings are in fact different in a number of ways. Firstly, on the bang or collapse surfaces $g_{\theta\theta}$ and $g_{\phi\phi}$ both go to zero, and g_{rr} either goes to zero or diverges, while on the shell crossing surfaces only g_{rr} goes to zero. Another difference is that shell crossings are timelike everywhere. The normal to the surface $R' = \text{const}$ is

$$n_\alpha \propto (\dot{R}', R'', 0, 0), \quad (2.23)$$

or, writing the locus of the surface as $t = b(r)$, then

$$n_\alpha \propto (1, -b', 0, 0), \quad (2.24)$$

so that

$$R'' = -b\dot{R}' \quad (2.25)$$

and $n_\alpha n^\alpha > 0$ gives $b'^2 > R'^2/(1+f)$, which implies b' may have any value on $R' = 0$, except zero. Other differences will be shown in chapters 3 and 4. I believe that shell crossings are not serious physical singularities, but rather, they occur due to the breakdown of the basic assumptions of the Tolman model. These assumptions are that the matter can be represented by comoving coordinates and a single particle four-velocity at each point. Furthermore, Lake (1984a) has pointed out that the metric is C^1 , but not C^2 at a shell crossing, and so the Einstein equations are not valid there. (At Σ_0 , the metric is not even C^1 .) Although there may be a way of resolving this problem, it cannot be dealt with in the context of the Tolman model. It is worth noting that the theorems which use the Raychaudhuri equation (1955 and 1957) to predict a divergence in the density, fail to distinguish shell crossings from more serious physical singularities. As Seifert (1979) has pointed out, even when the origin of a singularity is really hydrodynamic, the Einstein equations ensure that a curvature singularity also appears. Since shell crossings can also occur in non relativistic hydrodynamics, this may be the real source of the problem.

The function $a(r)$ not only determines the bang time, but also the relationship between Σ_0 and Σ_1 . At points where $a' = 0$, it is evident from eq (2.13) or (2.16) that $R' = 0$, whenever $R = 0$, so Σ_1 and Σ_0 intersect at $a' = 0$. Thus, if $a(r) = \text{const}$, the two surfaces are coincident. In eq (2.16) and its time derivative, the leading terms near Σ_0 are

$$R' = -a' \sqrt{\frac{F}{R}} \quad \text{and} \quad \dot{R}' = \frac{a' F}{2R^2} \quad (2.26)$$

(\dot{R}' is positive so the positive root of F/R must be chosen). Thus, where a' is positive, R' is negative and increasing in t , and where a' is negative, R' is positive but decreasing. Also the first three terms in eq (2.16) are

$$R' = -a' \sqrt{\frac{F}{R}} \left(1 + \frac{fR}{2f} \right) + \frac{RF'}{3F} + \dots \quad (2.27)$$

If $a' = 0$ at $r = r_0$, then for small values of R and $(r - r_0)$, the location of Σ_1 is given by

$$R_{\Sigma_1} \approx F \left(\frac{3a'}{F'} \right)^{2/3}, \quad (2.28)$$

for a' positive, but there is no solution for a' negative, because in this case Σ_1 occurs in $t < a$, where \dot{R} is negative. So, for $t > a$, Σ_1 only exists near Σ_0 where a' is positive, but it may extend indefinitely into the future, depending on the functions $a(r)$ and $f(r)$.

In general, the density calculated from eq (2.7) is negative on one side of a shell crossing surface, so that, even if the singularity is not truly physical, it is serious enough to make the metric unusable beyond it. Thus, unless one is interested in studying shell crossings, it is of interest to find the conditions that will ensure no shell crossings will form in a Tolman model. These are derived in Chapter 5.

Another kind of singularity in some Tolman models was found by Eardley and Smarr (1978) in a numerical study, and more recently by Christodoulou (1984) in a mathematical proof of a violation of cosmic censorship in a particular class of models. Cosmic censorship is the hypothesis, put forward

by Penrose (1969) which states that, starting from reasonable initial conditions, no singularities which are visible from arbitrarily large distances may form (global censorship), so that all singularities must be clothed by the formation of an event horizon. In a later discussion (e.g. Penrose 1979) he extended the protection of the cosmic censor to all observers, arguing that singularities should not be visible from anywhere, even inside a horizon (local censorship). This means that timelike singularities are not allowed. In a collapsing Tolman model, if the crunch singularity occurs first at the origin, then, given some apparently reasonable conditions, it can be shown that this single point on the crunch surface emits light rays, and is therefore naked, at least locally and sometimes globally. This singularity is considered in some detail in chapter 7.

Chapter 3

THE REDSHIFT

In this chapter an approximation is used in order to determine the behaviour of the redshift from the big bang “seen” by later observers. The restrictions on the redshift behaviour mentioned at the end of the last chapter will then be applied. This work has already appeared in the *Astrophysical Journal* (Hellaby and Lake 1984).

To calculate the redshift, the motions of the emitting particle, the light ray, and the observing particle are needed. If their tangent vectors are v_e^μ , k^μ , and v_o^μ , respectively, the redshift of the geometrical optics approximation, z , is given by the standard formula

$$(1 + z) = \frac{\chi_e}{\chi_o}, \quad (3.1)$$

where $\chi_e = v_e^\mu k_\mu$ and $\chi_o = v_o^\mu k_\mu$. The tangent vector to the light ray is, of course, geodesic, and the emitter is also assumed to be geodesic. All that is assumed about the observer is that χ_o is finite and non zero, which will be the case for any timelike motion at any regular point in spacetime.

As a preliminary, the results for the standard model will be briefly summarised. The Robertson-Walker metric is

$$ds^2 = -dt^2 + P^2(t) \left(\frac{dr^2}{1 - \epsilon r^2} + r^2 d\Omega^2 \right), \quad (3.2)$$

with scale factor P , obeying the usual Friedmann equations. It has timelike and null geodesic tangent vectors,

$$v_e^\mu \equiv \left(\sqrt{\frac{\gamma^2}{P^2} + 1}, \pm \frac{\sqrt{1 - \epsilon r^2}}{P^2} \sqrt{\gamma^2 - \frac{h_e^2}{r^2}}, 0, \frac{h_e}{P^2 r^2} \right) \quad (3.3)$$

and

$$k^\mu \equiv \left(\frac{1}{P}, \pm \frac{\sqrt{1 - \epsilon r^2}}{P^2} \sqrt{1 - \frac{h_n^2}{r^2}}, 0, \frac{h_n}{P^2 r^2} \right), \quad (3.4)$$

where $[(\gamma^2/P^2) + 1]^{1/2}$ is the dimensionless energy per unit mass in the comoving frame, so γ is an energy parameter, and h_e and h_n are the effective impact parameters for the timelike and null vectors (the emitter and the light ray) respectively, and all three are constants of the motion. In general, the orbits of the emitter and of the light ray will not be coplanar (though both are stably planar). In this case, however, the orbits have been chosen to lie in the plane $\theta = \pi/2$, since allowing v_e^μ a non zero θ component does not qualitatively change the behaviour of χ_e . The contraction of eqs (3.3) and (3.4) is then

$$\chi_e = \frac{1}{P^2} \left[-\sqrt{\gamma^2 + P^2} \pm \sqrt{\left(1 - \frac{h_n^2}{r^2}\right) \left(\gamma^2 - \frac{h_e^2}{r^2}\right) + \frac{h_e h_n}{r^2}} \right], \quad (3.5)$$

where the second term in brackets is positive if v_e^μ and k^μ are both incoming or both outgoing, and negative otherwise. For comoving emitters, $\gamma = 0$ and $h_e = 0$, so $\chi_e = -1/P$ and the redshift becomes infinite as $P \rightarrow 0$. For general geodesic emitters, however, an infinite redshift ($\chi_e \propto -1/P^2$) is not found for all cases. There are also “forward rays” which give a finite redshift. The light ray which is emitted straight ahead (i.e. $v_e^\phi/v_e^r = k^\phi/k^r$, which implies $h_e = \gamma h_n$, with the positive sign in eq (3.5)) has $\chi_e \rightarrow -1/2\gamma$ as $P \rightarrow 0$, giving a finite z . From the observer’s point of view, this corresponds to the emitter coming straight at him, and it can be explained by noting that the local proper speed of any geodesic with $\gamma \neq 0$ approaches c as $P \rightarrow 0$.

3.1 The geodesic equations

In this and the next section k^μ will be used for any geodesic tangent vector, null or timelike. The quantity k^μ is governed by the geodesic equation

$$k^\mu \nabla_\mu k^\nu = 0, \quad (3.6)$$

and the null or timelike condition

$$k^\mu k_\mu = \epsilon, \quad (3.7)$$

where $\epsilon = 0$ or -1 , respectively. Because the Tolman metric is spherically symmetric, there is no loss of generality in choosing $\theta = \pi/2$, so the θ and ϕ components of eq (3.6) give

$$k^\theta = 0, \quad \text{and} \quad k^\phi = \frac{h}{R^2}, \quad (3.8)$$

where h is the constant effective impact parameter. Eq (3.7) and the remaining components of eq (3.6) are written out explicitly for the Tolman metric below. There are only two independent equations, though eq (3.11) must be one of them. The indices here refer to particular coordinates, and there is no summation.

$$k^t \partial_t k^t + k^r \partial_r k^t + \frac{R' \dot{R}' k^{r2}}{y^2} + \frac{h^2 \dot{R}}{R^3} = 0, \quad (3.9)$$

$$k^r \partial_r k^r + k^t \partial_t k^r + \left(\frac{R''}{R'} - \frac{y'}{y} \right) k^{r2} + \frac{2\dot{R}' k^t k^r}{R'} - \frac{h^2 y^2}{R' R^3} = 0, \quad (3.10)$$

$$k^{t2} = \frac{R'^2 k^{r2}}{y^2} + \frac{h^2}{R^2} - \epsilon, \quad (3.11)$$

where¹

$$y^2 = 1 + f$$

Using eq (3.11) to eliminate k^t , eq (3.10) becomes

$$\left(\frac{R'^2 k^{r2}}{y^2} + \frac{h^2}{R^2} - \epsilon \right) \left(\partial_t k^r + \frac{2\dot{R}' k^r}{R'} \right)^2 = \left[k^r \partial_r k^r + \left(\frac{R''}{R'} - \frac{y'}{y} \right) k^{r2} - \frac{h^2 y^2}{R' R^3} \right]^2, \quad (3.12)$$

and this can be written

$$\left(\frac{R'^2 k^{r2}}{y^2} + \frac{h^2}{R^2} - \epsilon \right) \left[\partial_t \left(\frac{2R' k^r}{y^2} \right) \right]^2 = \left[\partial_r \left(\frac{R'^2 k^{r2}}{y^2} + \frac{h^2}{R^2} \right) \right]^2. \quad (3.13)$$

¹Erratum: In the printed version, the variable f was used instead of y , so that f had a different meaning from this point till the end of this chapter. This change of meaning was, unfortunately, not pointed out.

This version is more useful than the equivalent equation in k^t , since, in the asymptotic forms that will be used, k^t can be found unambiguously from eq (3.11), given k^r , whereas the reverse is not necessarily true.

Equations (3.6) and (3.7) can be solved only for a few metrics with high symmetry (e.g. static spherically symmetric metrics). If the spacetime admits a conformal Killing vector, ξ_μ (such that ξ_μ satisfies $\nabla_\nu \xi_\mu = (1/2)\nabla_\alpha \xi^\alpha g_{\mu\nu}$), then some components of the null vector, but not the timelike vector, are easily found, because the contraction $\xi_\mu k^\mu$ is constant along the geodesic. In the Tolman metric, the Killing vectors of spherical symmetry immediately give the θ and ϕ components of the null vector. The r and t components can only be found if a conformal Killing vector is assumed to exist in the r - t plane. For an investigation of the redshift properties of the big bang, this approach is not general enough. In the next section a series expansion of k^μ , valid only in the vicinity of Σ_0 , is used. While this does not give a complete solution, it does give the limiting behaviour of k^μ , which is all that is needed. Though a series expansion does not cover all conceivable possibilities, it is certainly valid for a much wider class of solutions than the assumption of a conformal Killing vector allows.

3.2 Expansions of the tangent vectors near Σ_0

It is now assumed that, near Σ_0 , the t and r components of the tangent vectors can be expanded as series in powers of R , with coefficients that are functions of r only, in analogy with the expansions of \dot{R} and R' in eqs (2.15) and (2.16):

$$k^t = \sum_{i=1}^{\infty} A_i R^{\alpha_i} , \quad k^r = \sum_{i=1}^{\infty} B_i R^{\beta_i} , \quad (3.14)$$

where $A_i = A_i(r)$ and $B_i = B_i(r)$ are finite and non zero, and $\alpha_1 < \alpha_2 < \dots$, and $\beta_1 < \beta_2 < \dots$.

Though equations (2.15) and (2.16) are valid for any small R , eqs (3.14) are only required to be valid in the limit as $R \rightarrow 0$. Since the series for \dot{R} and R' contain only half and whole powers of R , the α 's and β 's are also expected to be multiples of $1/2$, as indeed is found. These expansions will then be applied to the geodesic equation, (3.13), and it is required that the equations be satisfied by the coefficients of each power of R separately. In fact just the leading terms will be retained, as only the limiting behaviour near Σ_0 is of interest.

Some functions, such as $\ln(R)$ and $\exp(1/R)$, while diverging at $R = 0$, cannot be approximated by any power law in the limit. It is possible, then, that k^t and k^r behave like these functions, but it is not very likely when \dot{R} and R' show no such behaviour, and these are the only other R -dependent functions in eq (3.13).

3.3 Calculation of the tangent vectors

Because only the leading terms in R are being kept, several different cases have to be considered separately. In particular, the leading term in equation (2.16) is different in the two cases $a' = 0$, and $a' \neq 0$; and eq (3.13) is sensitive to whether or not $h = 0$. Since the approach is essentially the same for each case, the calculations will be presented for the $a' \neq 0$ case only and all the results will be tabulated in the next section.

When $a' \neq 0$, the leading terms in \dot{R} , R' , and k^r (eqs (2.15), (2.16), and (3.14)) are

$$\dot{R} = \sqrt{\frac{F}{R}}, \quad R' = -a' \sqrt{\frac{F}{R}}, \quad \text{and} \quad k^r = BR^\beta, \quad (3.15)$$

where the subscript "1" on B and β has been dropped. Combining these with eq (3.13) leads to

$$\left(\frac{a'^2 FB^2}{y^2} R^{2\beta-1} - \epsilon + h^2 R^{-2} \right) \left[\partial_t \left(\frac{2a'^2 FB}{y^2} R^{\beta-1} \right) \right]^2 = \left[\partial_r \left(h^2 R^{-2} + \frac{a'^2 FB^2}{y^2} R^{2\beta-1} \right) \right]^2, \quad (3.16)$$

and evaluation of the derivatives, using equations (3.15), gives

$$\left(\frac{a'^2 FB^2}{y^2} R^{2\beta-1} - \epsilon + h^2 R^{-2} \right) \left[\frac{2a'^2 F^{3/2} B(\beta-1)}{y^2} R^{\beta-5/2} \right]^2 = \left[2h^2 a' F^{1/2} R^{-7/2} - \frac{a'^3 F^{3/2} B(2\beta-1)}{y^2} R^{2\beta-5/2} \right]^2,$$

which simplifies to

$$\left(\frac{a'^2 FB^2}{y^2} R^{2\beta-1} - \epsilon + h^2 R^{-2} \right) \left[\frac{2a' FB(\beta-1)}{y^2} R^\beta \right]^2 = \left[2h^2 R^{-1} - \frac{a'^2 FB(2\beta-1)}{y^2} R^{2\beta} \right]^2. \quad (3.17)$$

It may appear that, when $\beta = 1$, the leading term given in eq (3.17) for the time derivative in eq (3.16) does not exist. However, the time derivative in the earlier eq (3.13) is in fact the sum of two terms,

$$\partial_t \left(\frac{2R'^2 k^r}{y^2} \right) \equiv \frac{2}{y^2} \left[R'^2 \partial_r(k^r) + 2R' k^r \partial_t(R') \right]$$

both of the same order in R . This form of eq (3.13) also leads to eq (3.17) when the expressions (3.15) are applied, but $\beta = 1$ now indicates the two terms cancel exactly.

Consider first the case when $h = 0$, that of radial motion. Eq (3.17) simplifies to

$$\left(\frac{a'^2 FB^2}{y^2} R^{2\beta-1} - \epsilon \right) (\beta-1)^2 = \left[\frac{a' B(2\beta-1)}{2} R^\beta \right]^2. \quad (3.18)$$

Now if $\epsilon = 0$, the lowest power of R on the left hand side is $2\beta - 1$, while the lowest on the right is 2β . The requirement that the coefficients of $R^{2\beta-1}$ satisfy eq (3.18) yields

$$\frac{a'^2 FB^2(\beta-1)^2}{y^2} = 0. \quad (3.19)$$

Neither of the functions $B(r)$ or $F(r)$ is zero in general, and $a' = 0$ is not yet being considered, so the only possibility is that $\beta = 1$. Next take $\epsilon = -1$. If $\beta < 1/2$, the leading term in (3.18) does not contain ϵ , so eq (3.19) is obtained once again, and this cannot be satisfied for $\beta < 1/2$. Even if $\beta \geq 1/2$, the power of R on the right is always higher than that on the left. In these cases the lowest power is always R^0 , and the coefficient equations become

$$\left(\frac{a'^2 FB^2}{y^2} + 1 \right) \left(-\frac{1}{2} \right)^2 = 0,$$

when $\beta = 1/2$, which cannot be satisfied for any real value of B , or

$$(\beta - 1)^2 = 0 ,$$

when $\beta > 1/2$, and here again the result is $\beta = 1$.

Turn now to the case of non radial motion, $h \neq 0$. In eq (3.17), the term $h^2 R^{-2}$ is always of lower order than ϵ , so the asymptotic forms of k^r for the timelike and null vectors must be identical. Set $\epsilon = 0$. Suppose $\beta < -1/2$, then the lowest power in eq (3.17) is $4\beta - 1$ on the left hand side, and the coefficient equation is again (3.19), which does not allow $\beta < -1/2$. If $\beta = -1/2$, the lowest power is R^{-3} on the left and the coefficient equation,

$$\left(\frac{a'^2 F B^2}{y^2} + h^2 \right) \left[\frac{2a' F B (\beta - 1)}{y^2} \right]^2 = 0 ,$$

cannot be satisfied. Lastly, if $\beta > -1/2$, then eq (3.17) becomes

$$(h^2 R^{-2}) \left[\frac{2a' F B (\beta - 1)}{y^2} R^\beta \right]^2 = 4h^4 R^{-2} .$$

Clearly $\beta = 0$ is the only possibility, and this leads to

$$B = \pm \frac{h y^2}{a' F} . \quad (3.20)$$

There must of course be a constant of integration in the solution to eq (3.6). In the $h = 0$ case, the function $B(r)$ contains this constant and so is not determined, while in the $h \neq 0$ case, $B(r)$ is fully determined, so the constant must appear in higher order terms.

In summary, when $a' \neq 0$, it has been found that the leading term of the r component of the geodesic tangent vector is independent of whether $\epsilon = 0$ or -1 , and is given by

$$h = 0 : \quad k^r = B(r) R , \quad (3.21)$$

and

$$h \neq 0 : \quad k^r = \pm \frac{h y^2}{a' F} , \quad (3.22)$$

for the radial and non radial cases respectively.

The leading terms of k^t are easily found by applying eqs (3.14) and (3.15) to (3.11) as follows:

$$A^2 R^{2\alpha} = \frac{a'^2 F B^2}{y^2} R^{2\beta-1} + \frac{h^2}{R^2} - \epsilon ; \quad (3.23)$$

and the results, eqs (3.21) and (3.22), can then be inserted. Since both k^r and k^ϕ may be of either sign, it makes sense to choose only the positive root of eq (3.23), so that k^t is future oriented:

$$h = 0, \epsilon = 0 : \quad k^t = \left| \frac{a' B}{y} \sqrt{F R} \right| ; \quad (3.24)$$

$$h = 0, \epsilon = -1 : \quad k^t = 1 ; \quad (3.25)$$

$$h \neq 0 : \quad k^t = \left| \frac{h}{R} \left(1 + \frac{R y^2}{2F} \right) \right| . \quad (3.26)$$

The two terms given in eq (3.26) are required because, when the redshift is calculated for $h \neq 0$, the leading terms exactly cancel. Fortunately, this does not require a higher order calculation of k^r .

The argument for the case when $a' = 0$ (whether at a point or for all r) is similar, except that the expression for R' in eq (3.15) is replaced by $R' = F'R/3F$.

3.4 Shell crossing surfaces

The calculation of the tangent vectors near Σ_1 , where $R' = 0$, will only be outlined, as the method is quite similar to that given above. It is assumed that eq (2.25), which holds for $R' = 0$ identically, is also the dominant relationship between \dot{R}' and R'' near Σ_1 , and it is further assumed that, near Σ_1 , the geodesic tangent vectors can be written

$$k^t = \sum_{i=1}^{\infty} C_i R'^{\gamma_i} , \quad k^r = \sum_{i=1}^{\infty} D_i R'^{\delta_i} , \quad (3.27)$$

with the same conditions as for (3.14). Only the case when $R \neq 0$ is considered, since the case with both $R' = 0$ and $R = 0$ occurs when $a' = 0$ and $R = 0$, and has already been dealt with. Thus \dot{R} , \dot{R}' , and R'' are also finite. So now eq (3.13) becomes, to lowest order in R' ,

$$\left(\frac{D^2 R'^{2\delta+2}}{y^2} + \frac{h^2}{R^2} - \epsilon \right) \left[\partial_t \left(\frac{2D R'^{\delta+2}}{y^2} \right) \right]^2 = \left[\partial_r \left(\frac{D^2 R'^{2\delta+2}}{y^2} + \frac{h^2}{R^2} \right) \right]^2 , \quad (3.28)$$

and evaluating the derivatives gives

$$\left(\frac{D^2}{y^2} R'^{2\delta+2} + \frac{h^2}{R^2} - \epsilon \right) \left[\frac{2D(\delta+2)\dot{R}'}{y^2} R'^{\delta+1} \right]^2 = \left[\frac{D^2}{y^2} \left(\frac{2D'}{D} - \frac{2y'}{F} \right) R'^{2\delta+2} - \frac{D^2(2\delta+2)b'\dot{R}'}{y^2} R'^{2\delta+1} - \frac{2h^2}{R^3} R' \right]^2 . \quad (3.29)$$

To solve the lowest order equation, each of the cases $\delta < -1$, $\delta = -1$, $-1 < \delta < 0$, $\delta = 0$, and $\delta > 0$ is tried separately. The only viable solution is $\delta = -1$. (The case $\delta = 0$ leads to the condition

$$D = \sqrt{\frac{h^2}{b'^2 R^2} - \frac{\epsilon}{b'^2}} \pm \sqrt{\frac{h^2}{b'^2 R^2} - \frac{\epsilon}{b'^2} + \frac{h^2 y^2}{2b' \dot{R}' R^3}} ,$$

which is not acceptable since the second root becomes imaginary when b'/\dot{R}' is large and negative.) Thus for any h ,

$$k^r = \frac{D}{R'} \quad (3.30)$$

and, from eq (3.11),

$$k^t = \sqrt{\frac{D^2}{y^2} + \frac{h^2}{R^2} - \epsilon} . \quad (3.31)$$

3.5 General results for the redshift

In this section, v_e^μ will be used for the timelike tangent vectors of the emitters once again, and k^μ will be kept for the null tangent vectors (light rays). The subscript e indicates parameters belonging to v_e^μ , and n indicates those belonging to k^μ . In the calculations above it was assumed that both the emitter and the light ray lie in the plane $\theta = \pi/2$. In general, however, there will be an angle ψ between the planes of the two orbits. So the null orbit is taken to lie in the $\theta = \pi/2$ plane and the

emitter's tangent vector is given a rotation, remembering that the emitter must be instantaneously at $\theta = \pi/2$ to emit a light ray in that plane. Thus (3.8) is replaced by

$$v_e^\theta = \frac{h_e \sin \psi}{R^2}, v_e^\phi = \frac{h_e \cos \psi}{R^2}, \quad (3.32)$$

the other components remaining unchanged. The modulus sign will be dropped because v_e^μ will be contracted with k^μ , and it is possible to specify both h_e and h_n to be positive, choosing $\cos \psi$ to be negative when the emitter and the light ray are revolving in opposite directions. The limiting behaviour of the null and timelike geodesic tangent vectors is given in table 1. For the sake of brevity

$$\omega = \frac{F'}{3Fy} \quad (3.33)$$

has been used.

TABLE 1. Limiting behaviour of the null and time-like vectors near Σ_0

Case	Leading terms in k^μ	Leading terms in v_e^μ
$a' \neq 0$, $h \neq 0$	$k^t = \frac{h_n}{R} \left(1 + \frac{Ry^2}{2F}\right)$ $k^r = \pm \frac{h_n y^2}{a'F}$ $k^\phi = \frac{h_n}{R^2}$	$v_e^t = \frac{h_e}{R} \left(1 + \frac{Ry^2}{2F}\right)$ $v_e^r = \pm \frac{h_e y^2}{a'F}$ $v_e^\phi = \frac{h_e \cos \psi}{R^2}$
$a' \neq 0$, $h = 0$	$k^t = \left \frac{a' B_n}{y} \sqrt{FR} \right $ $k^r = B_n R$	$v_e^t = 1$ $v_e^r = B_e R$
$a' = 0$, $h \neq 0$	$k^t = \frac{1}{R} \sqrt{\omega^2 B_n^2 + h_n^2}$ $k^r = \frac{B_n}{R^2}$ $k^\phi = \frac{h_n}{R^2}$	$v_e^t = \frac{1}{R} \sqrt{\omega^2 B_e^2 + h_e^2}$ $v_e^r = \frac{B_e}{R^2}$ $v_e^\phi = \pm \frac{h_e \cos \psi}{R^2}$
$a' = 0$, $h = 0$	$k^t = \frac{1}{R} \omega B_n $ $k^r = \frac{B_n}{R^2}$	$v_e^t = \frac{1}{R} \omega B_e $ $v_e^r = \frac{B_e}{R^2}$

Note that the lowest order solutions for $a' = 0$ become exact for the Robertson-walker case. (For the $a' = 0$, $h \neq 0$ case, there appears to be a second solution with $k^r \propto R^{-3/2}$ and $A^2 = h^2$. This solution is rejected because, although it also appears in the series analysis of the dust Robertson-Walker case to lowest order, it does not satisfy the higher order coefficient equations.)

The last step in finding the redshift is the calculation of the contraction $\chi_e (= g_{\mu\nu} k^\mu v_e^\nu)$. Since χ_o in equation (3.1) is assumed finite, the redshift, z , obeys

$$(1+z) \propto \chi_e. \quad (3.34)$$

The results are summarised in table 2 for comoving emitters [$v_e^\mu \equiv (1, 0, 0, 0)$], and in table 3 for general geodesic emitters. The fact that χ_e becomes zero (or infinite) as $R \rightarrow 0$ does not mean that the emitted frequency is infinite (or zero), but that the observed frequency is zero (or infinite). Both χ_e and χ_o are expected to be negative.

TABLE 2. Limiting behaviour of χ_e for comoving emitters, and the resulting redshift from Σ_0

Case	Leading terms in χ_e	Behaviour of $(1+z)$
$a' \neq 0,$ $h_n = 0$	$-\left \frac{a'B_n}{y}\sqrt{FR}\right $	$\rightarrow 0$
$a' \neq 0,$ $h_n \neq 0$	$-\frac{h_n}{R}$	$\rightarrow \infty$
$a' = 0,$ $h_n = 0$	$-\frac{ \omega B_n }{R}$	$\rightarrow \infty$
$a' = 0,$ $h_n \neq 0$	$-\frac{1}{R}\sqrt{\omega^2 B_n^2 + h_n^2}$	$\rightarrow \infty$

It is clear from table 2 that, with comoving emitters, the models with $a' = 0$ everywhere have well behaved (i.e. infinite) redshifts, while those with $a' \neq 0$ in general have divergent energy fluxes in the radial direction. The situation is basically the same when the emitting particles are geodesic, except that finite redshifts occur along those rays emitted in the direction of the particle's motion (the forward direction), as they do in the Robertson-walker case (beginning of this chapter). The cases which include forward rays are noted in table 3, and the last term in each of the expressions for χ_e in these cases was obtained by combining equations (3.7) and (3.1) with the known behaviour of k^r .

Such an infinite blueshift along radial rays has been calculated for a particular $a(r)$ by Szekeres (1980), and for the self similar Tolman model by Dyer (1979). It should be emphasised that, unlike the the case of the past Schwarzschild singularity, this is not a forward ray effect. It occurs along radial rays from radial emitters only, and even occurs for comoving emitters, which do not approach light speed near Σ_0 .

Lastly, the redshift near Σ_1 can be given for all cases by a single expression:

$$\chi_e = -\sqrt{\left(\frac{D_n^2}{y^2} + \frac{h_n^2}{R^2}\right)\left(\frac{D_e^2}{y^2} + \frac{h_e^2}{R^2} + 1\right)} + \frac{D_n D_e}{y^2} + \frac{h_n h_e \cos \psi}{R^2}, \quad (3.35)$$

and this is always finite. So, although ρ and K both diverge on Σ_1 , its redshift behaviour is quite regular.

3.6 Discussion

The principal result of this investigation is as follows. The requirement of no infinite blueshift from the big bang is only satisfied if the bang time, $a(r)$, is constant everywhere, i.e. if the bang is

simultaneous. The stronger requirement, of only infinite redshifts, does not result in a stronger condition than $a' = 0$ if one considers only comoving emitters. The finite redshifts that do appear along forward rays from non comoving emitters appear also in the Robertson-Walker case. Since they only occur along a single direction from each emitting particle, they do not yield a finite amount of energy to be received by later observers, so cosmic censorship is not violated in this case either, and $a' = 0$ will still suffice. Therefore the stronger redshift requirement is unnecessary.

TABLE 3. Limiting behaviour of χ_e for geodesic emitters, and the resulting redshift from Σ_0

Case	Leading terms in χ_e	Behaviour of $(1+z)$
$a' \neq 0,$ $h_e = 0,$ $h_n = 0$	$-\left \frac{a'B_n}{y}\sqrt{FR}\right $	$\rightarrow 0$
$a' \neq 0,$ $h_e = 0,$ $h_n \neq 0$	$-\frac{h_n}{R}$	$\rightarrow \infty$
$a' \neq 0,$ $h_e \neq 0,$ $h_n = 0$	$-h_e\left \frac{a'B_n}{y}\sqrt{\frac{F}{R}}\right $	$\rightarrow \infty$
$a' \neq 0,$ $h_e \neq 0,$ $h_n \neq 0$	$-\frac{h_e h_n}{R^2}(1 - \cos \psi) - \frac{h_e h_n y^2}{R}(1 \pm 1) - \frac{h_n}{2h_e}$	$\rightarrow \infty^*$
$a' = 0,$ $h_e = 0,$ $h_n = 0$	$-\frac{\omega^2}{R^2}(B_n B_e - B_n B_e) - \omega^2 \left \frac{B_n}{B_e}\right $	$\rightarrow \infty^*$
$a' = 0,$ $h_e = 0,$ $h_n \neq 0$	$-\frac{1}{R^2} \left(\omega^2 B_e \sqrt{B_n^2 + \frac{h_n^2}{\omega^2}} - \omega^2 B_e B_n \right)$	$\rightarrow \infty$
$a' = 0,$ $h_e \neq 0,$ $h_n = 0$	$-\frac{1}{R^2} \left(\omega^2 B_n \sqrt{B_e^2 + \frac{h_e^2}{\omega^2}} - \omega^2 B_n B_e \right)$	$\rightarrow \infty$
$a' = 0,$ $h_e \neq 0,$ $h_n \neq 0$	$-\frac{1}{R^2} \left[\sqrt{(\omega^2 B_e^2 + h_e^2)(\omega^2 B_n^2 + h_n^2)} - \omega^2 B_n B_e - h_e h_n \cos \psi \right] - \frac{h_n}{2h_e}$	$\rightarrow \infty^*$

* Except along the forward rays, see the text.

This result, that $a' = 0$, leads to three further conclusions: (a) It is this very condition which eliminates decaying mode fluctuations in the Tolman metric (which cause divergences in the density contrast and the curvature contrast on Σ_0), leaving only the growing modes (Silk 1977). (b) Furthermore, in the classification scheme of the velocity dominated singularities of irrotational comoving

dust metrics given by Eardley, Liang, and Sachs (1972), Σ_0 is a $[2/3, 2/3, 2/3]$, or Friedmann-like, singularity if $a' = 0$, and it is a $[2/3, 2/3, -1/3]$, or Heckmann-Schucking-like, singularity otherwise. (Σ_1 is a $[0, 0, 1]$ singularity.) The three numbers are the powers of $(t - a)$ that dominate the behaviour of the metric components along three perpendicular spacelike directions, the third one being the radial direction in this case. Clearly the condition $a = \text{const}$ is a significant one. (c) It has been shown by Bonnor (1974) that all parabolic Tolman models approach homogeneity at late times, and that a class of hyperbolic models also become asymptotically homogeneous. The only models which satisfy both $a' = 0$ everywhere, and the condition of asymptotic homogeneity are the flat and open dust Robertson-Walker models. For the elliptic model, the nearest equivalent of the asymptotic homogeneity condition is that the crunch time be simultaneous. Then once again only the Robertson-Walker model satisfies both conditions. However, the homogeneity condition is concerned with the observed homogeneity of the universe and is therefore only applicable on the very large scale, whereas $a' = 0$ applies on all scales. Since there are only growing modes in $a' = 0$ models, it is concluded that, in the context of the Tolman models, the universe is homogeneous at all times on very large scales, while the bang time is constant on all scales (above the Planck length). Thus the Robertson-Walker model is the only good large scale model.

Chapter 4

SURFACE LAYERS AND REGULAR EXTREMA

Although none of the material presented here is original, it seems appropriate to review it before continuing. A surface layer occurs if there is a discontinuity in the physical properties of a spacetime on some three dimensional hypersurface, Σ , but the metric components are not badly behaved there. In fact, part of one spacetime may be joined to another with a surface layer at the junction between them (Israel 1966). Neither the bang nor shell crossing surfaces, Σ_0 and Σ_1 , qualify as the location of a surface layer, as the metric is badly behaved at both of them, however another difference between these two singular surfaces may be seen by examining the surface stresses. The former has a divergent surface stress, while the latter does not.

4.1 Surface layers

The procedure for calculating a surface layer in spherical symmetry was detailed recently by Lake (1984b). Consider a timelike or spacelike spherically symmetric hypersurface, Σ , separating two manifolds, V^+ and V^- , where V^+ has a Tolman metric, (2.1), and V^- has some spherically symmetric metric, in which r is everywhere a spacelike coordinate. The intrinsic metric of Σ is

$$ds^2 = -\epsilon d\tau^2 + R^2(\tau)d\Omega^2, \quad (4.1)$$

where $\epsilon = +1$ for timelike surfaces, and -1 for spacelike surfaces. Suppose Σ follows the path

$$r = r(\tau), \quad t = t(\tau), \quad t^{*2} = \frac{R'^2}{1+f} r^{*2} + \epsilon, \quad (4.2)$$

where $*$ $\equiv \partial/\partial\tau$. The unit normal to the surface is

$$n_\alpha \equiv \kappa \frac{R'}{\sqrt{1+f}} \left(-r^*, t^*, 0, 0 \right), \quad n_\alpha n^\alpha = \epsilon \quad (4.3)$$

where $\kappa = \pm 1$, chosen so that n_α always points towards r increasing i.e. $n_r > 0$. (If $n_r = 0$, then $n_t > 0$ can be chosen.) Thus $\kappa = +1$ where $R' > 0$, and -1 where $R' < 0$. The extrinsic curvature, or second fundamental form of the surface is defined by

$$K_{ij} = n_{\alpha;\beta} e_i^\alpha e_j^\beta, \quad (4.4)$$

where e_i^α are the base vectors of the surface expressed in the coordinates of the enveloping manifold. Specifically,

$$e_\tau^t = \dot{t}^* , \quad e_\tau^r = \dot{r}^* , \quad e_\theta^\theta = 1 , \quad e_\phi^\phi = 1 . \quad (4.5)$$

Equations (4.3), (4.4) and (4.5) give the extrinsic curvature as

$$K_{\theta\theta} = \kappa \left[-R \left(C \dot{R} \dot{r}^* + \frac{1}{C} R' \dot{t}^* \right) \right] , \quad (4.6)$$

$$K_{\phi\phi} = K_{\theta\theta} \sin^2 \theta , \quad (4.7)$$

$$K_{\tau\tau} = \kappa \left[2C \left(\dot{r}^* \dot{t}^* - \dot{t}^* \dot{r}^* \right) + \left(2\dot{C} \dot{t}^* \dot{r}^* + C' \dot{t}^* \dot{r}^* - C^2 \dot{C} \dot{r}^* \right) \right] , \quad (4.8)$$

where $C = R' / \sqrt{(1+f)}$. Now if there is a jump in the values of K_{ij} across the surface Σ such that

$$\gamma_{ij} = K_{ij}^+ - K_{ij}^- \neq 0 , \quad (4.9)$$

then Σ is a surface layer whose surface stress energy tensor is defined by

$$8\pi S_{ij} = \epsilon (\gamma g_{ij} - \gamma_{ij}) , \quad (4.10)$$

where g_{ij} is the intrinsic metric tensor of Σ , given by eq (4.1), and $\gamma = g^{ij} \gamma_{ij}$ (Israel 1966). The surface density, σ , is defined by the eigenvalue equation

$$S_{ij} u^i = -\sigma u_j ,$$

and yields the surface mass, M , of the shell

$$M = 4\pi R^2 \sigma = -\epsilon \gamma_{\theta\theta} . \quad (4.11)$$

If the surface is ideal, i.e.

$$S_{ij} = \epsilon (\sigma + P) u_i u_j + P g_{ij} ,$$

then the surface tension, $-P$, is given by

$$8\pi R^2 (-P) = R^2 \gamma_{\tau\tau} - \epsilon \gamma_{\theta\theta} . \quad (4.12)$$

If all components of γ_{ij} are zero, then there is no surface stress, and Σ is called a boundary surface, since the discontinuity across Σ is of higher order.

It is clear from eqs (4.6) to (4.8) that K_{ij} is finite even on a shell crossing surface ($R' = C\sqrt{(1+f)} = 0$), so that the surface mass, the surface density and the surface tension are finite for any reasonable interior, V^- , as they are when Σ is not a shell crossing (Lake 1984a). However, since the density diverges as $R' = 0$ is approached, shell crossings are not merely surface layers, and this construction cannot make them well behaved.

For the bang or crunch surfaces Σ is spacelike, $\epsilon = -1$, and follows $t = a(r)$, so that, in the limit as $R \rightarrow 0$,

$$\dot{r}^* = \left(C^2 - a'^2 \right)^{-1/2} \quad (4.13)$$

$$\dot{t}^* = a' \dot{r}^* \quad (4.14)$$

and, using eqs (2.26), it follows that

$$K_{\theta\theta} = \kappa \left[\frac{-R}{(C^2 - a'^2)^{1/2}} \left(C \dot{R} + \frac{R a'}{C} \right) \right] , \quad (4.15)$$

and

$$K_{\tau\tau} = \kappa \left[-2Ca'' + 2\dot{C}a'^2 + C'a' - C^2\dot{C} \right] \frac{1}{(C^2 - a'^2)^{3/2}} . \quad (4.16)$$

These can be evaluated using the approximate forms for $R \rightarrow 0$, of eqs (2.15) and (2.16) and their radial derivatives. In all cases (4.15) becomes

$$K_{\theta\theta} = -\kappa\sqrt{FR} , \quad (4.17)$$

whereas (4.16), for $a' \neq 0$, becomes

$$K_{\tau\tau} = \frac{\kappa}{2}\sqrt{\frac{F}{R^3}} , \quad (4.18)$$

while for $a' = 0$, $a'' \neq 0$, it is

$$K_{\tau\tau} = -\kappa \frac{18F^2(1+f)a''}{R^2F'^2} , \quad (4.19)$$

and for $a' = 0$, $a'' = 0$, it is

$$K_{\tau\tau} = -\kappa\sqrt{\frac{F}{R^3}} . \quad (4.20)$$

In all cases, though, $K_{\theta\theta}$ goes to zero on Σ_0 , and $K_{\tau\tau}$ diverges. If it is possible to match an interior to Σ_0 at all, it is obvious that the only way that a divergent surface stress could be avoided is for V^- to have a similar singularity here. Otherwise it is clear from (4.11) and (4.12) that all the surface stresses diverge on Σ_0 .

Rather than dealing with surface stresses in the above, which involve the introduction of another metric and which are therefore not manifestly properties of the metric being considered, it could merely be pointed out that the second fundamental form diverges at one surface, and not at the other.

4.2 Regular extrema

A regular extremum (or point of inflection) in R along constant time slices may occur without causing a shell crossing, provided ρ does not diverge, as was made clear by Zel'dovich and Grishchuk (1984). By eq (2.7), this implies

$$F' = 0 \quad (4.21)$$

wherever $R' = 0$, and also that the surface $R' = 0$ remains at fixed r , say r_m . Consider eq (2.13) at r_m . Since the coefficients of a' and f' are different functions of time, then

$$a' = 0 \quad (4.22)$$

and

$$f' = 0 \quad (4.23)$$

must also obtain at r_m . Thus the condition for a regular extremum in $R(r, t)$ is that equations (4.21), (4.22), and (4.23) all hold at the same r . However, the extrinsic curvature shows a jump in its $\theta\theta$ component here. For a timelike surface following $r = \text{const}$, the proper time derivatives are

$$\overset{*}{r} = 0 , \quad \overset{**}{r} = 0 , \quad \overset{*}{t} = 1 , \quad \overset{**}{t} = 0 , \quad (4.24)$$

so that the extrinsic curvature becomes

$$K_{\tau\tau} = 0 , \quad K_{\theta\theta} = -\kappa R \sqrt{1+f} . \quad (4.25)$$

If the surface is a regular maximum, then R' changes sign across it, and so κ changes sign. This means there is at this radius a surface layer with mass

$$M = 2R\sqrt{1+f}, \quad (4.26)$$

and whose equation of state is

$$\sigma = 2P \quad (4.27)$$

(Bonnor 1984). Only if $f = -1$ is there no surface layer. Despite this, F , ρ , and $g_{\alpha\beta}$ are all continuous and finite through the layer, so the metric is well behaved in every other way. Thus this layer is quite acceptable and is no different from the surface layers that have been used to study the development of voids in the galaxy distribution recently (e.g. Lake and Pim 1985). For a regular minimum the surface layer has a negative mass, while an inflection point does not have a surface layer. In this last case, a coordinate transformation can be found which removes the inflection point in at least one of the arbitrary functions, and therefore in R .

Chapter 5

THE CONDITIONS FOR NO SHELL CROSSINGS

In this chapter, the necessary and sufficient conditions which ensure that no shell crossings will occur in Tolman models will be derived. The argument will consider only the case $t \geq a$. The argument and results for $t \leq a$ are easily found by replacing $t - a$ with $a - t$, and a' with $-a'$. Shell crossings were defined in chapter 2 to be surfaces on which $R' = 0$, and where the density, ρ , diverges. If $R' = 0$ but the density is finite, then there is no shell crossing, just a regular extremum. The conditions for each type of time evolution will be considered separately.

5.1 Elliptic regions, $f < 0$

The method used here is somewhat different from the one used previously (Hellaby and Lake 1985), because a fault in that version was pointed out recently by Bonnor, but the results and conclusions remain unchanged. The radial derivative of R may be written as

$$\frac{R'}{R} = \frac{F'}{F} (1 - \phi_1) + \frac{f'}{f} \left(\frac{3}{2} \phi_1 - 1 \right) - \frac{2(-f)^{3/2} a'}{F} \phi_2 \quad (5.1)$$

where

$$\phi_1(\eta) = \frac{\sin \eta (\eta - \sin \eta)}{(1 - \cos \eta)^2}, \quad (5.2)$$

and

$$\phi_2(\eta) = \frac{\sin \eta}{(1 - \cos \eta)^2}. \quad (5.3)$$

The functions ϕ_1 and ϕ_2 are shown in fig 1 (page 31). For $R' > 0$, it is clear from eq (2.7) that

$$F' \geq 0 \quad (5.4)$$

is required for positive density. Consider the evolution of eq (5.1) with time, i.e. as η goes from 0 to 2π . At early times ($\eta \rightarrow 0$), ϕ_2 dominates, going to $+\infty$, so

$$a' \leq 0 \quad (5.5)$$

is required for $R' > 0$. At late times ($\eta \rightarrow 2\pi$), $\phi_1 \rightarrow 2\pi\phi_2$, meaning eq (5.1) becomes

$$\frac{R'}{R} = \left[-2\pi \left(\frac{F'}{F} - \frac{3f'}{2f} \right) - \frac{2(-f)^{3/2} a'}{F} \right] \phi_2, \quad (5.6)$$

with ϕ_2 going to $-\infty$, so that the third condition for $R' > 0$ is found to be

$$a' \geq \frac{-\pi F}{(-f)^{3/2}} \left(\frac{F'}{F} - \frac{3f'}{2f} \right). \quad (5.7)$$

Of course, conditions (5.4), (5.5), and (5.7) also imply

$$\frac{F'}{F} \geq \frac{3f'}{2f}. \quad (5.8)$$

To demonstrate the sufficiency of these three conditions, the functions α , β , and ϕ_3 are defined as follows:

$$\left(\frac{F'}{F} - \frac{f'}{f} \right) = \alpha(r) \left(\frac{F'}{F} - \frac{3f'}{2f} \right), \quad (5.9)$$

$$\left(\frac{F'}{F} - \frac{3f'}{2f} \right) = -\beta(r) \frac{2(-f)^{3/2} a'}{F}, \quad (5.10)$$

$$\phi_3 = \frac{-\phi_2}{\alpha - \phi_1}. \quad (5.11)$$

Examples of the function ϕ_3 are plotted in fig 1 (page 31) for $\alpha = 2/3$, and in fig 2 (page 31) for $\alpha = 0.1, 0$, and -0.3 . For all $\alpha < 2/3$, ϕ_3 has no upper limit, whereas for $\alpha \geq 2/3$, ϕ_3 never exceeds $1/2\pi$ (at $\eta = 2\pi$). With these, eq (5.1) takes the form

$$\frac{R'}{R} = \frac{-2(-f)^{3/2} a'}{F} (\beta - \phi_3)(\alpha - \phi_1) \quad (5.12)$$

and conditions (5.4) and (5.7) become

$$\alpha \geq \frac{2}{3}, \quad \text{and} \quad \beta \geq \frac{1}{2\pi}, \quad (5.13)$$

while (5.5) remains the same. It is then obvious from (5.5), (5.13) and the figures that R' is always positive in eq (5.12). The converse of these conditions must hold for $R' < 0$. If both $F' = 0$ and $f' = 0$, then $a' = 0$ follows from (5.5) and (5.7), so $R' = 0$. Conditions (5.4) and (5.5) have an obvious meaning, and (5.7) ensures the crunch time increases with r , wherever R' is positive. Thus (5.5) and (5.7) together ensure that $q' > 0$, and therefore $p' > 0$, i.e. the time from bang to crunch and the radius of maximum expansion, defined in eq (2.12), both increase with R .

5.2 Hyperbolic regions, $f > 0$

It is a bit easier to derive the conditions for no shell crossings in this case. From eq (2.3), the radial derivative of R is given by

$$\frac{R'}{R} = \frac{F'}{F} (1 - \phi_4) + \frac{f'}{f} \left(\frac{3}{2} \phi_4 - 1 \right) - \frac{2f^{3/2} a'}{F} \phi_5, \quad (5.14)$$

where

$$\phi_4 = \frac{\sinh \eta (\sinh \eta - \eta)}{(\cosh \eta - 1)^2}, \quad (5.15)$$

and

$$\phi_5 = \frac{\sinh \eta}{(\cosh \eta - 1)^2}. \quad (5.16)$$

The functions $\phi_4(\eta)$ and $\phi_5(\eta)$ are shown in fig 3 (page 32). Again consider the evolution of eq (5.1) as η goes from 0 to ∞ . At early times (small η), ϕ_5 dominates, going to $+\infty$, so

$$a' \leq 0 \quad (5.17)$$

is once more required for $R' > 0$. At late times $\phi_5 \rightarrow 0$, and $(1 - \phi_4) \rightarrow 0$, so $(3\phi_4/2 - 1)$ dominates, requiring

$$f' \geq 0. \quad (5.18)$$

As before the positivity of the density implies

$$F' \geq 0. \quad (5.19)$$

Since $2/3 \leq \phi_4 \leq 1$, it is obvious that conditions (5.17), (5.18), and (5.19) are sufficient as well as necessary. The converse of these conditions holds for $R' < 0$.

An interesting feature of the conditions for elliptic regions is that, unlike the hyperbolic case, $f' \leq 0$ is not required for $R' > 0$. It was shown in chapter 2 that eq (2.4) gives the early time behaviour of all models and eq (2.6) gives the late time behaviour of hyperbolic models. Thus in hyperbolic models, f is not important at early times, but at late times the shells of matter sort themselves in order of increasing f , so, where f is not an increasing function of r , a shell crossing will sooner or later develop. Of course the effect of the function f increases with time in elliptic models also, but, since the lifetime of the models is finite (except where $f \rightarrow 0$), it is possible for f' to be positive. Indeed, if f is negative and f' positive, condition (5.7) is easier to satisfy, so that the transition zone from an elliptic region towards a hyperbolic or parabolic region is not hard to construct.

5.3 Parabolic regions, $f = 0$

The boundary between an elliptic and a hyperbolic region deserves special consideration since the parameter η is not valid there. Eq (2.14) for the radial derivative of R is

$$\frac{R'}{R} = \frac{F'}{3F} - \frac{2a'}{3(t-a)} + \frac{3f'}{10} \left[\frac{2(t-a)^2}{3F^2} \right]^{1/3} + O(f), \quad (5.20)$$

and, since the coefficients of F' , f' , and a' are all different functions of t , it is evident that the conditions for no shell crossings are the same in this case as for hyperbolic regions. For an extended parabolic region $f' = 0$, but otherwise the same conditions obtain here also.

Incidentally, it can now be verified that the density remains finite at a regular maximum, r_m , provided there are no shell crossings in the vicinity. Eq (2.13), with conditions (5.17) - (5.19), or (5.4), (5.5), and (5.7), shows that R' cannot approach zero faster than F' does, so eq (2.7) must remain finite.

5.4 The origin

There are a few restrictions on the arbitrary functions near the origin that are implied by the requirement of no shell crossings.

It was shown in chapter 2 that the requirement of a regular origin, where the density is finite and the type of time evolution does not change, implies eq (2.18), given (2.17). If $s > 2/3$, then the behaviour becomes parabolic at the origin. This is quite acceptable in a hyperbolic model, but in an elliptic model it means that the time from bang to crunch must be decreasing as R increases, since there is no crunch surface in the parabolic case. This is not allowed if shell crossings are to be avoided.

On the other hand, $s < 2/3$ causes no problems in elliptic models, as there is nothing wrong with the time from bang to crunch going to zero at the origin, and the explosive evolution that results in hyperbolic models does not cause shell crossings either, a result which is perhaps surprising at first.

Turning now to the shape of the bang surface near the origin, it is clear from conditions (5.5) and (5.17), that $a' \rightarrow +\infty$ is not possible at all at the origin, though $a' \rightarrow -\infty$ is acceptable. For the same reason, $a \rightarrow -\infty$ at the origin is not allowed. In hyperbolic and parabolic models, $a \rightarrow +\infty$ is possible, but in elliptic models, since the time of the crunch increases outwards, $a \rightarrow +\infty$ implies that the time from bang to crunch is infinite at finite F , meaning f is zero. Since f is necessarily zero at the origin, the model is completely parabolic. Clearly, a must be finite at the origin in elliptic models.

5.5 Other formulations

When the Tolman metric is being used to make realistic models of density fluctuations, it often makes more sense to give the arbitrary functions in terms of the variation of physical properties along some initial spacelike surface at some time t_0 , where $t_0 > a$ everywhere in the region of interest. Bondi (1947) chooses the functions $R(r, t_0(r))$, $\dot{R}(r, t_0(r))$, and either $M(r)$ or $\rho(r, t_0(r))$, while Tolman (1934) sets t_0 constant, and specifies ω , $\dot{\omega}$, and $\ddot{\omega}$, where $e^\omega = R^2$.

It turns out that the conditions for no shell crossings in terms of these quantities are not at all simple. The most important reason is that the quantity \dot{R}' is normally negative near the bang, becoming positive at later times. The procedure to check whether the conditions are satisfied for the choice of $R_0(r)$, $\dot{R}_0(r)$, and $M(r)$ along a surface of constant t_0 is as follows.

Firstly, because t is constant along the surface the partial radial derivative is also the total derivative along the surface, which affords a considerable simplification. Thus, it can easily be checked that $M' \geq 0$ everywhere that $R'_0 > 0$. Next, $f(r)$ is found from

$$f = \dot{R}_0^2 - \frac{F}{R_0} \quad (5.21)$$

and f' can be compared with R'_0 . Thirdly, $a(r)$ is found from

$$a = t_0 - \frac{F}{2f^{3/2}} \left[\frac{2fR}{F} \sqrt{1 + \frac{F}{fR}} - \cosh^{-1} \left(\frac{2fR}{F} + 1 \right) \right], \quad (5.22)$$

and then differentiated. Since the derivative could be quite long, and since it contains the function \cosh^{-1} , it would be very tedious to check that $a' \geq 0$ everywhere that $R' > 0$.

In fact, the case given above is one of the easier ones. If ρ is given at t_0 instead of M , then an integration is needed to get M , and if the initial surface, $t_0(r)$, is not constant, then there are extra terms to convert the derivative from total to partial. Therefore, if it is important that the model contain no shell crossings, it may well be easier to play with the functions F , f , and a , in order to

obtain the desired parameters at t_0 . In practice, a shell crossing to the past of the initial surface may not be of concern. If so, the easiest way around the problem, is to choose a parabolic or hyperbolic model and specify $\dot{R}' > 0$ everywhere on the initial surface, as this will not eliminate many viable futures. For the elliptic model, it is not so simple in general, but there is one nice possibility, which is to specify R and M along the surface of maximum expansion, $\dot{R} = 0$. The function q (eq (2.12)) is found from

$$q(r) = \frac{R^3(r, t_0(r))}{2M(r)}, \quad (5.23)$$

and the bang and crunch times are

$$a(r) = t_0(r) - \frac{\pi}{2}q(r), \quad \text{and} \quad \tilde{a}(r) = t_0(r) + \frac{\pi}{2}q(r) \quad (5.24)$$

so it is straightforward to compare M' , a' , and \tilde{a}' with R' . If shell crossings at early times do not matter, then the calculation of a' may be omitted. The restriction of choosing the parameters at the point of maximum expansion need not always be a large problem. For example, if the model is to start at time $t_1 = \text{const}$, with a central region that is expanding more slowly than the surrounding background, then $(t_0 - t_1)$ should be chosen to be smaller in the central region. However, t_1 should not be too early, otherwise the central region may be expanding faster than the background.

5.6 Discussion

It is quite common in the literature (e.g. Hellaby and Lake 1984; Landau and Lifshitz 1975, footnote p 317) to see the conditions for no shell crossings given as $R' > 0$, $F' > 0$. These are actually too restrictive, and they exclude the regular maxima that must occur in closed models with well behaved coordinate systems. (The usual Robertson-Walker coordinates of eq (3.2) are defective at $r = 1$ in closed models.) As far as I know, Zel'dovich and Grishchuk are the first to have explicitly pointed out that, in a closed model, both R' and F' must be negative near one of the origins.

The conditions derived here, and summarised in table 4, are not particularly restrictive; there is just one upper or lower bound on the gradient of each arbitrary function at each point. The examples of Tolman models given in the next chapter are all free of shell crossings.

The considerations of this chapter were motivated by a recent paper by Zel'dovich and Grishchuk (1984). However, the conclusions arrived at here are different.

First, the initial condition they have chosen at time t_0 , which results in their equation (5), is perhaps too restrictive. As they say, wherever $R'(r, t_0) = 0$ (r_m , say), this condition requires

$$f(r_m) = -1, \quad (5.25)$$

but this will only be true if surface layers are disallowed, which they do not say. Since the function $f(r)$ must obey eq (2.11), eq (5.21) also implies

$$f'(r_m) = 0. \quad (5.26)$$

Zel'dovich and Grishchuk naturally specify that the density is everywhere finite at t_0 , so eq (2.7) further implies

$$F'(r_m) = 0. \quad (5.27)$$

Then, by putting eqs (5.22) and (5.23) in (2.13), it follows that

$$a'(r_m) = 0 \quad (5.28)$$

is also required at r_m . While eqs (5.22) to (5.24) are all necessary for a regular extremum in R , (5.21) is not. Eqs (5.22) to (5.24) also ensure that $R'(r_m, t) = 0$ at all times, and (5.21) ensures that recollapse occurs at r_m , which is the result they obtain in their paper. Specific counter examples to their hypothesis will be given in chapter 6.

To obtain a model with neither surface layers nor shell crossings, however, condition (5.21) is required, so that the surface mass is zero at r_m . It then follows from table 1 that models which include a hyperbolic or parabolic section cannot be closed. This can be seen by noting that, at the boundary between an elliptic and a hyperbolic region, where $f = 0$, the areal radius, R , must be increasing in the direction of the hyperbolic region. Thus, there may be an origin on the elliptic side, but no maximum in R is allowed on the hyperbolic side, so there can be no second origin. The same is true for the boundary between an elliptic and a parabolic region.

TABLE 4. The conditions for no shell crossings.

These are the necessary and sufficient conditions for the Tolman models which have $t \geq a$. The conditions for the case $t \leq a$ are obtained by replacing a' with $-a'$ below.

$f \geq 0$	$f < 0$
$R' > 0$	
$a' \leq 0$	$a' \leq 0$
$f' \leq 0$	$a' \geq \frac{-\pi F}{(-f)^{3/2}} \left(\frac{F'}{F} - \frac{3f'}{2f} \right)$
$F' \geq 0$	$F' \geq 0$
but no more than two equalities at once	but not both $F' = 0$ and $f' = 0$ at once
$R' = 0$	
$a' = 0$	$a' = 0$
$f' = 0$	$f' = 0$
$F' = 0$	$F' = 0$
$R' < 0$	
$a' \geq 0$	$a' \geq 0$
$f' \leq 0$	$a' \leq \frac{-\pi F}{(-f)^{3/2}} \left(\frac{F'}{F} - \frac{3f'}{2f} \right)$
$F' \leq 0$	$F' \leq 0$
but no more than two equalities at once	but not both $F' = 0$ and $f' = 0$ at once

5.7 Figures

Fig 1. The behaviour of the functions $\phi_1(\eta)$, $\phi_2(\eta)$, and $\phi_3(\eta, \alpha = 2/3)$, defined by eqs (5.2), (5.3), and (5.11). For all values of $\alpha \geq 2/3$, ϕ_3 is similar to the curve shown, and, in particular, the upper limit is always $1/2\pi$.

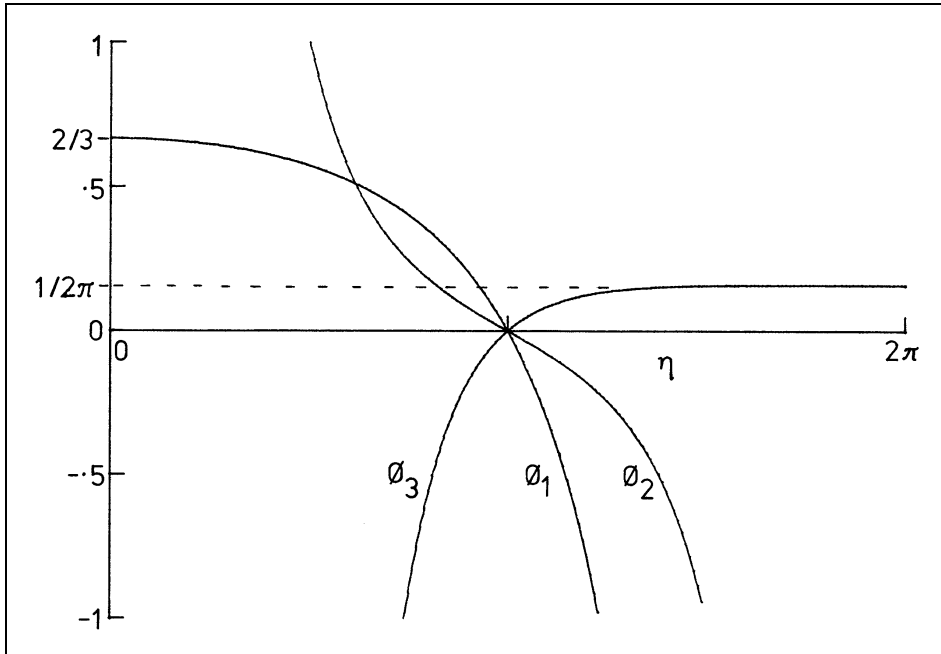


Fig. 1

Fig 2. The function $\phi_3(\eta, \alpha)$ has three possible forms other than the one shown in Fig 1, but none of them have a finite upper limit. The sample curves shown here are labelled by their values of α .

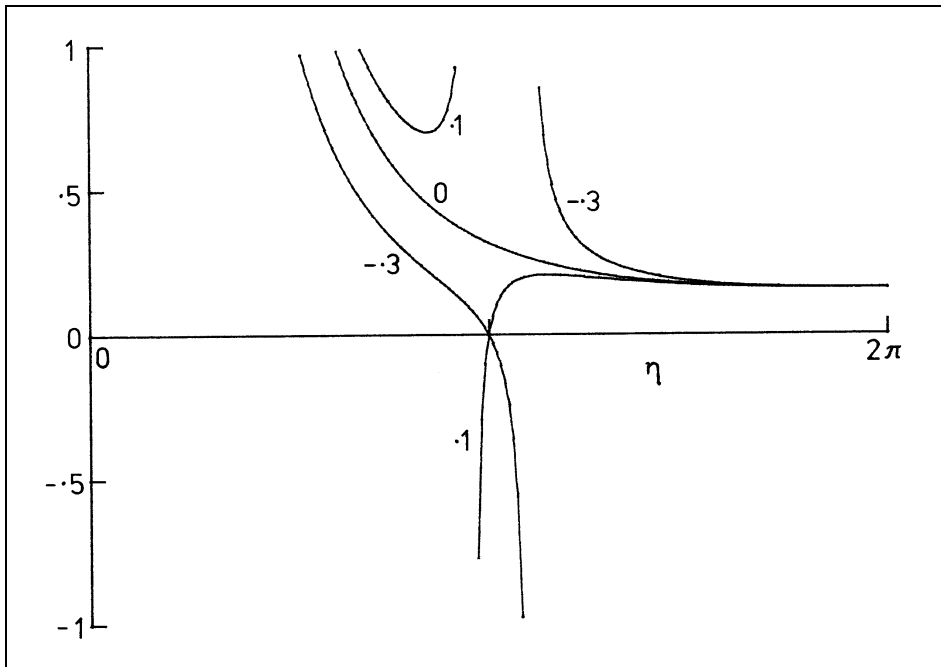


Fig. 2

Fig 3. The behaviour of the functions $\phi_4(\eta)$ and $\phi_5(\eta)$, defined in eqs (5.15) and (5.16).

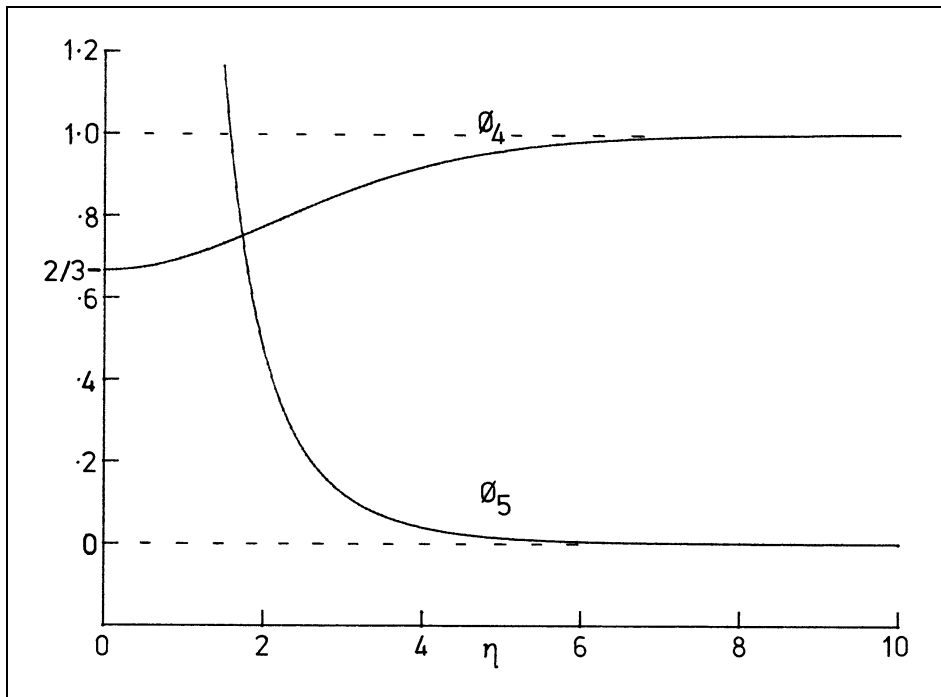


Fig. 3

Chapter 6

SOME EXAMPLES

In this chapter a few specific Tolman models will be presented and discussed. Each one illustrates a particular point.

6.1 A closed hyperbolic model

For the first example, the three arbitrary Tolman functions are chosen to be

$$F = F_0 \gamma^m , \quad (6.1a)$$

$$f = f_0 \gamma^n , \quad (6.1b)$$

$$a = -a_0 \gamma^i , \quad (6.1c)$$

where $\gamma = \gamma(r)$ is a positive function of r that goes to zero at $r = 0$, and m , n , and i are all positive, as are F_0 , f_0 , and a_0 . Such models are hyperbolic, with no shell crossings, but regularity at the origin would require $2m = 3n$. If, for example,

$$\gamma(r) = 3 \sin\left(\frac{\pi r}{\lambda}\right) + 2 \sin\left(\frac{3\pi r}{\lambda}\right) , \quad (6.2)$$

is specified, then for fixed t , $R(r, t)$ has two maxima and one minimum, and it has a second origin at $r = \lambda$, where $R(\lambda, t) = 0$. In other words, the model is closed, though everywhere hyperbolic. As shown in chapter 4, there must be surface layers at these extrema.

6.2 An open elliptic model

The choice of arbitrary functions for the second example is

$$F = \frac{F_0 r^m}{1 + br^n} , \quad (6.3a)$$

$$f = \frac{-f_0 r^n}{1 + br^n} , \quad (6.3b)$$

$$a = -a_0 r^i \sqrt{1 + br^n} , \quad (6.3c)$$

$$(6.3d)$$

where the constants m, n, i, F_0, f_0 , and a_0 are all positive, and the conditions

$$a_0 \leq \frac{\pi F_0}{f_0^{3/2}} \quad \text{and} \quad 2i = 2m - 3n \quad (6.4)$$

ensure no shell crossings will form. Also $2m = 3n$ would give a regular origin. In this case there is only one origin, and the constant $t, \theta = \pi/2$ sections become conical at large r , so the space is elliptic, yet open. The original version of this example was defective, since it was not actually free of shell crossings. This was pointed out by Bonnor, who also gave a valid example (Bonnor 1985).

6.3 A closed hybrid model

The three functions are next defined by

$$F = F_0 r^3 (\lambda - r)^3, \quad (6.5a)$$

$$f = f_0 (br^3 - r^2) [b(\lambda - r)^3 - (\lambda - r)^2], \quad (6.5b)$$

$$a = a_0 (r^2 - \lambda r), \quad (6.5c)$$

where a_0, F_0, f_0 , and λ are all greater than zero, and $b > 2/\lambda$. The condition $f \geq -1$ puts an upper limit on f_0 in terms of b and λ , which is very long but not very instructive. It is clear that equations (6.5) cause no shell crossings in the hyperbolic region, and in the elliptic regions it is near the origins that the conditions for no shell crossings are hardest to satisfy. For small r , condition (5.7) gives

$$\frac{(b\lambda - 1)^{5/2}}{b^2} \leq \frac{3\pi F_0}{2a_0 f_0^{3/2}}. \quad (6.6)$$

The model then has no shell crossings and consists of a hyperbolic region between two elliptic regions, each of which contains a regular origin (at $r = 0$, and $r = \lambda$). As above, the maximum at $r = \lambda/2$ has a surface layer. There is no hyperbolic region if $b \leq 2/\lambda$. The evolution of the function $R(r, t)$ is shown in fig 4 (page 35) for $a_0 = 5, f_0 = 1, F_0 = 1, b = 3$, and $\lambda = 1$. This example demonstrates that a closed Tolman model, containing both hyperbolic and elliptic regions, need not recollapse. Since no shell crossings form, the hyperbolic region remains and expands indefinitely. This violates Zel'dovich and Grishchuk's hypothesis that a closed hybrid model inevitably develops shell crossings which lead to the eventual recollapse of the model.

6.4 A model with no origin

The last choice of arbitrary functions is

$$f = -1 + B^2 \exp\left(\frac{2r}{r_0}\right), \quad (6.7a)$$

$$F = A^3 \left(1 + C \exp\left[\frac{r}{r_0}\right]\right)^3, \quad (6.7b)$$

$$a = 0, \quad (6.7c)$$

where A, B, C , and r_0 are all positive. In this model the whole space emerges from the bang simultaneously, and without an origin. As $r \rightarrow -\infty$, the constant $t, \theta = \pi/2$ sections become

cylinders, while in the other direction, the space has a fairly normal structure. At $r = -r_0 \ln(B)$ the model changes from elliptic to hyperbolic evolution, so at late times there is a singular origin whose mass increases asymptotically to the limiting value of $A^3(1 + C/B)^3$, while the rest of the space continues to expand indefinitely. There are no shell crossings.

6.5 Figure

Fig 4. The evolution of the function $R(r, t)$ for the metric functions given in section 6(c), with $a_0 = 5$, $f_0 = 1$, $F_0 = 1$, $b = 3$, and $\lambda = 1$. Successive curves, receding into the page, are the functions $R(r)$ at successively later times. Before the bang, and after the crunch, R has been set to zero. The divisions between the central hyperbolic region and the two elliptic regions are marked along each curve.

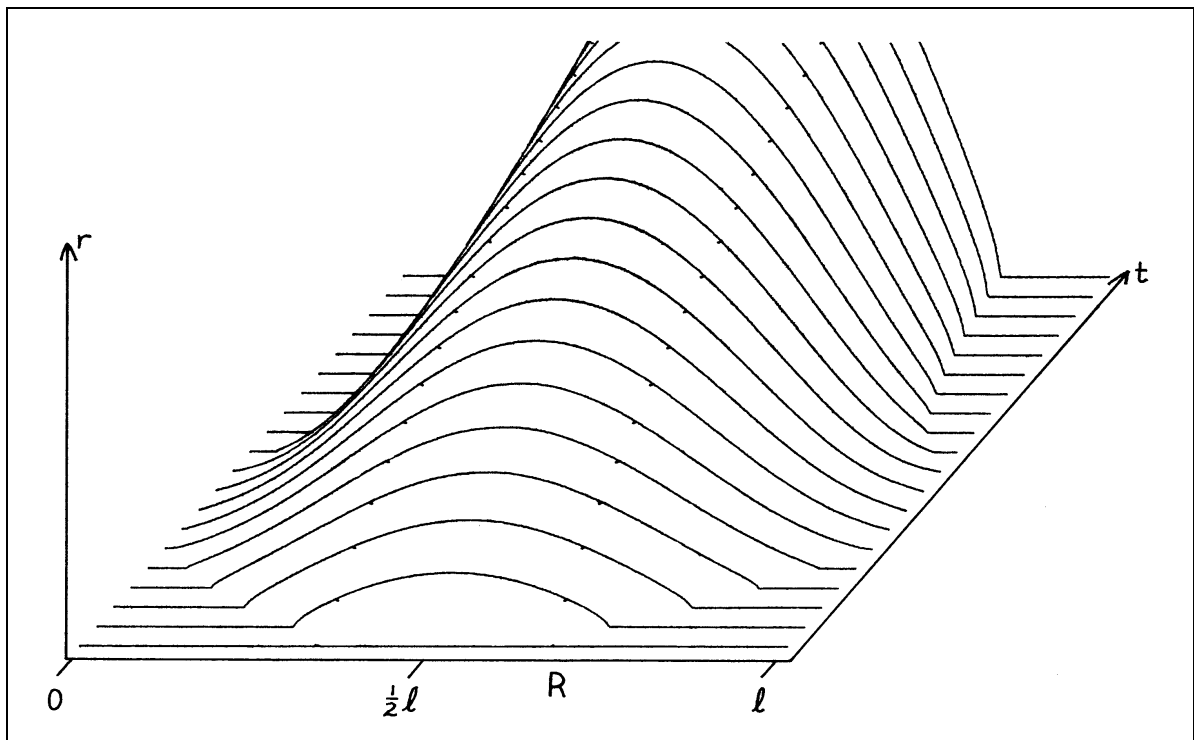


Fig. 4

Chapter 7

THE E.S.C. SINGULARITY

Last summer, a very interesting violation of cosmic censorship was published by Christodoulou (1984). In outline, he took a spherically symmetric dust cloud of finite size, and allowed it to collapse. The exterior was described by the Schwarzschild vacuum, while the interior consisted of an elliptic Tolman model, whose arbitrary functions were chosen such that the cloud was initially at rest, and the density fell to zero at the surface of the cloud. Further, he imposed a strong continuity condition at the origin, which is important for the proof, but seems entirely reasonable. Specifically, the condition was that the density must be an even, C^∞ function of r , even when r is carried through zero to negative values. Obviously the intent was to ensure that there is nothing irregular about the origin in the initial conditions. In this model, the crunch singularity occurs first at the centre of symmetry, $r = 0$, and spreads to increasing radius with time, thus ensuring that the model is free of shell crossings. The crunch singularity joins to the future singularity of the exterior Schwarzschild manifold, and the apparent horizon, defined as the locus of points where the expansion of the wave fronts of radial light rays is zero, joins to the Schwarzschild event horizon. Christodoulou then showed that, for a certain class of models, the first ray to emerge from that initial point on the singularity, could reach the exterior of the cloud a finite time before the cloud entered the horizon, and escape to infinity, thus constituting a global violation of cosmic censorship. (A ray is said to emerge from a singularity if its path can be traced back to arbitrarily small affine distances from that singularity.)

This singularity was first discovered in a study of numerical relativity conducted by Eardley and Smarr (1978). The primary aim of the paper was to investigate ways of slicing the spacetime to obtain the best coverage by the numerical grid, whilst avoiding the singularity. Their model was also a dust cloud surrounded by vacuum, but the interior was a parabolic Tolman metric, and they calculated a large variety of cases to compare their results with the known analytic solutions. They too found that, in models where this singularity existed, light could be propagated from the initial singular point, and could in some cases reach future null infinity. The three conformal diagrams they drew for these spacetimes are reproduced in fig 5 (page 7.8), and they show respectively no violation of cosmic censorship, a local violation, and a global violation.

I have chosen to call this central point on the crunch surface, together with its effects, the ESC singularity, after its discoverers, though Eardley and Smarr named it a shell focussing singularity. In their paper they comment that this singularity “has hitherto escaped notice in these models for 40 years”, and they find it “surprising that these phenomena occur in the family of Tolman-Bondi spacetimes, which are thought to be well understood”. In fact, this singularity had not received any more attention until Christodoulou’s paper came along, and even he was not aware of their work until the referee drew his attention to it. Perhaps one reason is that Eardley and Smarr give no explanation of this singularity, other than tabulating which types of model it occurs in, nor do they say how they

came across it, or derived the conditions for its existence. In the analytical treatment, the existence of rays emerging from this singularity does not become apparent without carefully examining the geodesic equation. Since no general solution is known, even for the radial null geodesics, this has not been easy to do.

And indeed the existence of this singularity is surprising, especially since the crunch surface is spacelike, as was shown in chapter 2. However, more careful examination of the arguments shows that this result is not valid when both r and η are small simultaneously. The results of chapter 3 also become doubtful at the origin, since it was assumed that the functions $A_i(r)$ and $B_i(r)$ are non zero, and this may not be valid here. In fact, Christodoulou calculated a discontinuity in the redshift observed at infinity.

The ESC singularity is investigated in this chapter, with the aim of making it clearer what is happening physically, and in particular, a conformal diagram is calculated. The emphasis is on the behaviour of the Tolman model near the ESC singularity, and the question of whether the violation of cosmic censorship is local or global in a Schwarzschild exterior is not of great concern here. Only some of the cases of interest have been covered, and so the conclusions are only tentative.

7.1 The light rays

In this case, it is the crunch surface that is of interest, so the region $t < a$ is used. (One merely has to substitute $(a - t)$ for $(t - a)$, and $-a'$ for a' in all the equations of preceding chapters.) Also, since all the unexpected behaviour happens near the crunch surface, i.e. when η is small, it is sufficient to use a parabolic Tolman model, as the other types (elliptic and hyperbolic) have the same behaviour here. Thirdly, it is assumed that the density is not zero anywhere in the neighbourhood of the origin, so that one may choose the radial coordinate by specifying

$$F = r^3 . \quad (7.1)$$

Thus the evolution of the function R is given by

$$R = \frac{rg^2}{4} , \quad (7.2)$$

where

$$g = [12(a - t)]^{1/3} \quad (7.3)$$

so that

$$\dot{R} = -\frac{2r}{g} , \quad (7.4)$$

and

$$R' = \frac{g^2}{4} + \frac{2ra'}{g} . \quad (7.5)$$

From the metric, eq (2.1), the radial null geodesics obey

$$\frac{dt}{dr} = \varepsilon R' = \varepsilon \left(\frac{g^2}{4} + \frac{2ra'}{g} \right) , \quad (7.6)$$

where $\varepsilon = +1$ for outgoing rays, and -1 for incoming rays. This can be converted to an equation in g as the "time" variable using (7.3),

$$g^3 g' = 4ga' - \varepsilon(g^3 + 8a'r) . \quad (7.7)$$

It is now necessary to choose a form for the function $a(r)$. Christodoulou chose it to be a series in even, positive powers of r , in order to fulfil his continuity condition, i.e.

$$a = a_0 + a_1 r^2 + a_2 r^4 + \dots .$$

He found that the violation only occurred if a_1 , the coefficient of r^2 , was non zero. Consequently, the form

$$a = a_0 + a_1 r^m , \quad m > 0 , \quad a_1 > 0 , \quad (7.8)$$

is chosen so that cases with and without a violation can be studied, as well as other values of m , not considered by him. (If a_1 were less than 0, there would be shell crossings.) This is the form assumed by Eardley and Smarr, though they used only integer values of m . (Their r is not quite the same, since they defined r by $M = F/2 = r^3$.) The higher order terms are not important for this investigation, and are omitted here. With this choice, eq (7.7) becomes

$$g^3 g' = 4m a_1 g r^{m-1} - \varepsilon (g^3 + 8m a_1 r^m) . \quad (7.9)$$

The constant a_1 may be removed by the transformations

$$s = \frac{r}{a_1^w} , \quad q = \frac{g}{a_1^w} , \quad (7.10)$$

which lead to

$$q^3 q' = 4m a_1^{w(m-3)+1} q s^{m-1} - \varepsilon (q^3 + 8m a_1^{w(m-3)+1} s^m) .$$

Here the dash indicates the derivative with respect to s , but since q is always a function of s , and g is always a function of r , no confusion will arise. By setting $w = 1/(3-m)$, the factors of a_1 can be eliminated for all cases except $m = 3$ (which is the self similar parabolic Tolman model), viz:

$$q^3 q' = 4m q s^{m-1} - \varepsilon (q^3 + 8m s^m) . \quad (7.11)$$

For most cases, then, the paths of the radial light rays do not depend on the value of a_1 , except as a scaling factor.

Firstly the case studied by Christodoulou will be considered, i.e. $m = 2$. Eq (7.11) becomes

$$q^3 q' = 8q s - \varepsilon (q^3 + 16s^2) , \quad (7.12)$$

but even in this form there is no obvious solution, nor is it listed by Kamke (1944). As a first indication of the behaviour of this equation, the gradient, q' , is plotted in the q - s plane as an array of inclined line segments, in fig 6 (page 7.8). This figure uses the convention that incoming rays are plotted on the left side of the origin, with negative s values, and outgoing rays are on the right side with positive s values. The diagram may be thought of as a slice through the origin, showing only the left to right rays, and it makes clear the fact that light rays do in fact pass through the origin. This convention will be maintained for all the ray diagrams. From the figure it does appear that there are indeed rays that emerge from the origin. In order to find the behaviour for small s and small q , series expansions will once more be resorted to. If there is a ray that passes through the origin at $q = 0$, then, for s sufficiently close to zero, it is assumed to follow

$$q = \sum_{i=1}^{\infty} q_i s^{n_i} , \quad (7.13)$$

where $q_i > 0$, $n_i > 0$, and $n_{i+1} > n_i$ for all i . The first term of this series is inserted into eq (7.12),

$$n q_1 s^{4n_1-1} = 8 q_1 s^{n_1+1} - \varepsilon (q_1^3 s^{3n_1} + 16s^2) , \quad (7.14)$$

and the coefficients of the lowest powers are required to cancel. There are only two values of n which allow this to be done: (i) $n_1 = 2/3$, $q_1 = 12^{1/3}$, and (ii) $n_1 = 1$, $q_1 = 2\varepsilon$. Both of these may be extended to higher order. The most practical way to do this is to repeat the calculation for each higher power in turn, because if more than one extra term in the series is considered at once, it becomes hard to know how many terms to keep in the calculation, as the powers are not determined. At each stage the solution is found by requiring that $n_i > n_{i-1}$, and that the coefficient equation be consistent with previous results. There is always just one case each time that satisfies these requirements. The results are:

$$(i) \quad q = q_I v^2 - \varepsilon v^3 - \frac{q_I^2}{16} v^4 - \frac{4\varepsilon q_I}{27} v^5 + \dots, \quad (7.15)$$

where $v = s^{1/3}$ and $q_I = 12^{1/3}$;

$$(ii) \quad q = 2\varepsilon s + 3s^2 + \frac{39\varepsilon}{2}s^3 + \frac{387}{2}s^4 + \dots. \quad (7.16)$$

In the second case, s would have to be less than about .1 for the series to converge, but otherwise there is no problem, and they both have the form one would expect from the gradient graph. Also, only the $\varepsilon = +1$ solution of eq (7.16) lies in the positive q region, so the $\varepsilon = -1$ solution for $n = 1$ will be ignored. However, neither of these two solutions has an undetermined constant of integration. One of them, probably (7.15), must be a special case, and would not have a constant, but the other does need one. Using the transformation

$$q = bs$$

to define b as a function of s along the ray, eq (7.12) becomes

$$\frac{db}{ds} = \frac{8}{b^2 s^2} - \frac{1}{s} - \frac{16}{b^3 s^2} - \frac{b}{s}.$$

Since b is finite as $s \rightarrow 0$, this is approximately

$$\frac{db}{ds} = \frac{8(b-2)}{b^3 s^2},$$

which has the solution

$$\frac{1}{3}(b-2)^3 + 3(b-2)^2 + 12(b-2) + 8 \ln(b-2) = -\frac{8}{s} + 8 \ln(C),$$

where C is the constant of integration. As $s \rightarrow 0$, the first term on the right goes to $-\infty$, meaning the last term on the left must dominate the left hand side, so that

$$b = 2 + C e^{-1/s}, \quad (7.17)$$

and $b \rightarrow 2$, as expected. Since $e^{-1/s}$ goes to zero faster than any power of s , it would not appear in a series expansion. For the same reason, it causes a sharp turn off from the series solution of (7.16) once it does become significant. Of course eq (7.17) is still only an approximation, but it does indicate how the constant of integration appears, and demonstrates that there is a whole family of rays whose limiting form near $s = 0$, $q = 0$ is eq (7.16).

Clearly, eq (7.15) with $\varepsilon = +1$ is the very first ray to escape from the singular origin, and it is the ray that Christodoulou proved to exist. It is effectively the horizon of the ESC singularity, dividing the region which can be causally affected by it from the region that cannot. I call this the "critical ray", all later ones the "post critical rays", and the point from which they emerge the "critical point".

The incoming ray which hits this point is the “incoming critical ray” because it has the form (7.15) with $\varepsilon = -1$, rather than the form that all the other incoming rays have (see (7.19) below). If eq (7.15) is put into (7.3), the lowest order term is cancelled, giving

$$t = a_0 + \left[\left(\frac{3}{2} a_1 \right)^2 r^7 \right]^{1/3} \left[1 - \left(\frac{r}{768 a_1} \right)^{1/3} \dots \right], \quad (7.18)$$

and this is the reason for the factor of $x^{7/3}$ in Christodoulou’s eq (3.37). (In that equation, $x \propto r$, and $\zeta \propto t - a_0$, while θ is being defined there.)

Before proceeding to the numerical integration, an asymptotic form for the behaviour of the rays near $q = 0$, when $s = s_0 \neq 0$, is needed, and it is found to be

$$s = s_0 - \frac{q^4}{64s_0^2} - \frac{q^5}{160s_0^3} - \frac{q^6}{384s_0^4} - \frac{q^7}{896s_0^5} \left(1 - \frac{s_0}{2} \right) \dots \quad (7.19)$$

Now that the limiting behaviour near $q = 0$ has been found, the ray paths can easily be calculated numerically. Given the form of eq (7.12), it is quite easy to find the higher derivatives of q , so a Taylor series integration is appropriate. The program starts each ray with one of the approximate expressions derived above, but completes the majority of its path numerically, setting the integration interval automatically, based on the relative sizes of the terms in the Taylor expansion. The program is listed in the appendix, and the results are shown in fig 7 (page 7.8) for s - q coordinates, on 3 different scales. The ray paths in the r - t plane are shown in fig 8 (page 7.8), assuming $a_0 = 0$ and $a_1 = 1$. The limitation on the smoothness of these curves is not the program, but the amount of data the graph plotting routine can accept.

It should be remembered that q is not the time, but the cube root of the time before the crunch, and $q = 0$ corresponds to a surface that is curving upwards in the r - t plane. So in fact the rays never go backwards in time, though they may get further away from the crunch surface (in time, or in areal radius) as they go outwards. Given this, the s - q diagram shows the various rays paths much more clearly than the r - t diagram. In all these graphs, the rays are equally spaced in s on the crunch surface. Thus the spacing of the rays at earlier times gives an idea of the expansion between the rays, in the comoving frame. It can be seen that rays which pass through the origin and become outgoing well before reaching the crunch surface experience an overall compression, while those which are always incoming and never near the origin have an overall expansion. As the incoming critical ray is approached from either side, the expansion becomes greater, but occurs later in q . In the r - t graphs the expansion seems to occur at very roughly the same time for all rays, and appears to be associated with the “bending over”, or decrease in gradient of the rays. On the other hand, rays which are distant from the incoming critical ray are not much affected by the presence of the ESC singularity.

The scaled radius where the outgoing critical ray hits the singularity once again is s_{crit} , and its value in this particular model is .2602, though this value would change if the model were not parabolic, or if there were higher terms in eq (7.8) for the shape of the crunch surface. It is the largest radius which any of the critical rays reach and is therefore the extent of the violation of cosmic censorship within the model, since nothing outside s_{crit} can be causally affected by the ESC singularity. If $M_{crit} = (a_1 s_{crit})^3 / 2$ is the total mass affected by the violation, and $t_{crit} = (a_1)^3 (s_{crit})^2$ is its duration, then the ratio $M_{crit} / t_{crit} = s_{crit} / 2$ is independent of the scale of the model. In order to produce a global violation, it is necessary to put the boundary of the cloud not just within s_{crit} , but before the outgoing critical ray crosses the apparent horizon. The apparent horizon is the locus of points where the expansion of the wave fronts of light is zero, in other words the rate of change

of the areal radius along the rays is zero, $\nabla_\alpha k^\alpha = 0$, and it is given by

$$g = 2r , \quad \text{or} \quad q = 2s , \quad (7.20)$$

for the outgoing rays. Along this locus $g' = q' = -1$. Since the asymptotic form of the post critical rays, eq (7.16), reduces to the apparent horizon at $s = 0$, it is clear that the rays all fall below this line before turning upwards and crossing it.

7.2 The conformal diagram

Having integrated the paths of the light rays, the next step is to calculate a conformal diagram. In such a diagram, the light rays are used as coordinates, so that u is constant along the left to right rays, and v is constant along the right to left rays. This means that the light rays are just two perpendicular sets of parallel straight lines, and the causal relationships are then quite obvious.

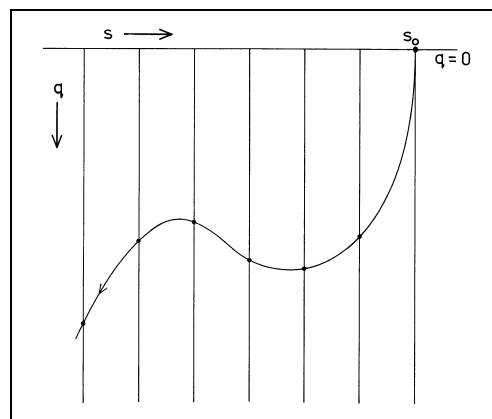
Before any calculations can be done, a method of choosing the u and v coordinates must be specified. It is normal to do this by the value of some parameter along a well defined surface. Since the latest post critical rays exist for a vanishingly short time, only surfaces which pass through the critical point parallel to the crunch surface will include them. Therefore the simplest choice is to label each ray by its value of s_0 where it hits the crunch singularity. Specifically, left to right rays, such as in fig 7, are labelled by

$$u = -s_0 , \quad (7.21)$$

and right to left rays, those in the mirror reflection of fig 7, are labelled by

$$v = s_0 . \quad (7.22)$$

The diagram is calculated numerically in the following manner. Starting with the s - q plane, a grid of lines of constant s is set up, as in the sketch below.



From the top of each grid line the light ray which hits the singularity there is selected, and labelled by its s_0 value. The ray is integrated backwards from that point, and every time it crosses a grid line the s and q values are recorded. In this way, the s - q plane is covered by a new grid of u and v values. By linear interpolation between these points, it is then possible to calculate a set of u and v values along any given curve (such as $s = \text{const}$ or $t = \text{const}$), which may be plotted in the u - v diagram. Reference to fig 7 shows that, if the incoming critical ray is approached from the left, it has to be labelled with $u = 0$, whereas if it is approached from the right, it appears to be a continuation of the outgoing critical ray, and must be labelled with $u = -s_{crit}$. Thus there is a jump in the value of u across this ray, owing to the later emergence of a whole set of rays between

these two limits. There is a similar effect for the v coordinate, and both these jumps must be written into the program. The program as it stands, is the maximum size allowed on the machine without memory management. Adding this utility would have added considerably to the time required to produce results. Up to 55 s grid lines could be used, which is less than ideal, but is enough to give a reasonably reliable picture. The program for this calculation is also given in the appendix.

Various families of curves are shown in the u - v diagram in fig 9 (page 7.8). The most noticeable feature is the central lozenge which the critical point has become, and which is singular, since ρ and K diverge there. The jumps in the u and v values have resulted in two furrows which continue out to infinity. In fact the curves are not discontinuous at these jumps but approach them smoothly, confirming that they are a real part of the u - v diagram. Nevertheless, the curves are not null in these furrows. The tangent vectors to the $s = \text{const}$ lines or the $t = \text{const}$ lines are well defined at these points. Thus the furrows are really just stretching the spacetime along two null directions, and the two sides of each furrow should be identified as the same ray. Another feature is that the $t = \text{const}$ lines tend to avoid the ESC singularity, in other words the rate of change of t with respect to u or v decreases towards the critical point, the lozenge being a single value of t and of r .

The diagrams derived here have one important difference from those drawn by Eardley and Smarr (fig 5), who have omitted the jump in the u and v values. When only half the diagram is drawn, this looks alright, but problems become apparent when it is remembered that the light rays do in fact pass through the origin, and the diagrams must allow a continuation across $r = 0$. Though the presence of these jumps may seem to be unsatisfactory, they are an inevitable feature of the u - v diagram of any spacetime in which a set of rays emerge from a single coordinate point.

Apart from these few features, the conformal diagram is not especially illuminating, and does not seem to contribute much to a physical understanding of what happens at an ESC singularity. What it does show most effectively is that the characteristics of the singularity are already beginning to appear just beforehand, since the various curves go continuously through the furrows.

7.3 The case of general m

For a better understanding of this singularity, it makes sense to compare the above results with a number of other cases, including those which do not have an ESC singularity, and any borderline case which may exist. In this section, some preliminary calculations and numerical results are presented.

As noted in the previous section, the case $m = 3$ is different from the other cases, since the factor of a_1 cannot be transformed away, so it is discussed separately. For $m \neq 3$, equation (7.11) obtains, and a first view of its behaviour is given for a range of m values in fig 10 (page 7.8), where the gradients are plotted as arrays of line segments in the s - q plane.

To find those models for which rays may emerge from a central critical point on the crunch surface, eq (7.11) may be solved to lowest order in s , using the first term in eq (7.13), and following the same procedure as above. The results are as follows.

$$\begin{aligned}
 \text{(a) } m < 3, \quad & \text{(i) } n_1 = m/3, \quad q_1 = 12^{1/3} ; \\
 & \text{(ii) } n_1 = 1, \quad q_1 = 2\varepsilon ; \\
 \text{(b) } m > 3, \quad & \text{(i) } n_1 = m/3, \quad q_1 = (-8m)^{1/3} ; \\
 & \text{(ii) } n_1 = 1, \quad q_1 = -\varepsilon .
 \end{aligned}$$

Since both s and q must be positive, those rays with $q_1 < 0$ may be ignored. Thus for the $m < 3$ cases, the $n_1 = 1$ solution only exists for $\varepsilon = +1$ (outgoing rays), as in the $m = 2$ case, while for $m > 3$, the $n_1 = 1, \varepsilon = -1$ ray is the only one to exist. Therefore there are no outgoing rays from this point in the $m > 3$ cases, so they do not have ESC singularities. This is borne out by fig 10. The series may be extended to higher order terms, as before:

(a)(i)

$$q = q_I s^{m/3} - \varepsilon s - \frac{mq_I^2}{4(6+m)} s^{2-m/3} - \frac{2\varepsilon mq_I}{27} s^{3-2m/3} \dots, \quad (7.23)$$

where $q_I = 12^{1/3}$,

(a)(ii)

$$q = 2\varepsilon s + \frac{6}{m} s^{4-m} + \frac{6\varepsilon}{m^2} (17-2m) s^{7-2m} + \frac{12}{m^3} (4m^2 - 66m + 245) s^{10-3m} \dots, \quad (7.24)$$

(b)(ii)

$$q = -\varepsilon s + q_2 s^{m-2} + q_3 s^{2m-5} + q_4 s^{3m-8} \dots, \quad (7.25)$$

where

$$q_2 = \frac{12m}{(m-2)}, \quad q_3 = \frac{384\varepsilon m^2}{(m-2)(2m-5)},$$

and

$$q_4 = \frac{192m^3(190m-443)}{(m-2)(2m-5)(3m-8)}.$$

Similarly, an expression is needed for the ray path near $q = 0$ when $s = s_0 \neq 0$. However, since there are non integer powers of s in eq (7.11), it is not suitable for a series expansion of s in powers of q . In this case, the first two terms on the right hand side may be neglected if q is small enough, and integration then leads to

$$q^4 = \frac{32\varepsilon m}{(m+1)} (s_0^{m+1} - s^{m+1}), \quad (7.26)$$

and this is sufficient for programming purposes.

The numerical integration, using the Taylor series method, has been carried out for a selection of m values less than 3. In its present form, there are numerical problems which prevent the program from working for $m < 1$, and for $m > 2.6$. For $m < 1$, the gradient is divergent at $s = 0, q \neq 0$, and so another approximate expression is needed to propagate the integration through this point. In the latter case the problem is less clear, but is most likely due to the smallness of the critical radius, and thus the smallness of the integration step required to generate accurate results. The results of these integrations are plotted in figs 11 and 12 (pages 7.8 & 7.8) for four m values, and all the graphs have been scaled so that the critical radius, s_{crit} , is at the same point in the diagram. Since the critical ray can be made to reach any desired maximum value of R by adjusting a_1 , this is the best way to compare the behaviour in each case. In fact there are no qualitative differences in behaviour between these four cases, and the only significant quantitative difference is the value of s_{crit} . One can be confident that the conformal diagrams for these cases will differ from fig 9 in equally subtle ways.

For comparison of these cases on the same scale, the outgoing critical rays are plotted on one graph for a variety of m values in fig 13 (page 7.8), while the dependence of s_{crit} on m is shown in fig 14 (page 7.8). Using the quantities M_{crit} and t_{crit} defined above, then $M_{crit}/t_{crit} = (s_{crit})^{3-m}/2$, giving s_{crit} a more direct physical meaning that is independent of a_1 . This ratio is graphed against m in fig 15 (page 7.8), and over the range that the data exists, it indicates that the ratio is approaching zero as m goes to 3. Therefore, for an ESC singularity which causes a violation of cosmic censorship

of a given duration, the amount of mass affected by the singularity decreases as m approaches 3. On the other hand, for a given affected mass, the duration of the violation increases as m goes to 3. So it is not clear whether the singularity becomes “stronger” or “weaker” towards $m = 3$. Because s_{crit} depends on the behaviour of the arbitrary metric functions away from the origin as well as near it, this is one aspect that might be made clearer by using higher terms in eq (7.8). Then it would be possible to vary the behaviour of the central singularity without much affecting the paths of the light rays at larger radii.

The adaptations of the program to integrate the $m > 3$ cases have not yet been tested properly.

7.4 The case $m = 3$

For this case, eq (7.9) must be used since the factors of a_1 cannot be removed. The gradient plots are shown in fig 16 (page 7.8) for three values of a_1 .

In fact, a further transformation of this equation with $m = 3$, casts it in separable form. Let

$$g = rb(r) , \quad (7.27)$$

then (7.9) becomes

$$b^3 b' r = -b^4 + 12a_1 b - \varepsilon b^3 - 24\varepsilon a_1 , \quad (7.28)$$

and the solution is

$$r = r_0 e^I , \quad (7.29)$$

where

$$I = \int_0^b \frac{b^3 db}{b^4 + \varepsilon b^3 - 12a_1 b + 24\varepsilon a_1} .$$

The lines of constant b are straight lines in the r - g plane, radiating from the point $r = 0, g = 0$, and they may be thought of as “angular coordinates” about that point. The integral is fairly complicated, and has to be integrated numerically anyway, so it would be much easier to do it by adapting the Taylor series method already developed, than to write a new program. However, there are some features which can be demonstrated analytically. The solution (7.29) is not valid for $r_0 = 0$, though there must be at least an incoming ray that reaches that point. There are some straight line solutions, $b' = 0$, with b given by the roots of the right hand side of eq (7.28), i.e. of

$$\Phi = b^4 + \varepsilon b^3 - 12a_1 b + 24\varepsilon a_1 = 0 . \quad (7.30)$$

There is always one root, b_1 , for the incoming rays, $\varepsilon = -1$, but for the outgoing rays, $\varepsilon = +1$, there are two roots, b_2 and b_3 , only if a_1 is large enough, otherwise there are none. The borderline case, when the two roots are degenerate, has

$$\frac{d\Phi}{db} = 4b^3 + 3\varepsilon b^2 - 12a_1 = 0 , \quad (7.31)$$

and cancelling a_1 between (7.30) and (7.31) leads to

$$b^2 - 2b - 2 , \quad (7.32)$$

which gives the solution

$$b_A = 1 + \sqrt{3} , \quad a_{1,A} = \frac{52 + 30\sqrt{3}}{12} . \quad (7.33)$$

This value of a_1 is the minimum for which any ray can emerge from the critical point, and it is in good agreement with the value calculated by Eardley (1974) and later by Eardley and Smarr. In fact, b_1 , b_2 , and b_3 are equivalent to the homothetic Killing horizons found by Eardley (1974) and by Dyer (1979). (Note that b here is the inverse of Dyer's parameter u .) Since b_A is an exact solution of (7.28), it extends out to infinity, meaning that it gets further from the crunch surface for all time. This also means that none of the earlier outgoing rays can reach the crunch surface, so that there is a future null infinity, as well as a past null infinity in this particular Tolman model. All of the later rays emerge from the critical point, and eventually hit the big crunch. If a_1 is larger than $a_{1,A}$, then there are two different roots of (7.30), so there are two straight line solutions for the paths of the light rays emerging from the critical point. Between these two rays, b_2 and b_3 , it is obvious from (7.28) that b' is positive, so the rays are moving away from b_2 (smaller b) and towards b_3 (larger b). This is also evident in fig 16(c), where the lines b_1 , b_2 , and b_3 are drawn in.

In terms of b , the gradient, g' , is

$$b^3 g' = -\varepsilon b^3 + 12a_1 b - 24\varepsilon a_1 = \Psi, \quad (7.34)$$

which shows that the gradient of the light rays is constant along lines of constant b . For $\varepsilon = -1$, g' is always positive, but for $\varepsilon = +1$, a region of negative gradient is possible between the two roots of $\Psi = 0$, b_4 and b_5 , depending on a_1 . The minimum value for which g' can go to zero is the degenerate root of $\Psi = 0$, which is found to be at

$$b_B = 3, \quad a_{1,B} = \frac{9}{4}. \quad (7.35)$$

Since $a_{1,B}$ is lower than $a_{1,A}$, there is a range of a_1 for which g' may be negative all the way up to the centre of the crunch surface, yet no rays emerge from that point. Fig 16(b) is an example of this case, and the lines b_1 , b_4 , and b_5 are marked on it.

The case which has a_1 between these two borderline values is probably the most interesting to investigate, since its conformal diagram would not contain any jump, while the lines would still display some of the bending noticed near the jump in fig 9. The case with a_1 larger than $a_{1,A}$ is not amenable to the present method of calculating the conformal diagram, since a whole set of its rays never reach the crunch surface, and so cannot be labelled by u and v in the prescribed manner. The case with a_1 less than $a_{1,B}$ appears, from fig 16(a), to behave like the $m > 3$ cases.

7.5 The orientation of the crunch surface

It was shown in chapter 2 that the bang and crunch surfaces are spacelike in the Tolman model, everywhere except possibly at the origin. The calculation is done specifically for the origin here.

The surfaces of constant $(a - t)$ have a normal vector, n_α , which is calculated from

$$n_\alpha \propto \partial_\alpha(a - t) \equiv (1, -a', 0, 0)$$

and the condition, $n_\alpha n^\alpha = \epsilon$, where $\epsilon = +1, 0$, or -1 , depending on whether the surface is timelike, null, or spacelike, respectively. It is found to be

$$n_\alpha = R' \sqrt{\frac{\epsilon}{a'^2 - R'^2}} (1, -a', 0, 0), \quad (7.36)$$

where R' is given by eq (7.5), and it is understood that the term under the square root is set to unity if $\epsilon = 0$. The tangent vector, u^α , found from $u^\alpha n_\alpha = 0$, and $u^\alpha u_\alpha = -\epsilon$, is

$$u^\alpha = \sqrt{\frac{\epsilon}{a'^2 - R'^2}} (a', 1, 0, 0) . \quad (7.37)$$

The value of ϵ is determined by the sign of $(a'^2 - R'^2)$, but, since a' must be positive, the surface is always simultaneous or outgoing in the comoving frame, in the sense that as r increases along the surface the time never decreases. If the comoving frame is badly behaved near the ESC singularity, this may not be a useful statement.

The ratio R'/a' is given by eqs (7.5) and (7.8), as

$$\frac{R'}{a'} = \frac{g^2 r^{1-m}}{4ma_1} + \frac{2r}{g} , \quad (7.38)$$

and, if its absolute value is larger than 1, the surface is spacelike, while if it is equal to or less than 1, the surface is null or timelike, respectively. Now it is necessary to approach the point $r = 0$, $g = 0$ along some definite path, since both terms of eq (7.38) are otherwise undefined at this point. Therefore, let

$$g = br^n , \quad n > 0 , \quad (7.39)$$

where b is now a constant, so that (7.38) becomes

$$\frac{R'}{a'} = \frac{b^2}{4ma_1} r^{2n-m+1} + \frac{2}{b} r^{1-n} . \quad (7.40)$$

The types of behaviour of (7.40) may be conveniently divided up as follows.

- (I). $R'/a' \rightarrow 0$, so that the surface is timelike. This is the case if $2n - m + 1 > 0$ and $1 - n > 0$, which leads to the conditions

$$m < 3 , \quad n < 1 , \quad n > \frac{m-1}{2} . \quad (7.41)$$

- (II). $R'/a' \rightarrow \text{const}$, which may give all three results for ϵ . There are three separate conditions for this case.

- (a) $2n - m + 1 = 0$ and $1 - n > 0$, which implies

$$m < 3 , \quad n < 1 , \quad n = \frac{m-1}{2} , \quad (7.42)$$

and the surface is spacelike, null, or timelike, depending on whether b is greater than, equal to, or less than $(4ma_1)^{1/2}$.

- (b) $2n - m + 1 > 0$ and $1 - n = 0$, which gives

$$m < 3 , \quad n = 1 , \quad (7.43)$$

so that if b is less than, equal to, or greater than 2, then the surface is spacelike, null or timelike.

(c) $2n - m + 1 = 0$ and $1 - n = 0$, yielding

$$m = 3, \quad n = 1. \quad (7.44)$$

In this case the surface is spacelike if

$$b^3 - 12a_1b + 24a_1 > 0,$$

and this is the Ψ of eq (7.34). Thus a spacelike surface is the only possibility if $a_1 < a_{1,B}$, but otherwise there is a range of b values between b_4 and b_5 for which the surface is timelike, or null at the ends of that range.

(III). $R'/a' \rightarrow \pm\infty$, so that the surface is spacelike. There are two possibilities here.

(a) $2n - m + 1 < 0$, in other words

$$\text{any } m, \quad n < \frac{m-1}{2}. \quad (7.45)$$

(b) $1 - n < 0$, implying

$$\text{any } m, \quad n > 1. \quad (7.46)$$

These results are summarised in a different order in table 5.

Table 5. Orientation of the crunch surface for different paths of approach to the origin.

$m < 3$	$n < 1$	$n < \frac{m-1}{2}$	spacelike
		$n = \frac{m-1}{2}$	$b^2 > 4ma_1$ spacelike
			$b^2 = 4ma_1$ null
			$b^2 < 4ma_1$ timelike
	$n > \frac{m-1}{2}$	timelike	
		$n = 1$	$b > 2$ timelike
			$b = 2$ null
			$b < 2$ spacelike
		$n > 1$	spacelike
		$m = 3$	$n < 1$
$n = 1$	$a_1 < a_{1,B}$ spacelike		
	$a_1 = a_{1,B}$		$b \neq b_B$ spacelike
			$b = b_B$ null
	$a_1 > a_{1,B}$		$b > b_4$ spacelike
			$b = b_4$ null
			$b_5 < b < b_4$ timelike
$n > 1$	$b = b_5$ null		
	$b < b_5$ spacelike		
	spacelike		
$m > 3$	spacelike		

7.6 Discussion

It is evident then, that the crunch surface is completely spacelike for $m > 3$, and also for $m = 3$ and $a_1 < a_{1,B}$. But for the other cases, there is not a definite answer. What this multiplicity of results means is not clear, though it does seem to imply more structure than was revealed by the conformal diagram. This would imply that such diagrams are not sufficient for displaying the full behaviour of the ESC singularity. The most puzzling point is that the conformal diagram shows there is an incoming null section to the ESC singularity, from which all the post critical rays emerge, while these calculations indicate that the crunch surface can only be simultaneous or outgoing. These results can only be reconciled if the comoving frame becomes incoming null at the critical point.

The conformal diagrams that were calculated have an important difference from those of Eardley and Smarr in the existence of a jump in the u and v values across the incoming critical ray, but their conditions for the presence of an ESC singularity have been borne out, and extended to the case of non integer m . Another difference is that they find the crunch surface is totally spacelike for all models that are free of an ESC singularity, whereas it was shown above that the orientation of the crunch surface becomes ill defined for values of a_1 which allow g' to become positive for outgoing rays, even though there are no critical or post critical rays present.

One thing that this investigation has not succeeded in is providing a possible physical reason for the appearance of the ESC singularity. It may be that the problem is merely one of insufficient continuity through the origin, but this would have to be demonstrated at events earlier than the big crunch. The origin of the value $m = 3$, is clearly the choice made in eq (7.1) for the form of the function $F(r)$, so the only obvious physical property that changes on either side of $m = 3$, is the rate of accumulation of mass onto the crunch surface, which is easily derived from the two arbitrary functions, a and F , as $dM/dt = F'/2a' = 3r^{3-m}/2ma_1$. Thus for $m < 3$, the initial rate of accumulation of mass onto the singularity is zero, for $m > 3$ it is divergent, and for $m = 3$ it is finite. The borderline values, $a_{1,A}$, and $a_{1,B}$, yield no special values of dM/dt , however. There probably is some significance to this point, but it needs some careful thought.

There is still plenty of work to be done before this singularity is understood. It would be useful to calculate a conformal diagram for some other cases, including a model without an ESC singularity, to show what features are always present, but particularly the $m = 3$ case with $a_{1,B} < a_1 < a_{1,A}$, mentioned above. It would also be of interest to calculate the behaviour of timelike and spacelike geodesics near ESC singularities, and it should be possible to use the approximate methods presented here. A further point to investigate is whether there is any similar behaviour near the crunch surface if a' passes through zero at points other than $r = 0$.

7.7 Note Added at Defence

As noted above, one possible cause of the ESC singularity is lack of sufficient continuity at the origin. A continuity condition can now be given which implies that this is the case. The condition is that, on some constant time slice, $t = \text{const}$, the density, ρ , expressed as a function of the mass, M , should be C^1 through the origin. In other words, as $r \rightarrow 0$,

$$\left. \frac{\partial \rho}{\partial M} \right|_t \rightarrow 0, \quad (7.47)$$

and for the model of eqs (7.1) and (7.8), this becomes

$$\left. \frac{\partial \rho}{\partial M} \right|_t = 2 \left. \frac{\partial \rho}{\partial F} \right|_t \rightarrow \frac{128ma_1(4 - 2m + m^2)}{\pi g^9 r^{3-m}} . \quad (7.48)$$

Satisfying this continuity condition obviously requires

$$m > 3 , \quad (7.49)$$

and eliminates all models containing an ESC singularity. This condition is expressed in terms of invariant physical quantities, and so is not coordinate dependent. More importantly, it applies at times prior to the crunch, including, for example, the initial conditions.

Although Christodoulou chose his r coordinate to be proportional to the proper radius near the origin, so that his continuity condition is invariant, it is apparent that the condition is not strong enough. At the origin, only the leading term in a Taylor expansion of the density is important, so it does not matter whether $\rho(r)$ is C^1 or C^∞ .

In further support of condition (7.47), it can be pointed out that it holds for any spherically symmetric distribution in Minkowski space where the density remains finite and non zero at the origin, and so should hold in the tangent space at the origin of a Riemannian space. If the density goes to zero at the origin in flat space, then $d\rho/dM \sim r^{-3}$. It is not known how the Tolman model behaves in this case. One would need to consider non parabolic models, as a parabolic model cannot have zero density at the origin unless it also contains shell crossings.

In conclusion, (7.47) is a new condition, whose usefulness may well extend beyond the Tolman model. It is important to investigate other models that violate it, for behaviour similar to the ESC singularity.

7.8 Figures

Fig 5. Reproductions of the conformal diagrams drawn by Eardley and Smarr, for a parabolic Tolman dust cloud embedded in a Schwarzschild vacuum. In all three diagrams, the shaded region is the Tolman interior, the hatched region is the fully causal domain which is unaffected by the ESC singularity, and the symbols I^+ , I^- , I^0 , \mathcal{I}^+ , and \mathcal{I}^- are respectively: future and past timelike infinities, spacelike infinity, and future and past null infinities. Diagram (a) is the case without an ESC singularity; (b) is the case with an ESC singularity where the violation of cosmic censorship is local, and the ESC horizon, H_E , (the outgoing critical ray) is inside the Schwarzschild horizon, H_S ; (c) is the case where the violation is global, and H_E is outside H_S .

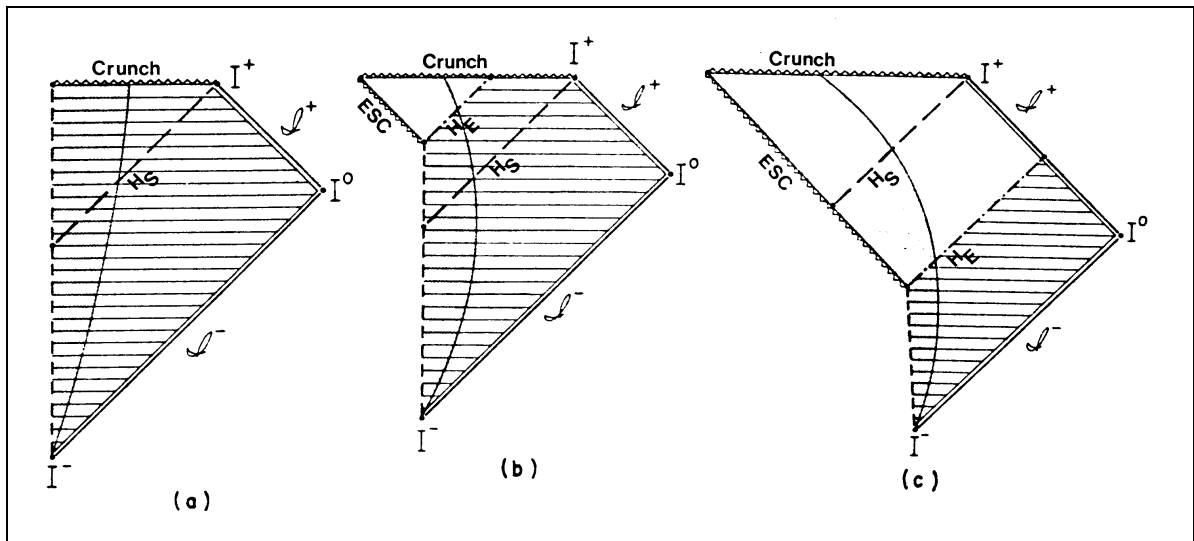


Fig. 5

Fig 6. The gradient, dq/ds , of the radial light rays in the s - q plane, as given by eq (7.12). Each of the line segments gives the direction of the light ray at its central point. Though negative s (radius) values are not strictly possible, this diagram plots incoming rays on the left of $s = 0$, and outgoing rays on the right. Since light rays do pass through $s = 0$, this gives a realistic picture of a slice through the origin, except that the right to left rays have been suppressed. All the rays go from left to right as time increases. This convention is used in all ray diagrams.

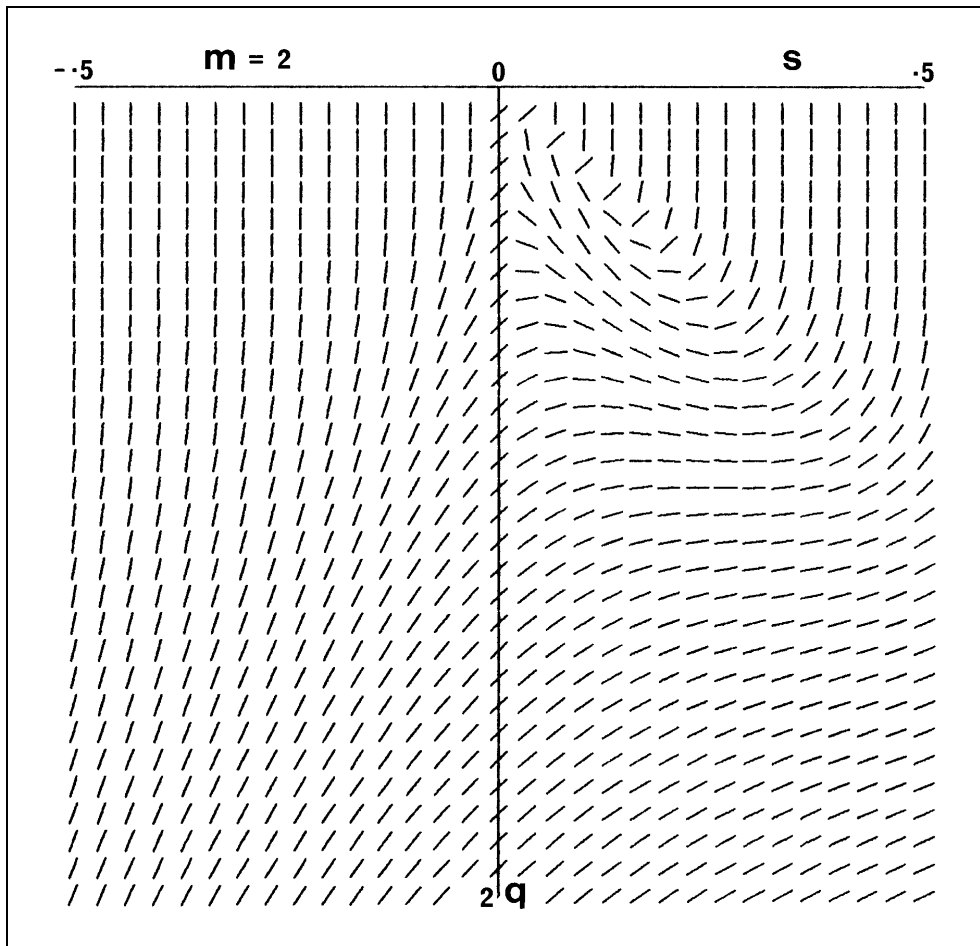


Fig. 6

Fig 7. The paths of the radial light rays near the ESC singularity are shown in the s - q plane, using the convention of fig 6 for the incoming and outgoing rays. The three diagrams are the same thing on three different scales.

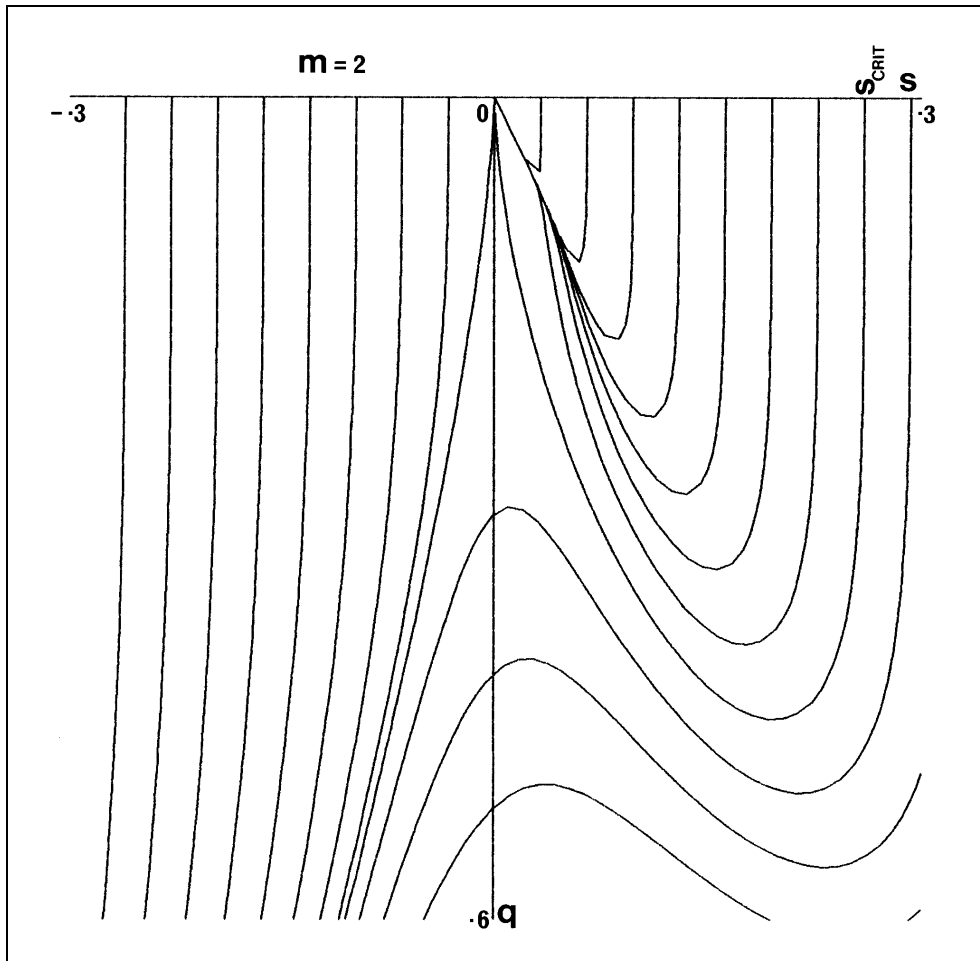


Fig. 7(a)

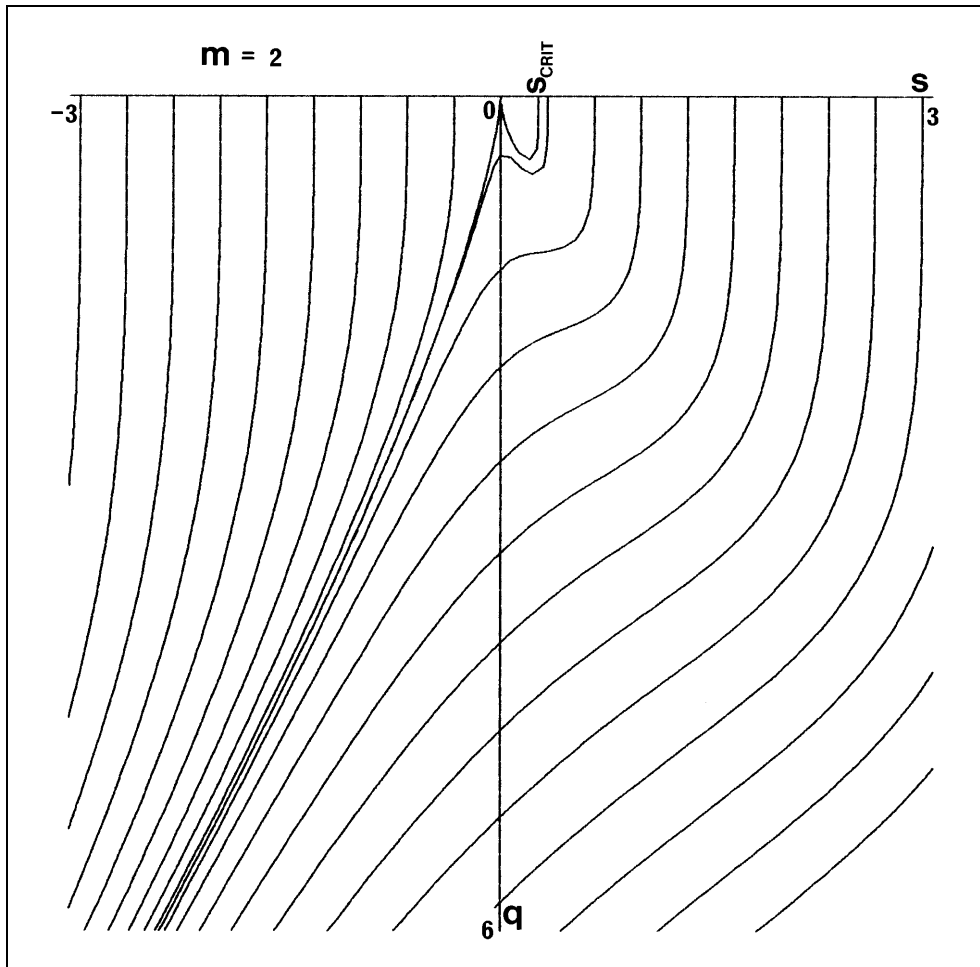


Fig. 7(b)

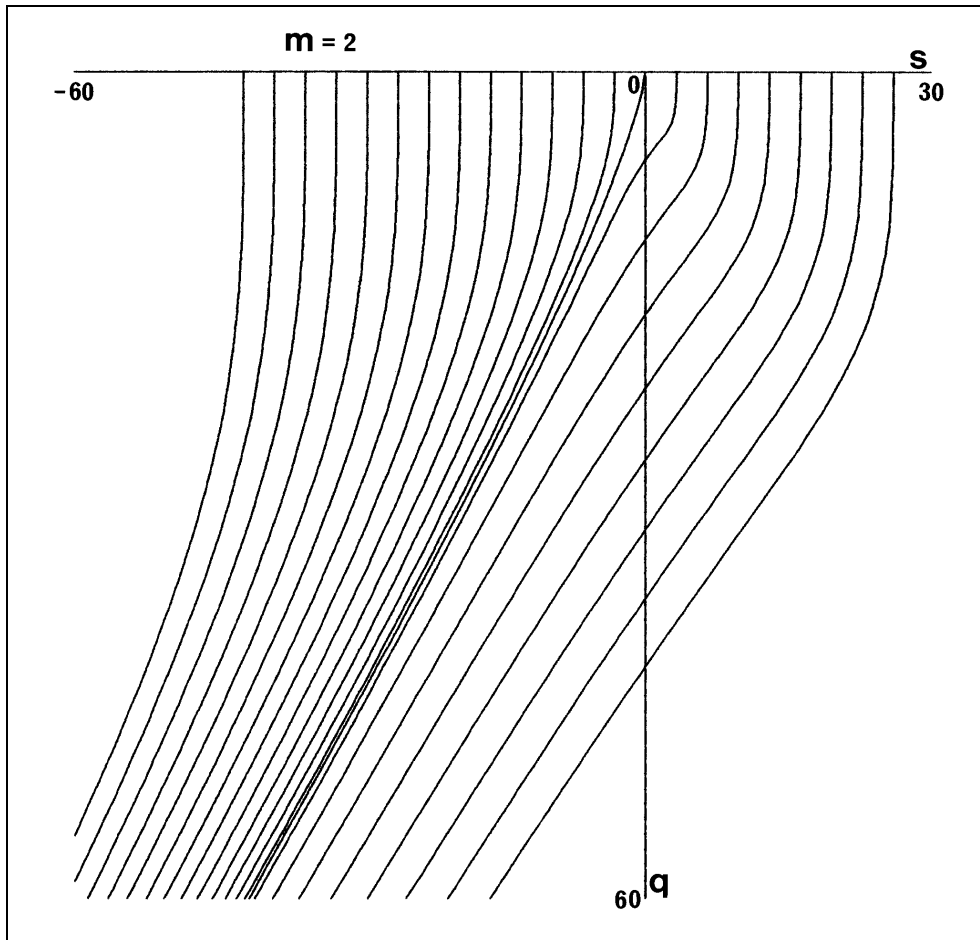


Fig. 7(c)

Fig 8. The paths of the radial light rays near the ESC singularity in the $r-t$ plane. The same curves as in figure 7 are shown for three comparable scales.

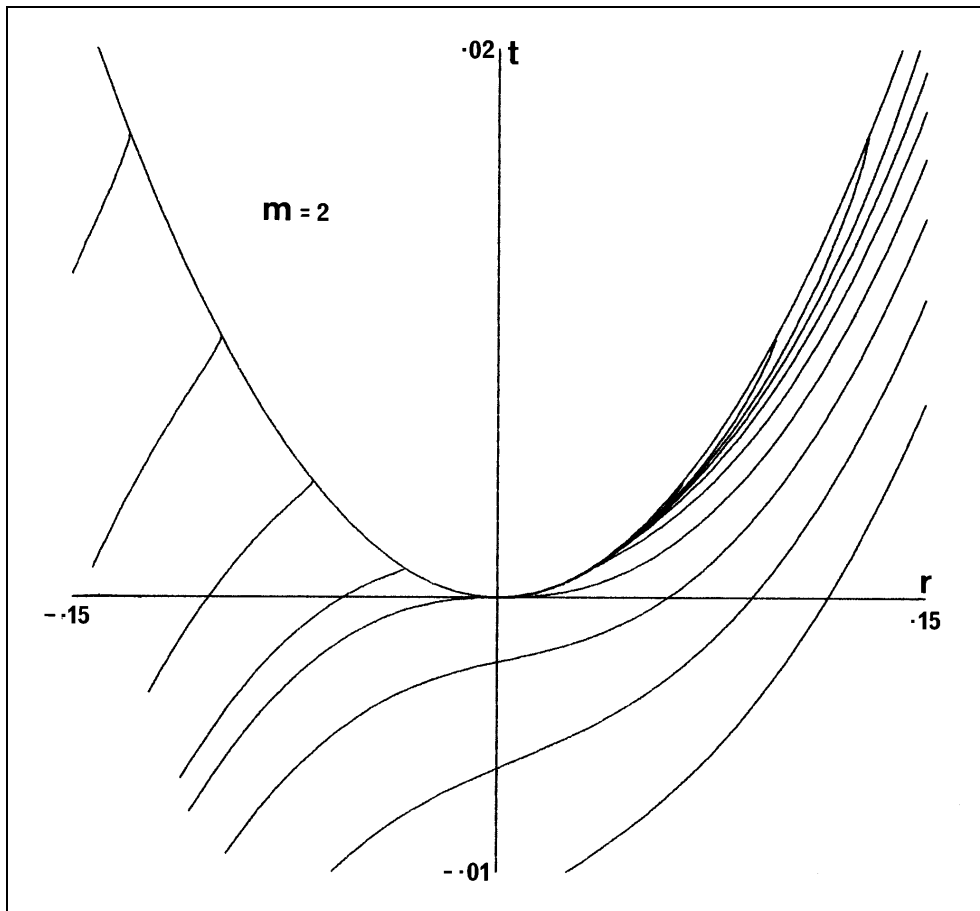


Fig. 8(a)

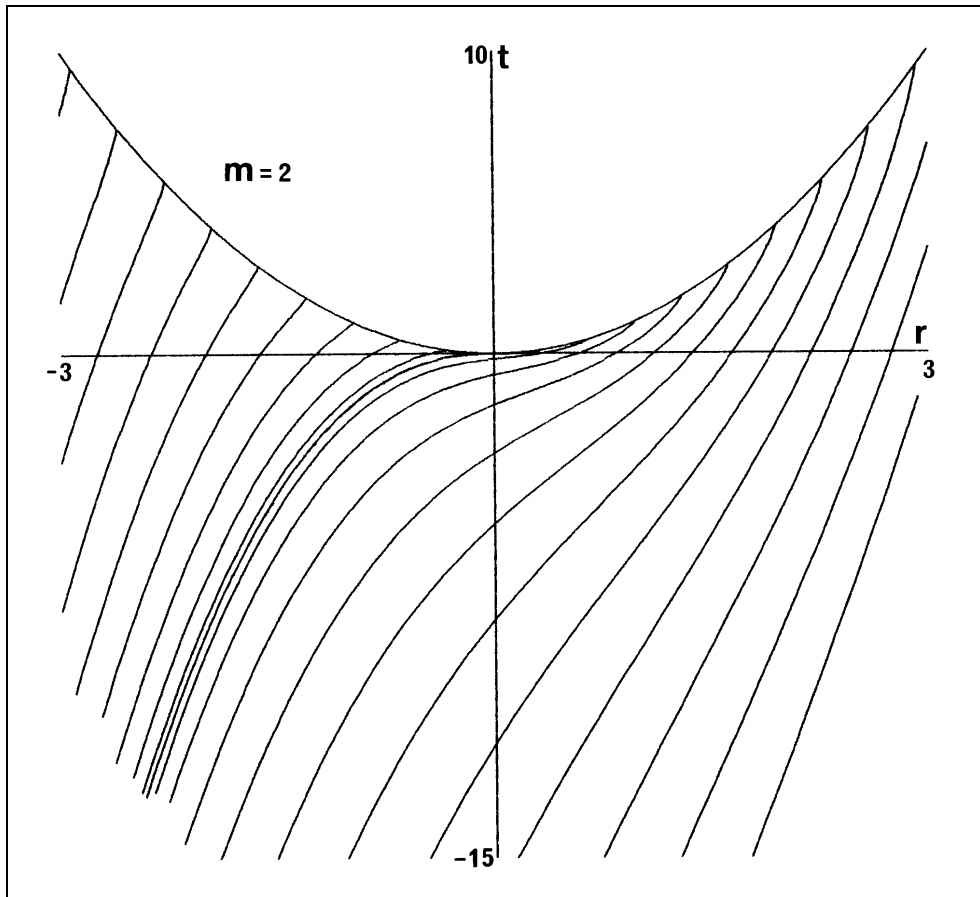


Fig. 8(b)

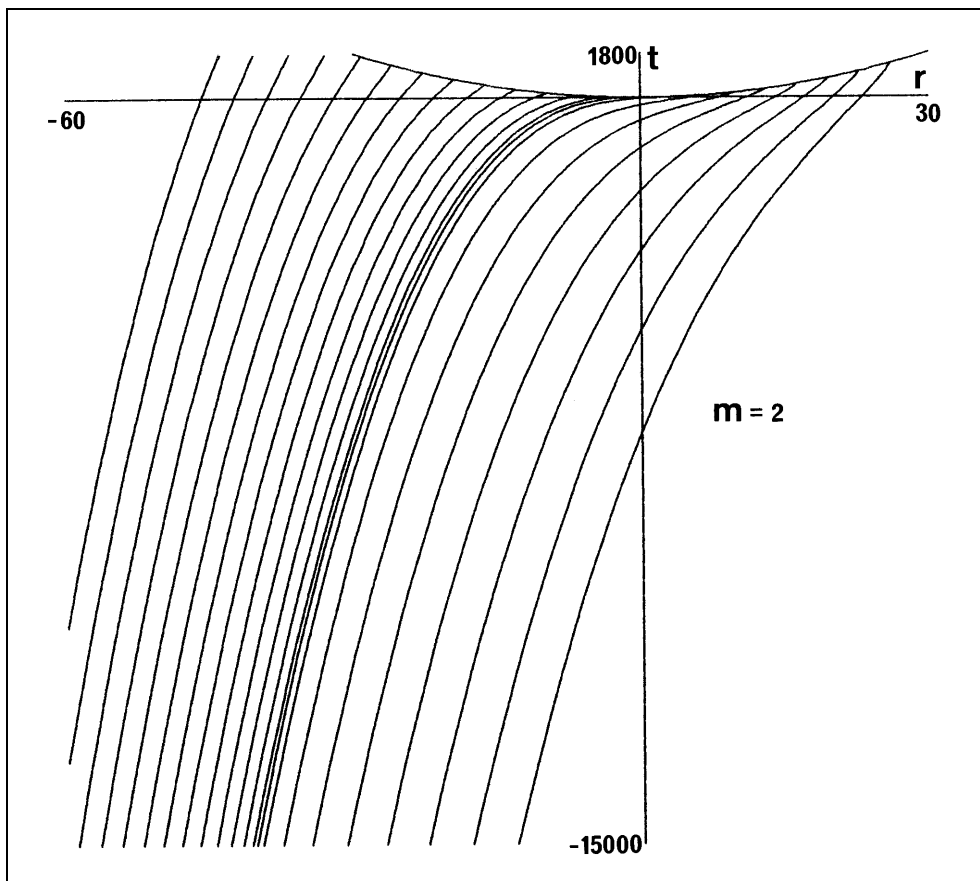


Fig. 8(c)

Fig 9. The conformal diagram for a parabolic Tolman model with arbitrary functions given by eqs (7.1) and (7.8) with $m = 2$, showing the region near the ESC singularity. Diagrams (a) to (e) show the curves of constant s , q , t , R , and ρ , respectively in the u - v plane. The light rays follow lines of constant u or constant v , and the origin is the central vertical line.

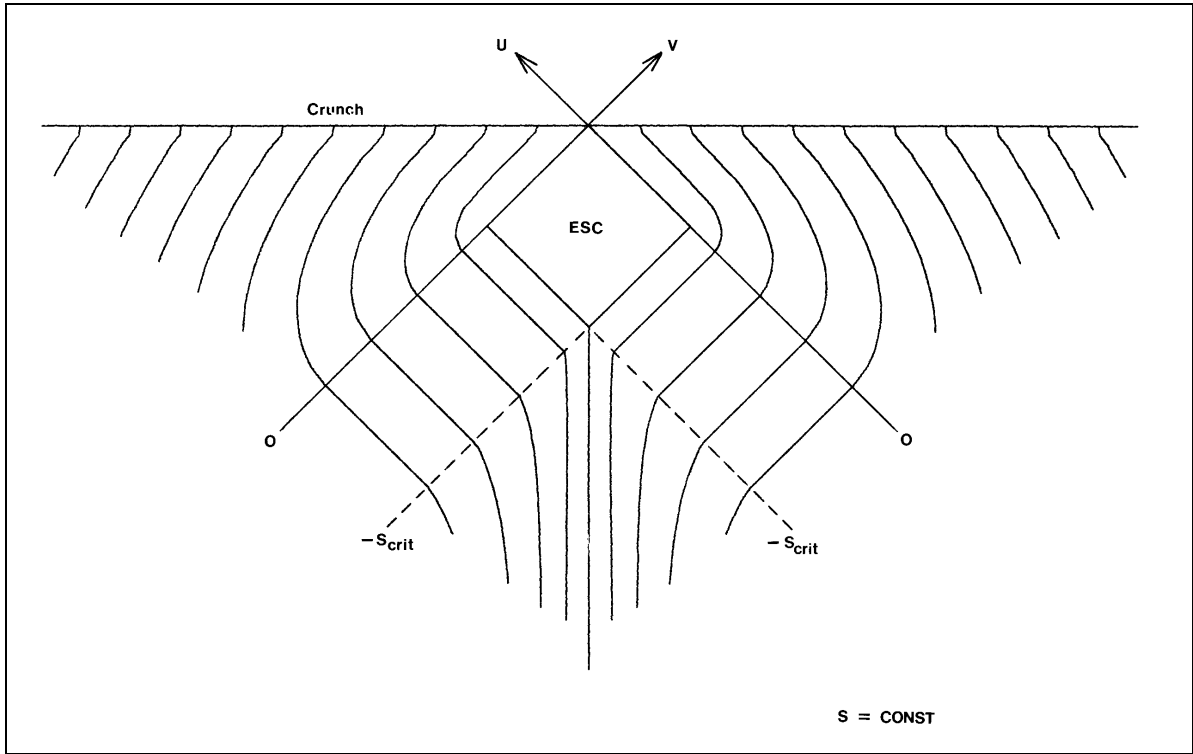


Fig. 9a

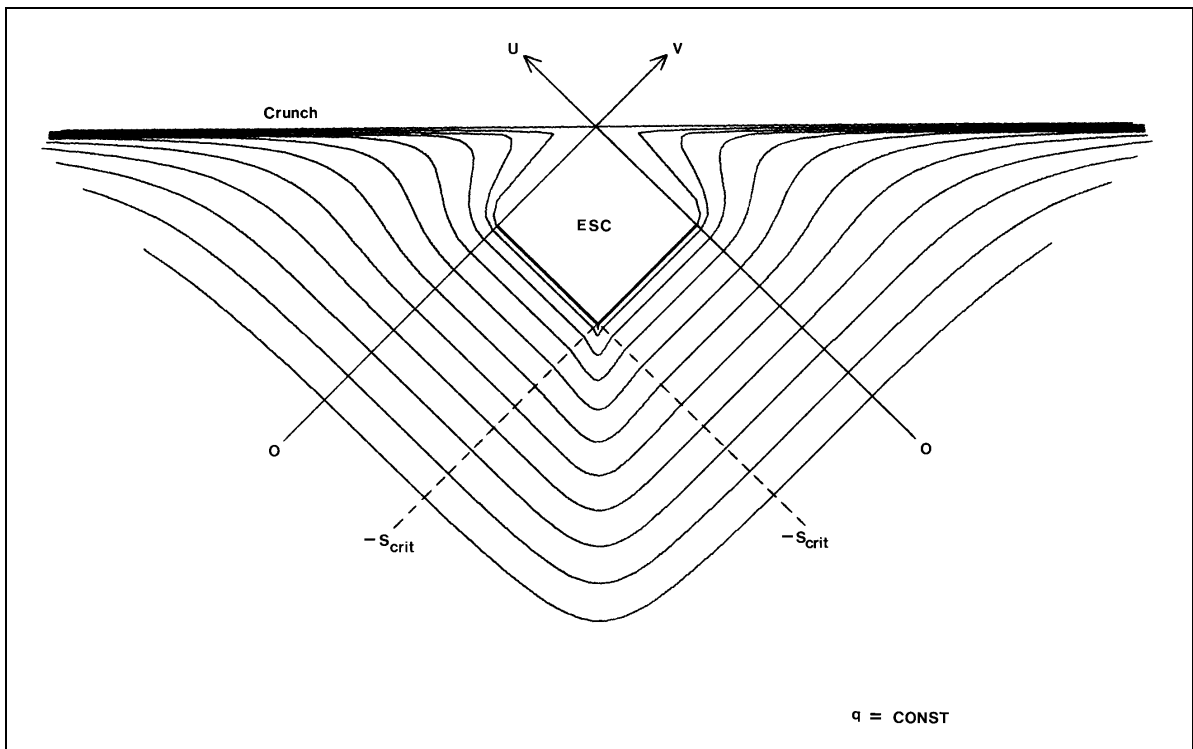


Fig. 9b

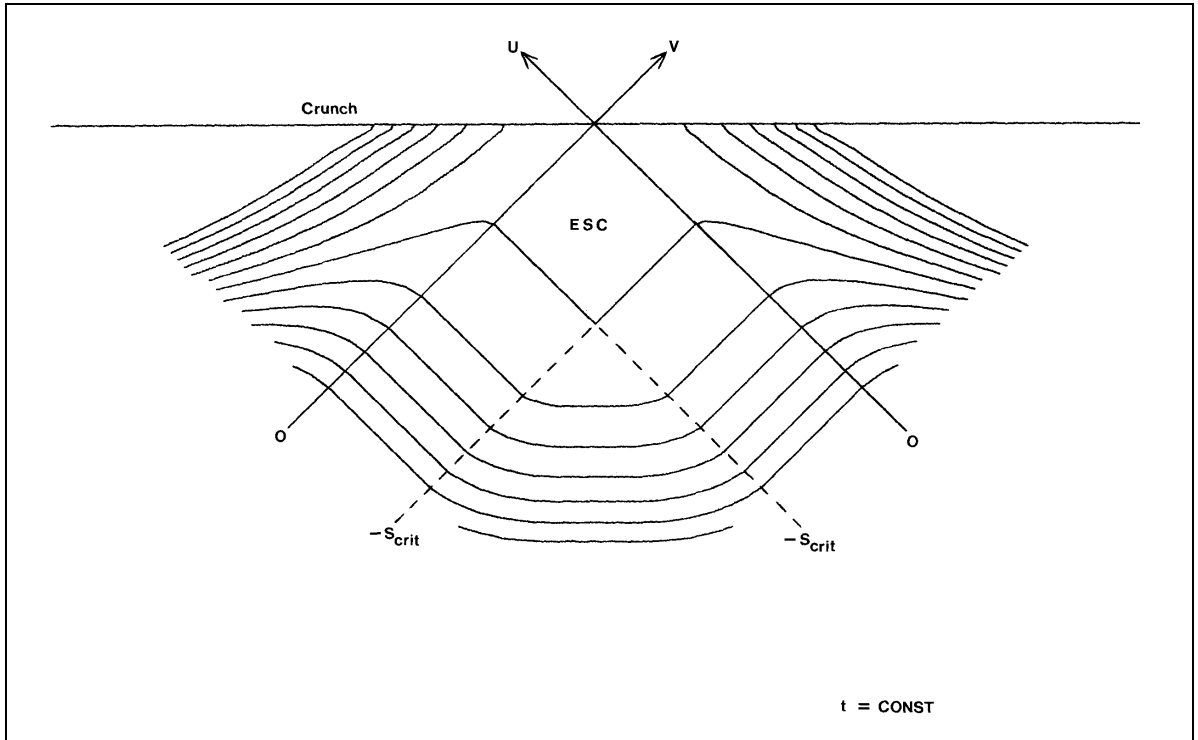


Fig. 9c

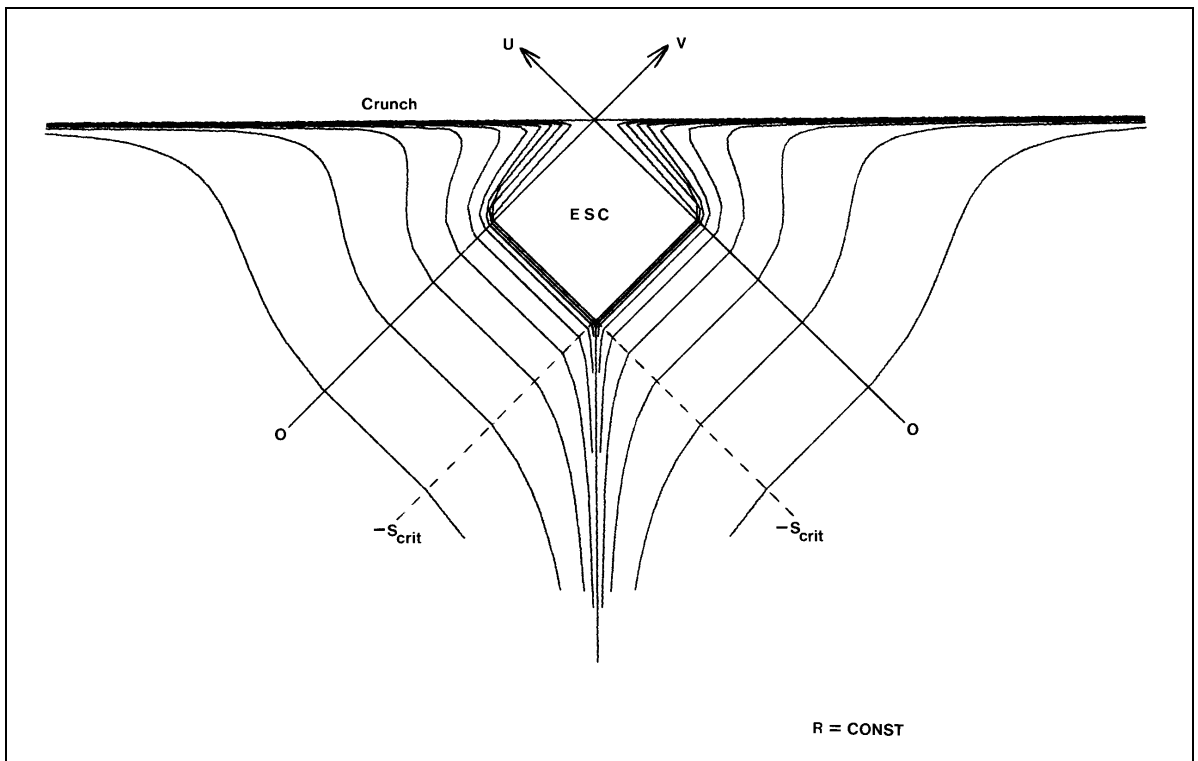


Fig. 9d

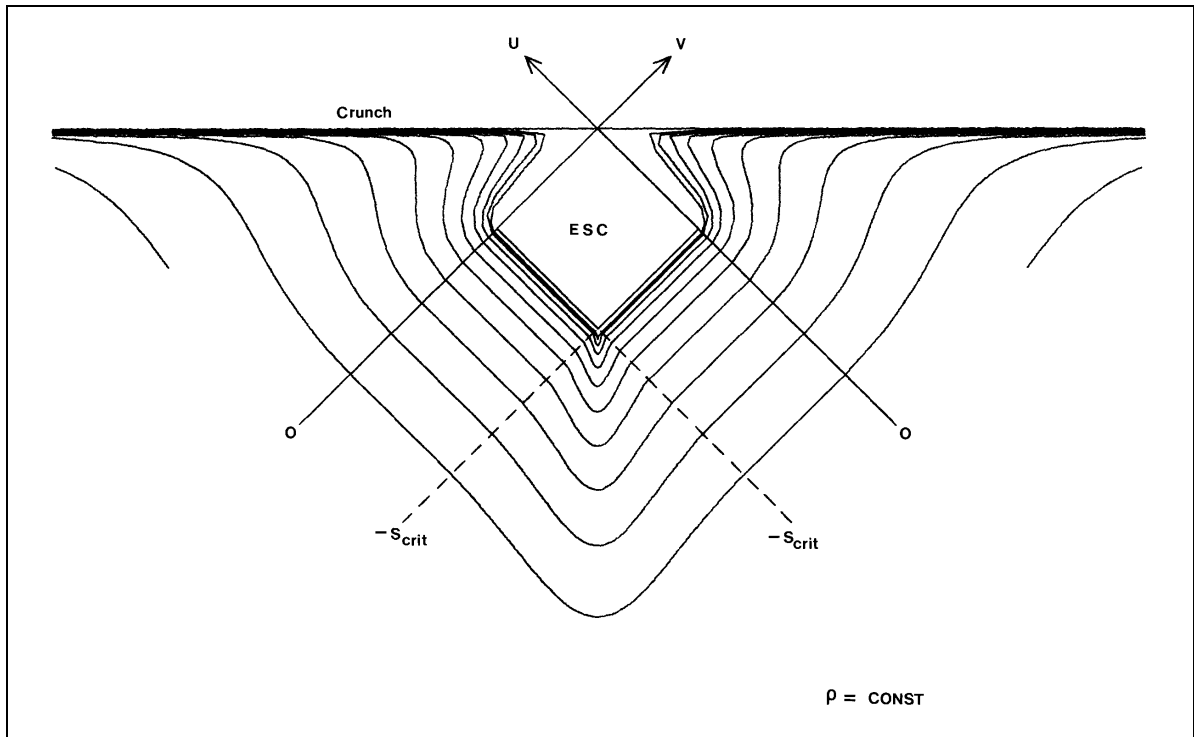


Fig. 9e

Fig 10. The gradient, dq/ds , of the radial light rays in the s - q plane, given by eq (7.11), for a variety of values of m , as labelled on each diagram.

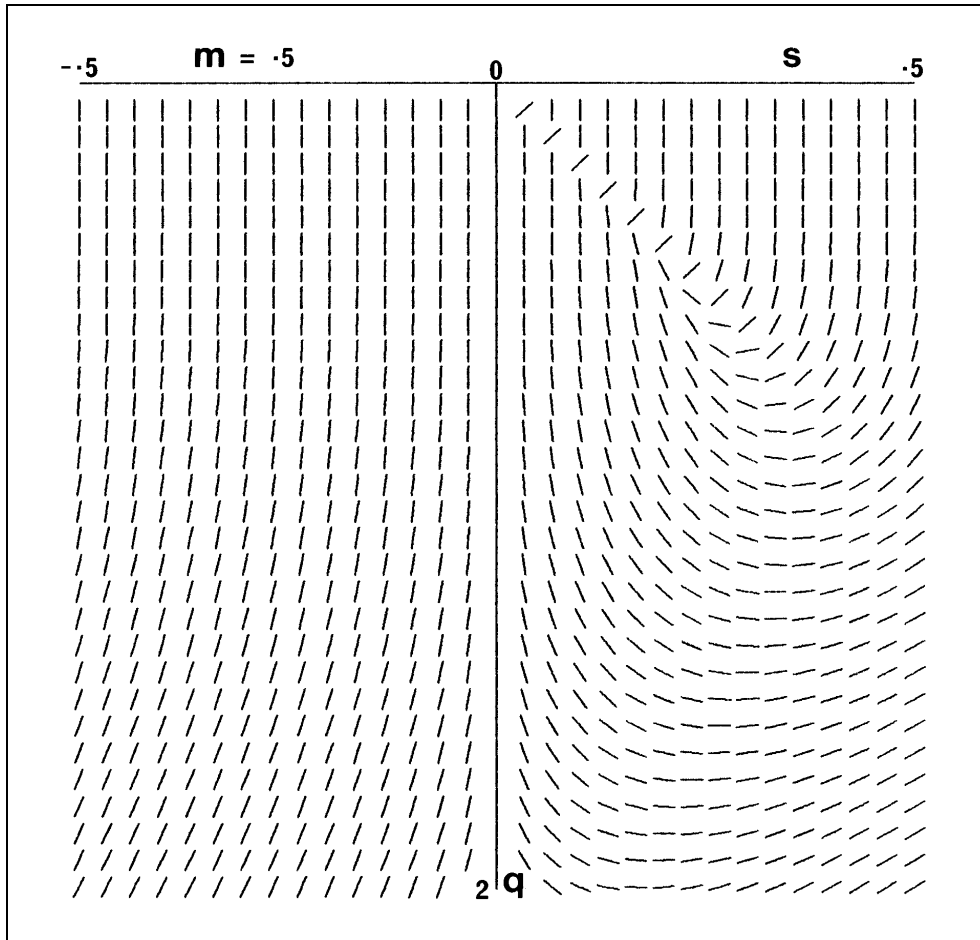


Fig. 10(a)

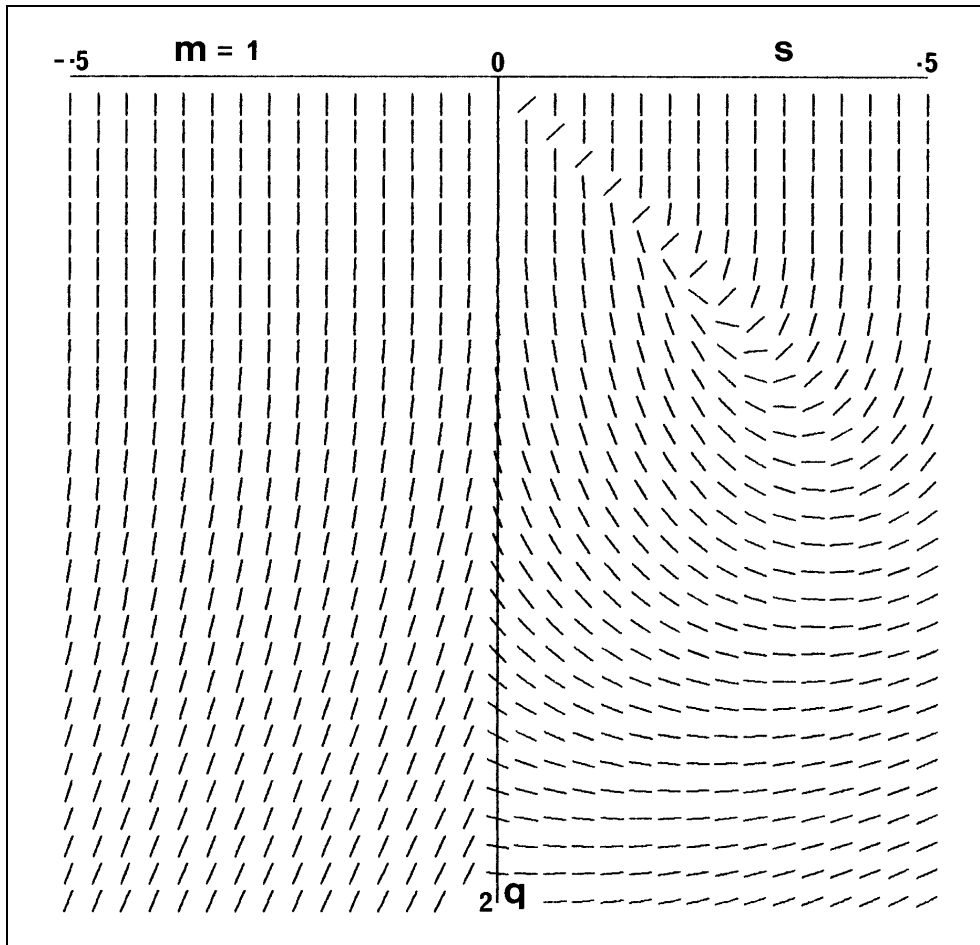


Fig. 10(b)

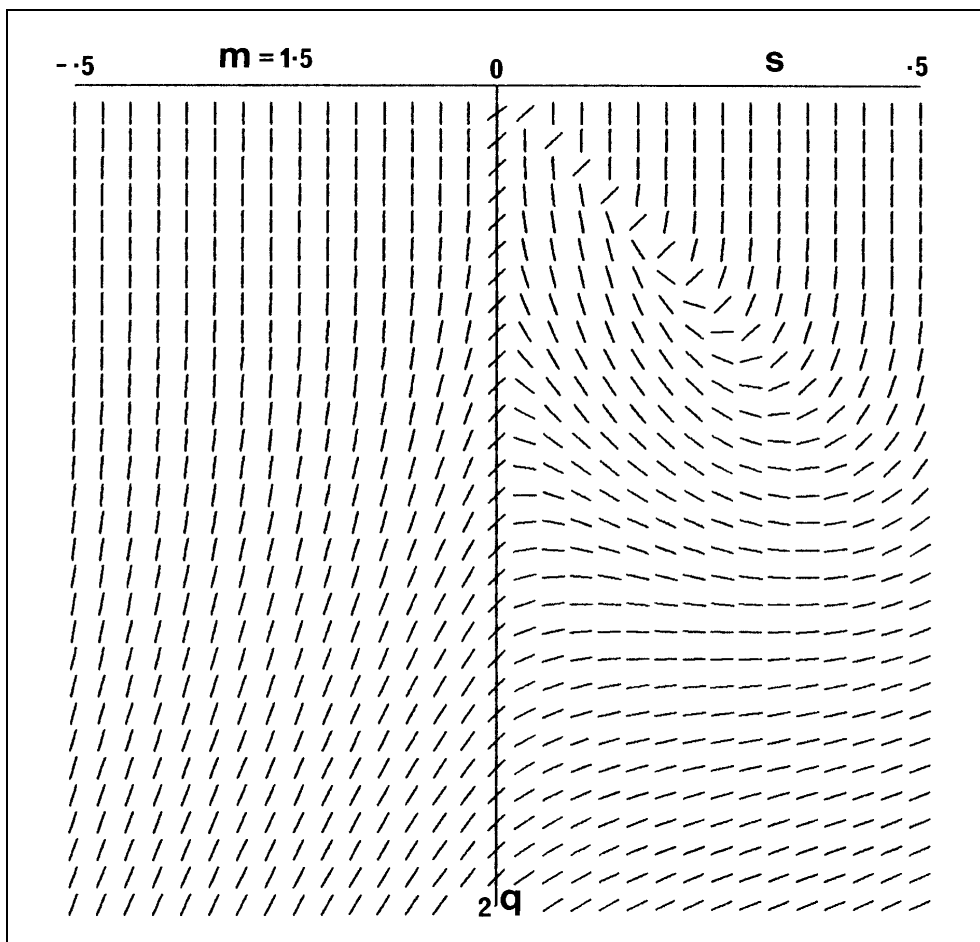


Fig. 10(c)

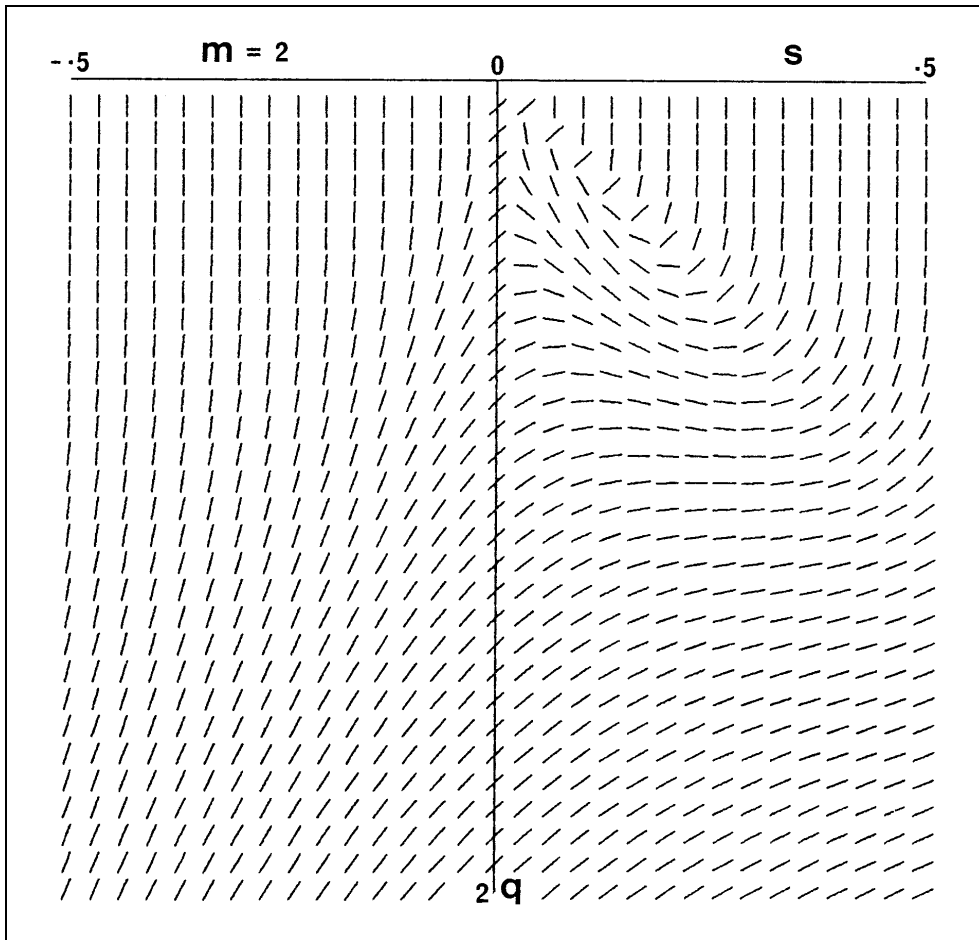


Fig. 10(d)

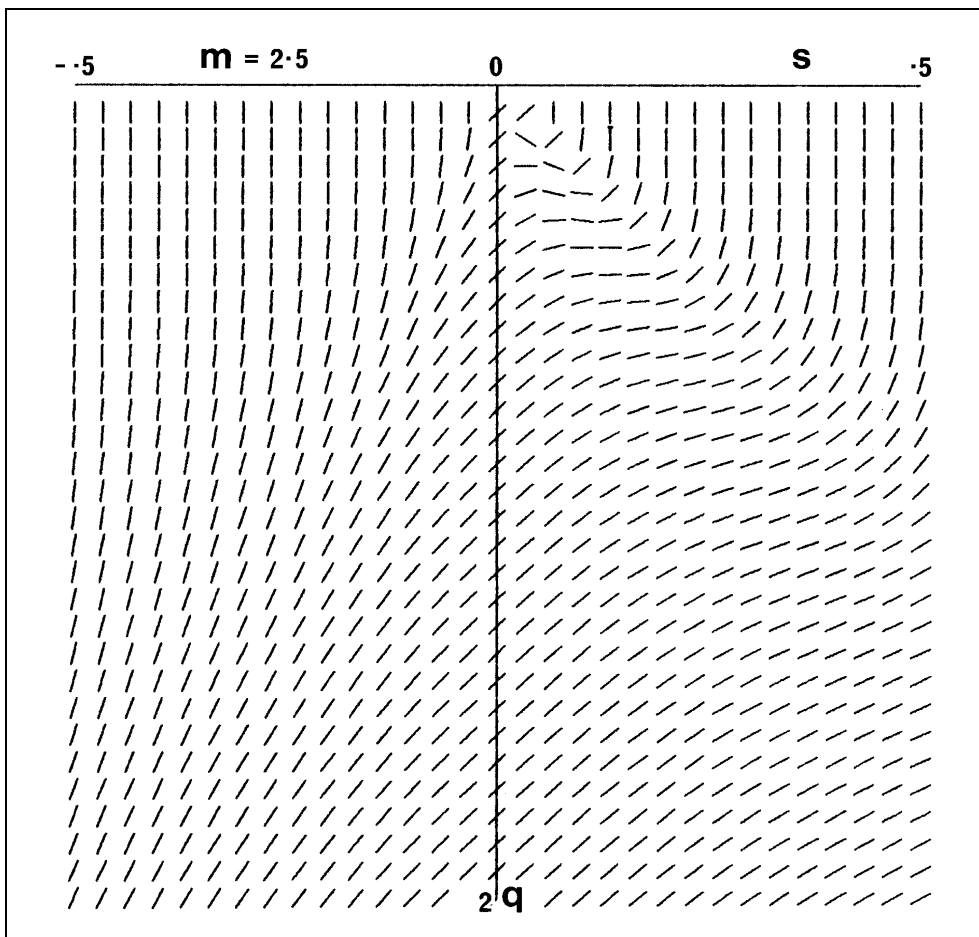


Fig. 10(e)

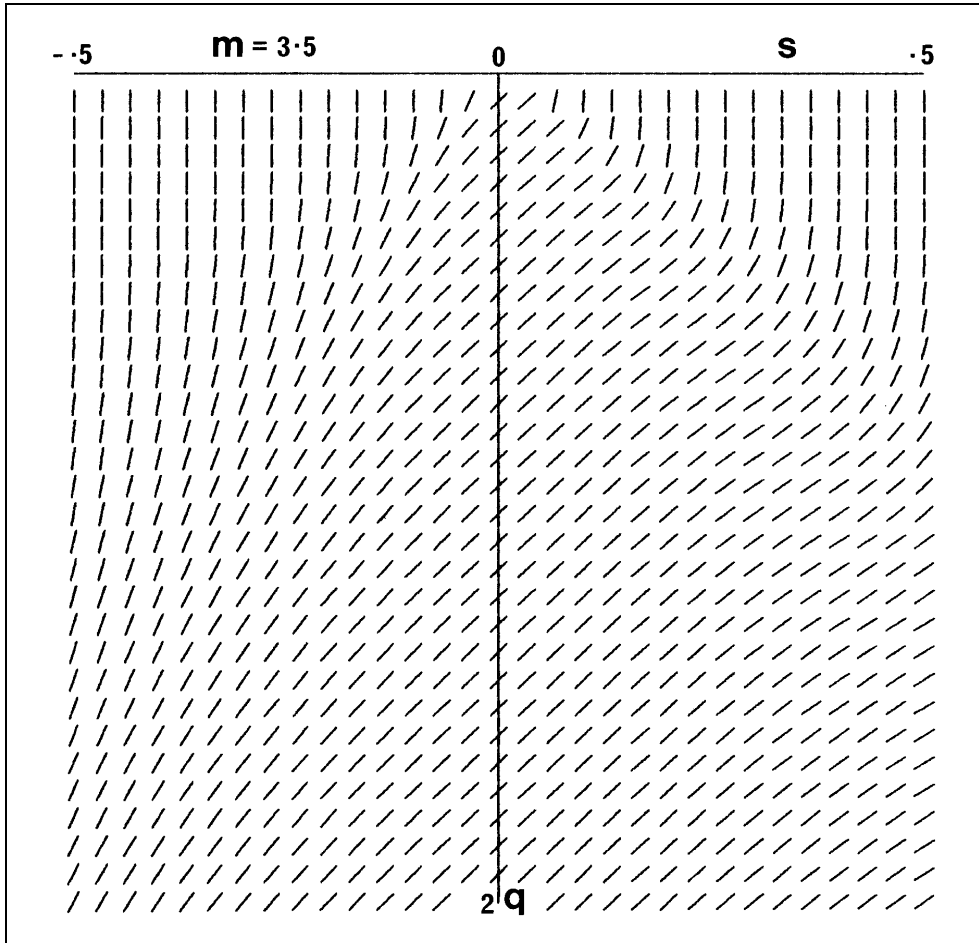


Fig. 10(f)

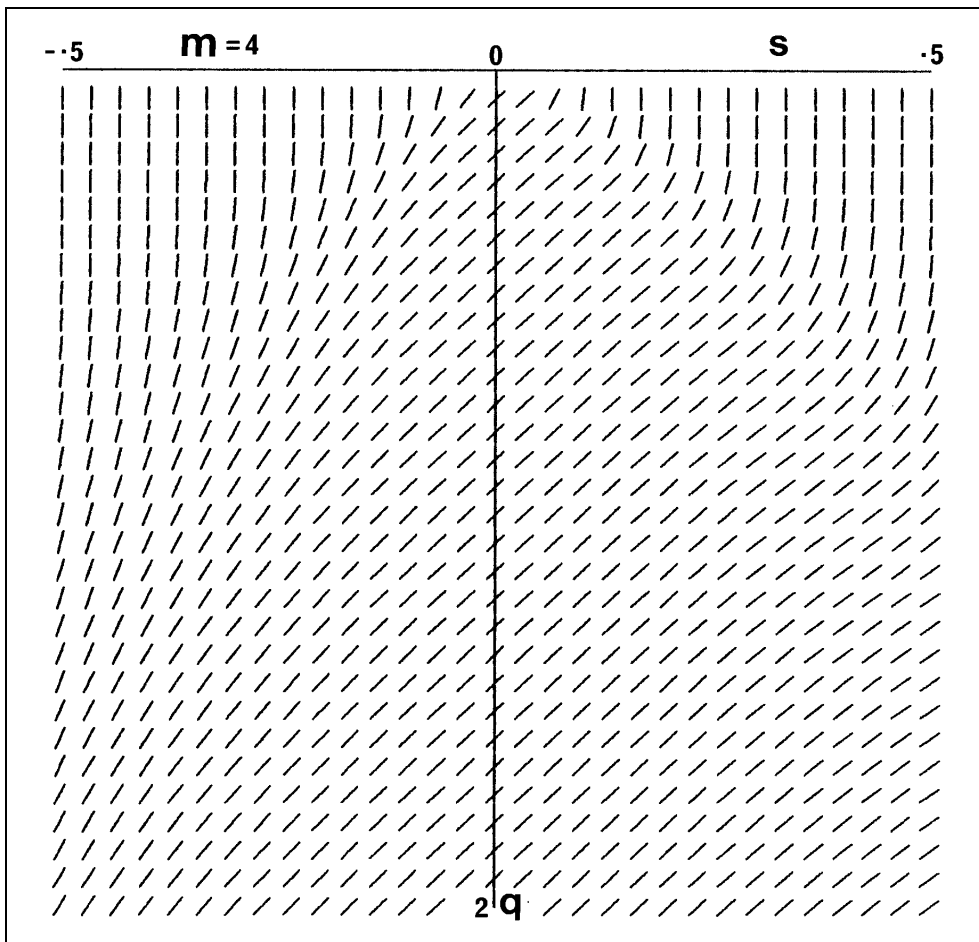


Fig. 10(g)

Fig 11. The paths of the radial light rays near the ESC singularity are shown in the s - q plane, for several values of m between 1 and 2.5. They have all been scaled so that s_{crit} is the same size in every diagram.

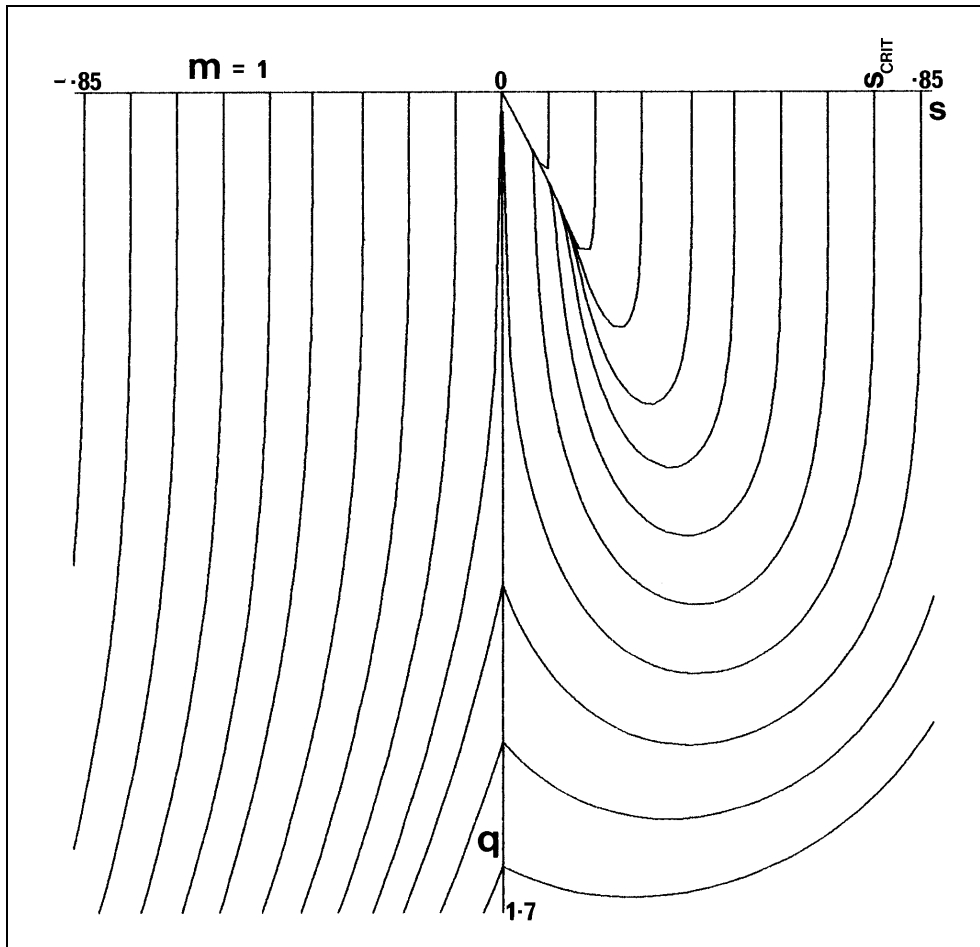


Fig. 11(a)

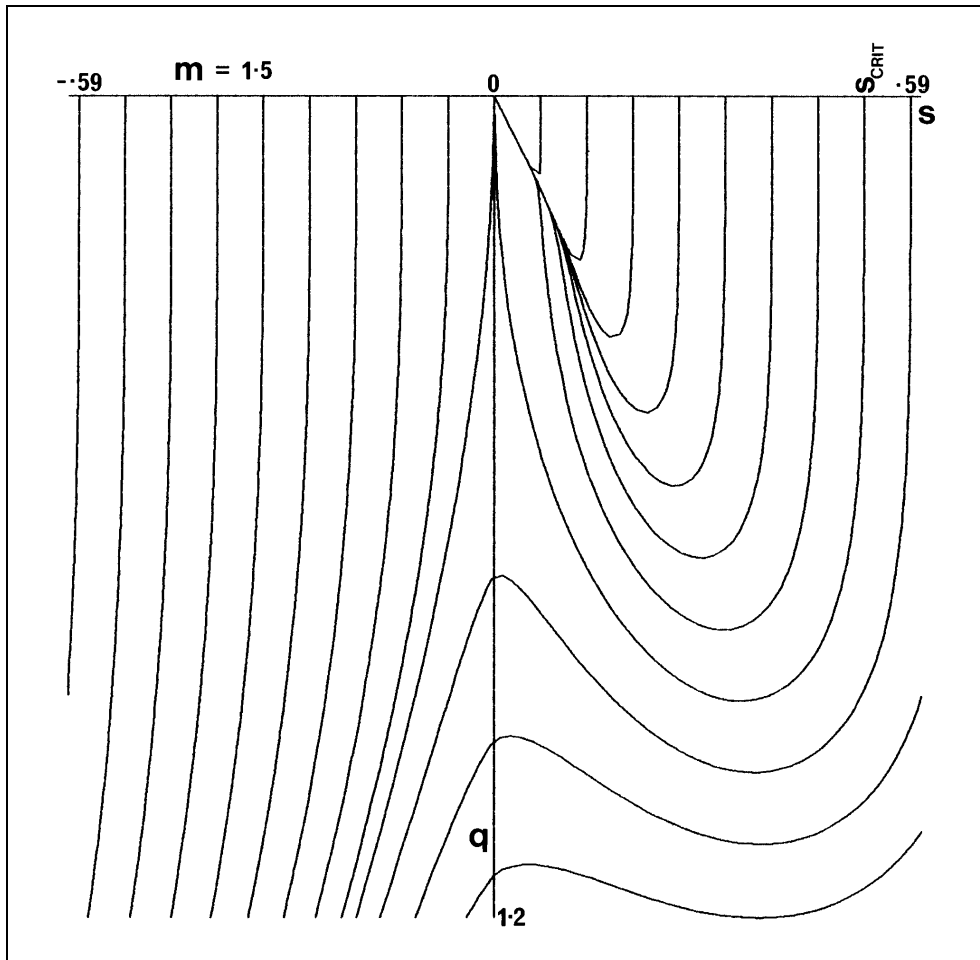


Fig. 11(b)

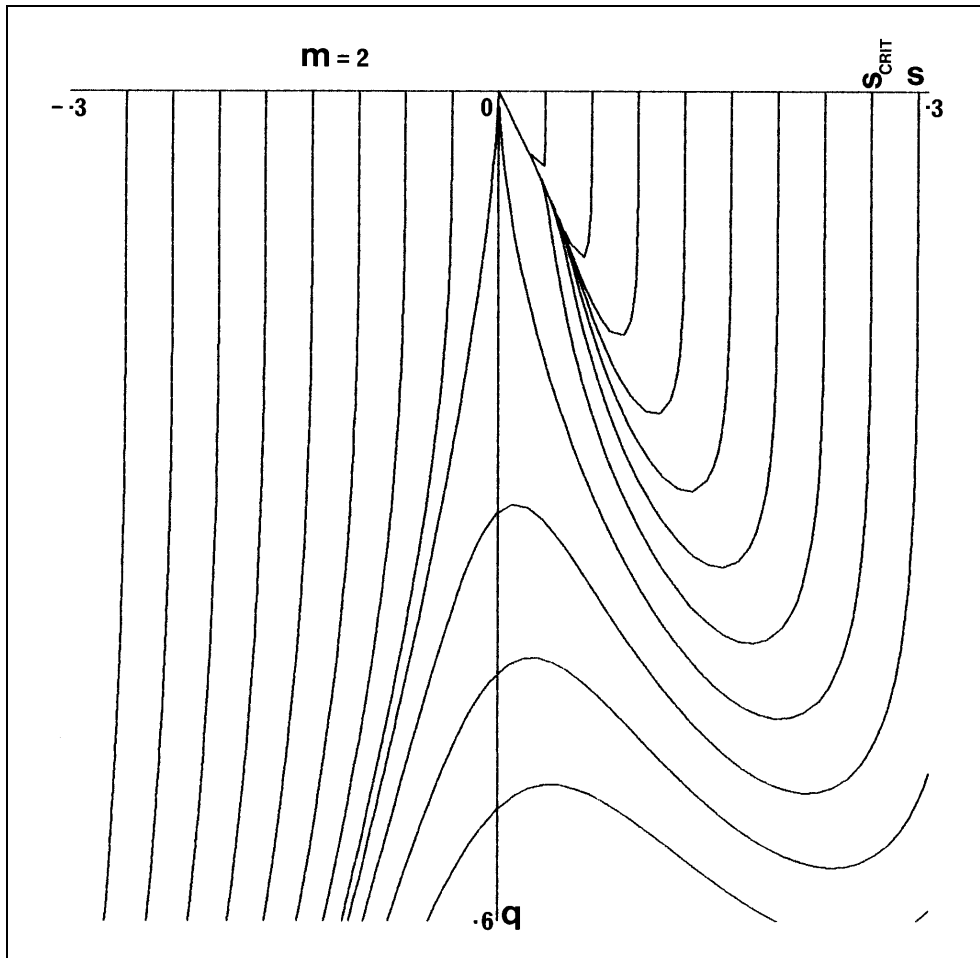


Fig. 11(c)

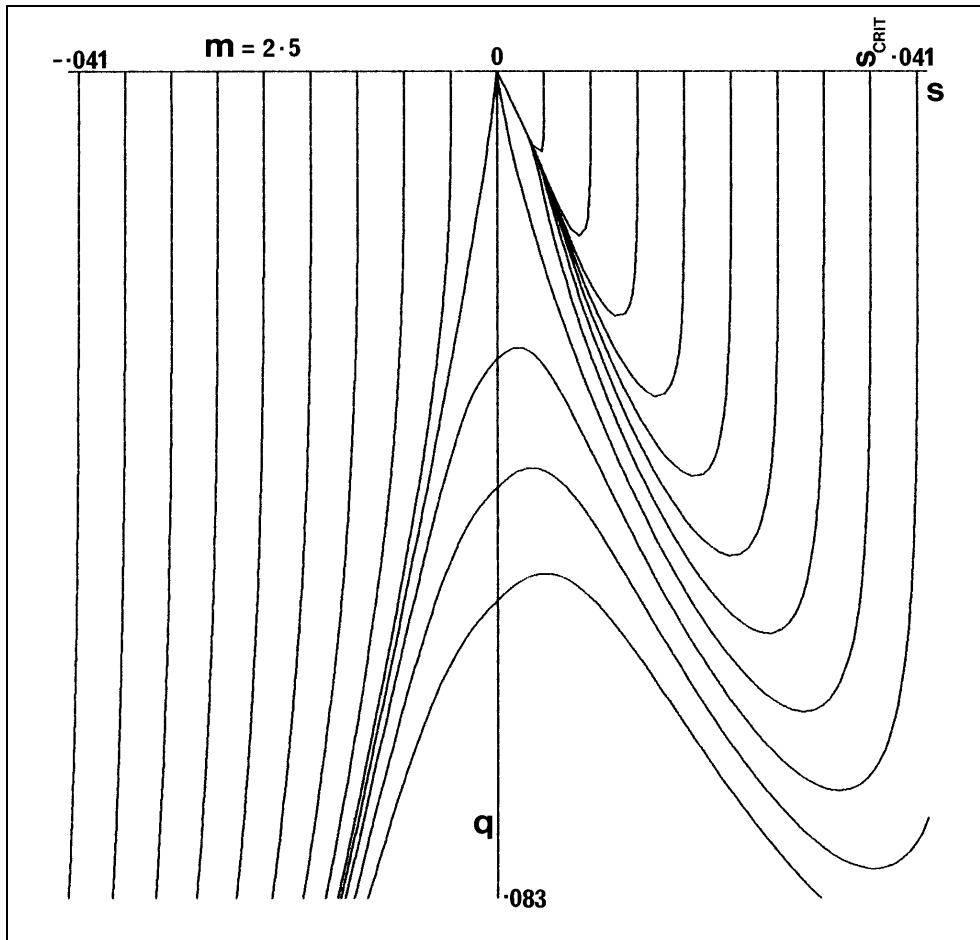


Fig. 11(d)

Fig 12. The paths of the radial light rays near the ESC singularity are shown in the $r-t$ plane, for several values of m between 1 and 2.5. The curves are the same as in fig 11.

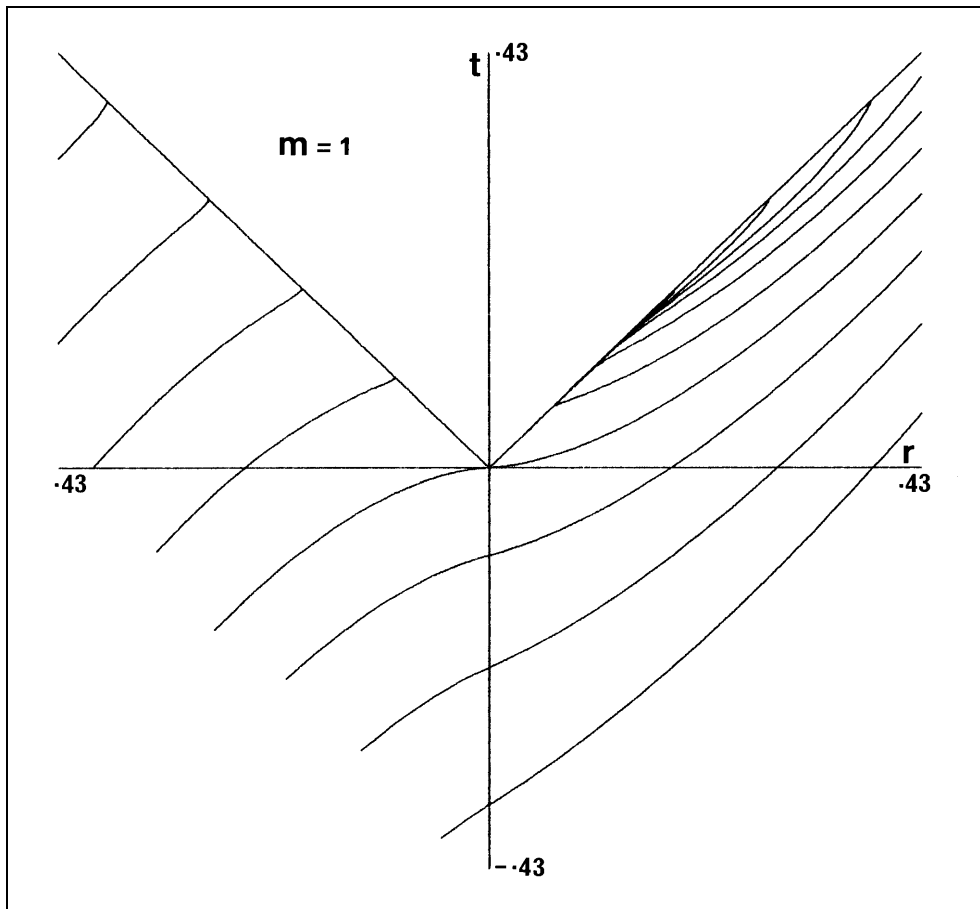


Fig 12(a)

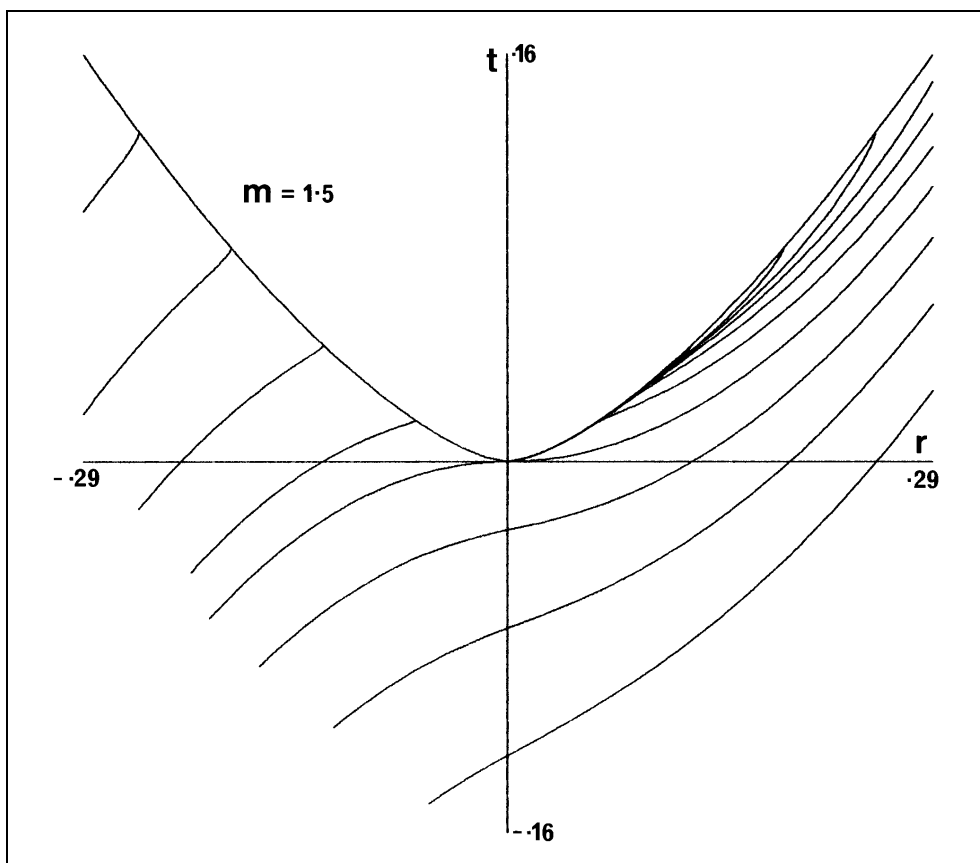


Fig 12(b)

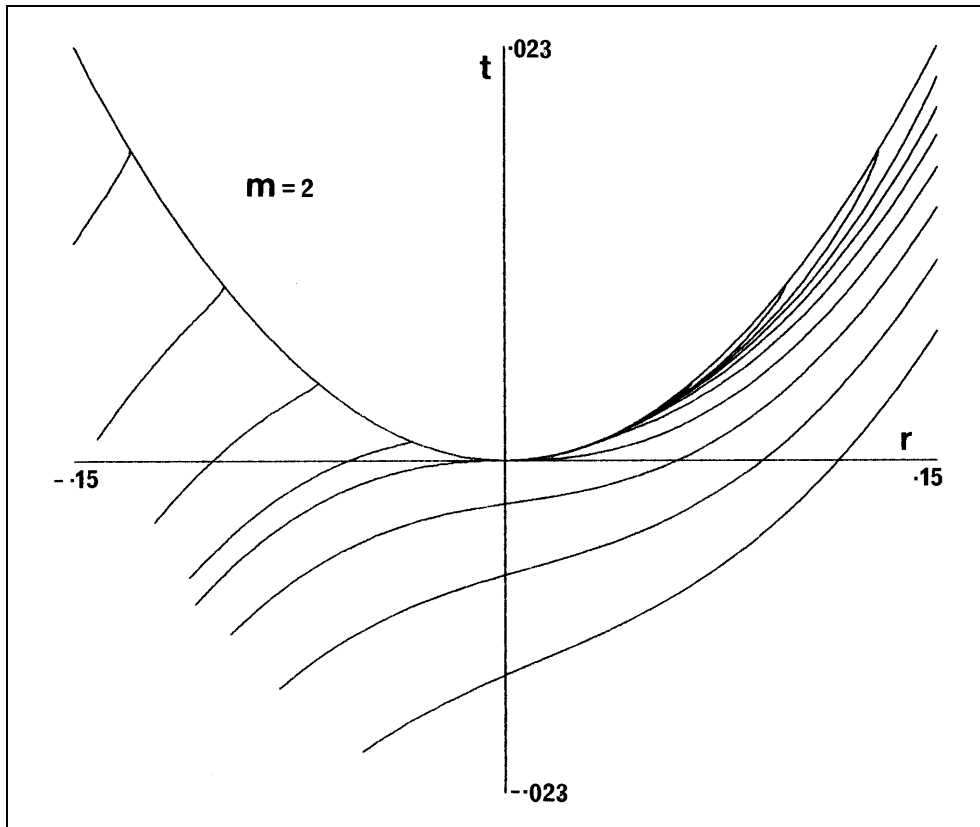


Fig 12(c)

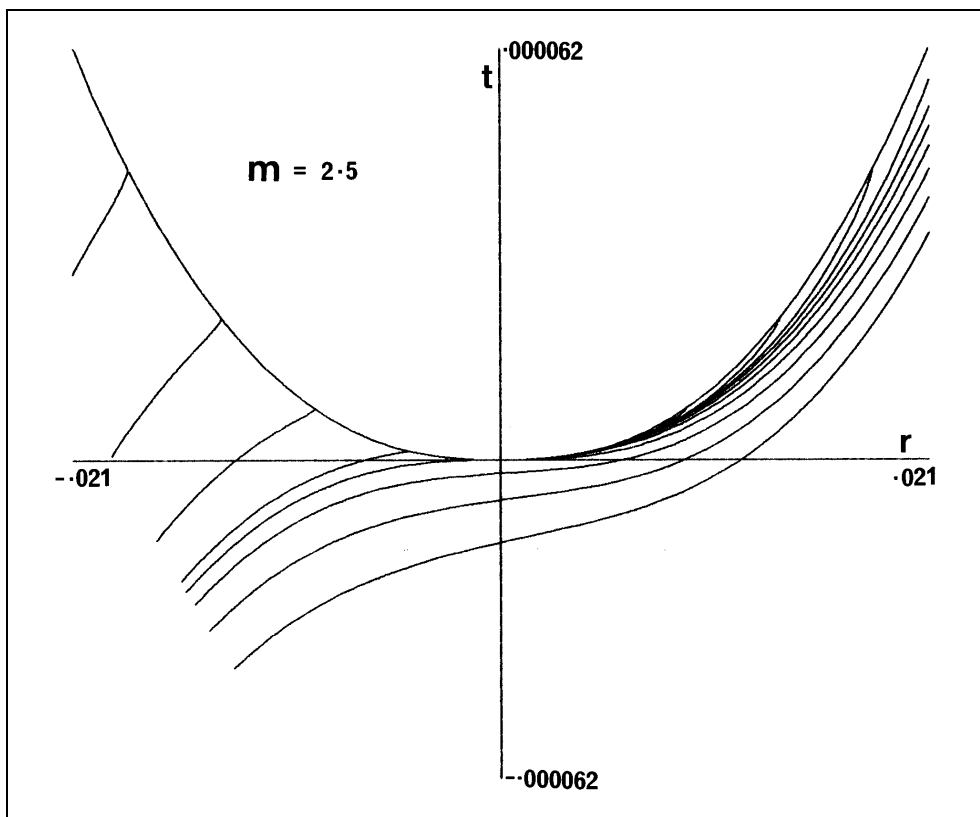


Fig 12(d)

Fig 13. The outgoing critical rays in the s - q plane for several values of m between 1 and 2.6, shown on the same scale.

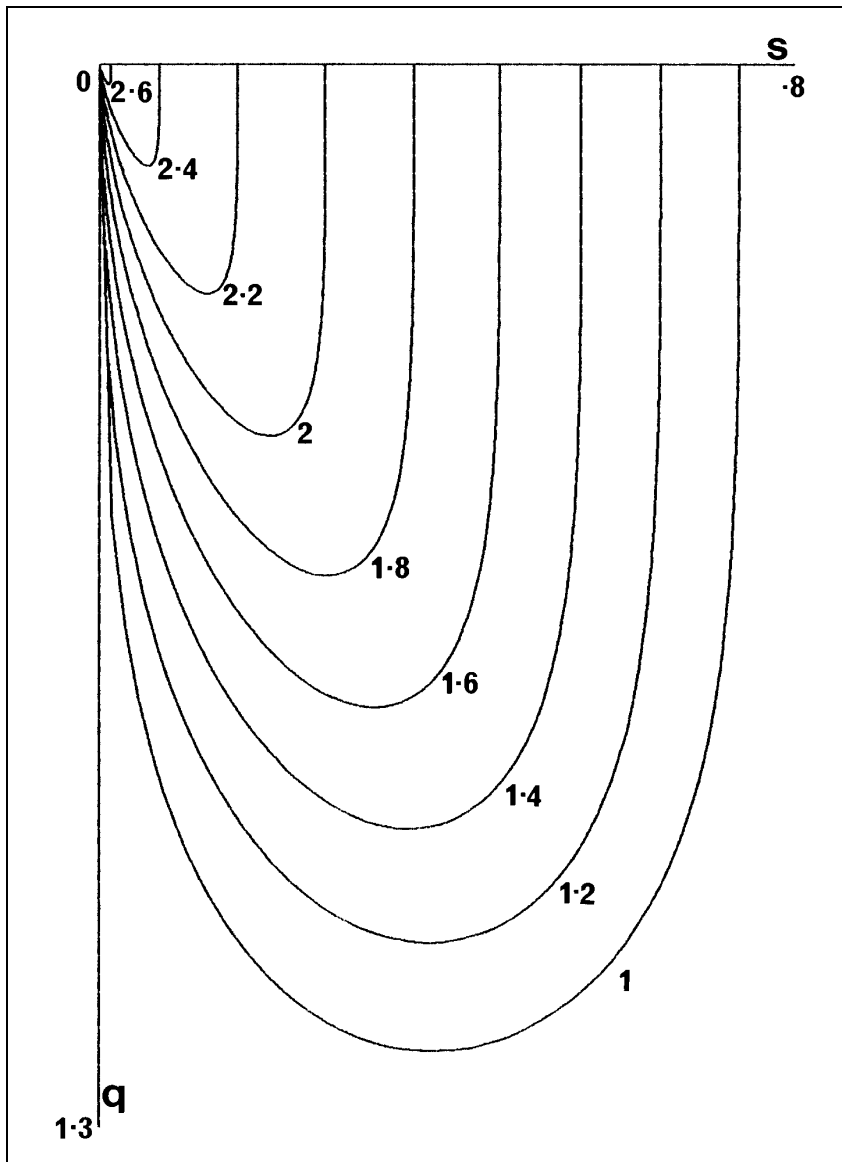


Fig. 13

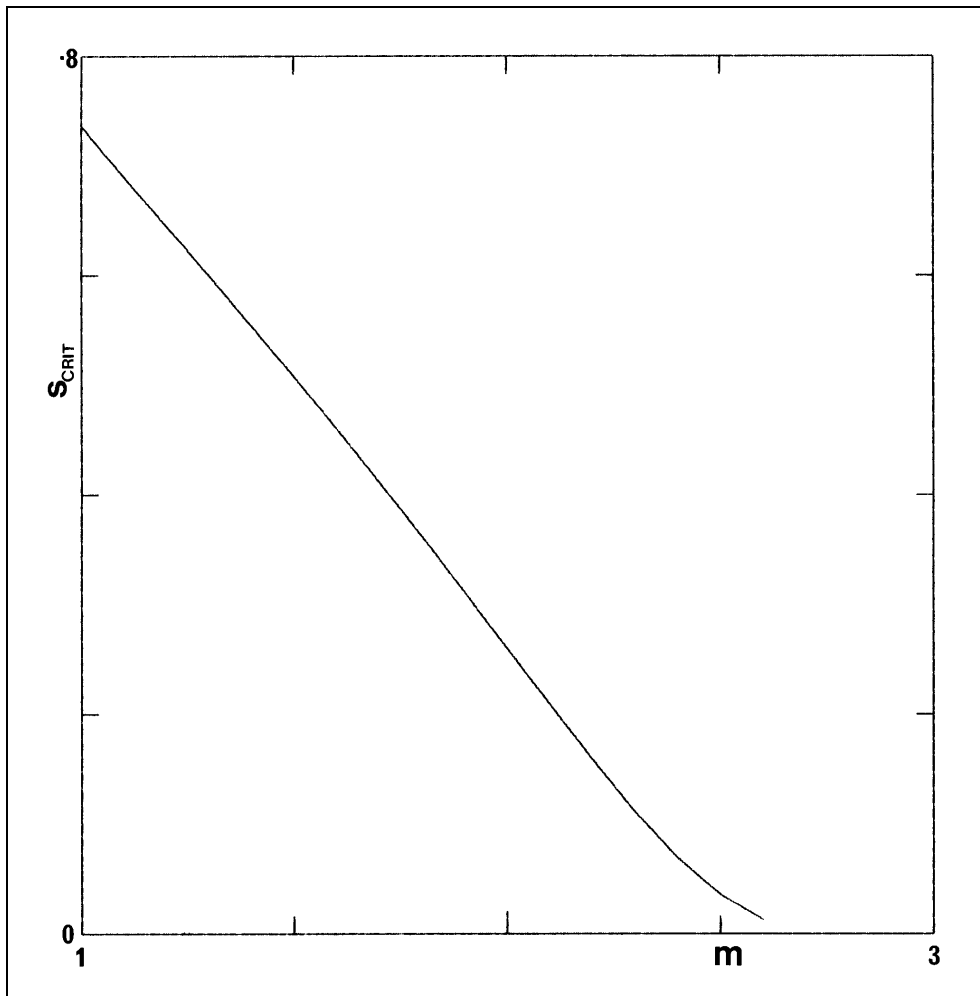
Fig 14. The critical radius, s_{crit} , as a function of m , in the range 1 to 2.6.

Fig. 14

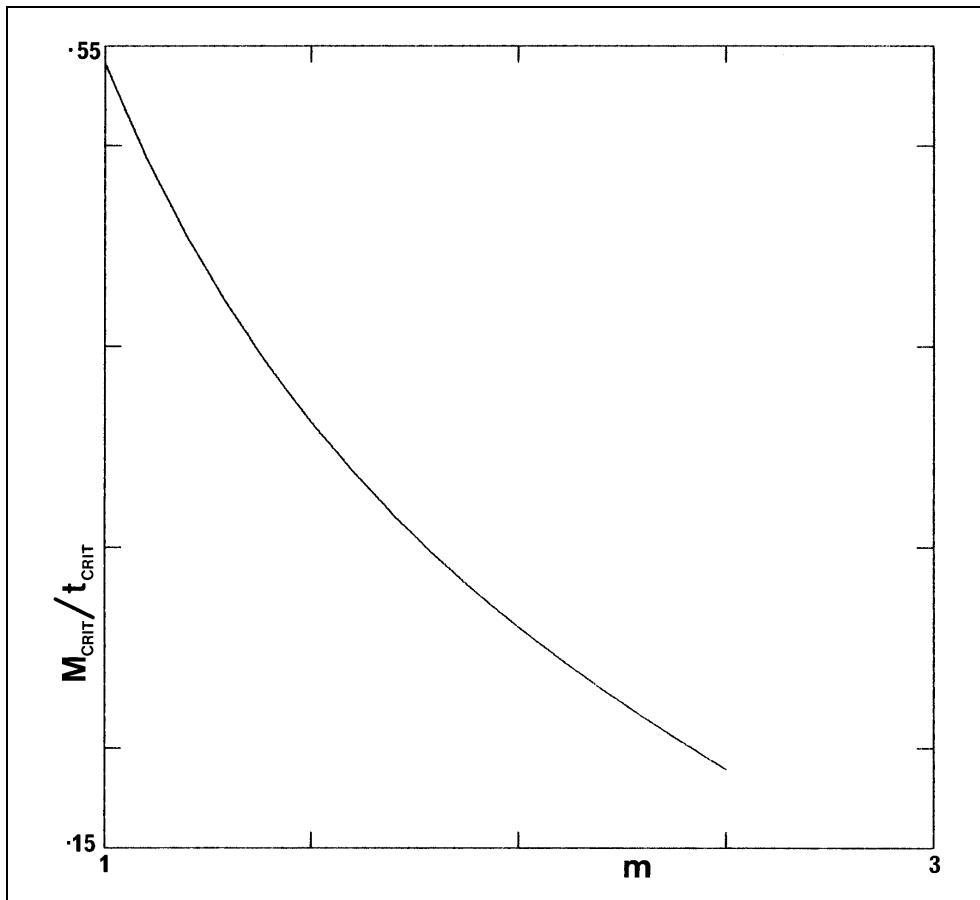
Fig 15. The ratio M_{crit}/t_{crit} as a function of m .

Fig. 15

Fig 16. The gradient, dg/dr , of the radial light rays in the $r-g$ plane, given by eq (7.9), for $m = 3$, and a variety of values of a_1 , as labelled on each diagram. The line b_1 is the incoming critical ray, which is a straight line in these coordinates. The outgoing critical ray is b_3 , while b_2 is one of the post critical rays that is also a straight line. The lines b_4 , and b_5 are loci of $dg/dr = 0$.

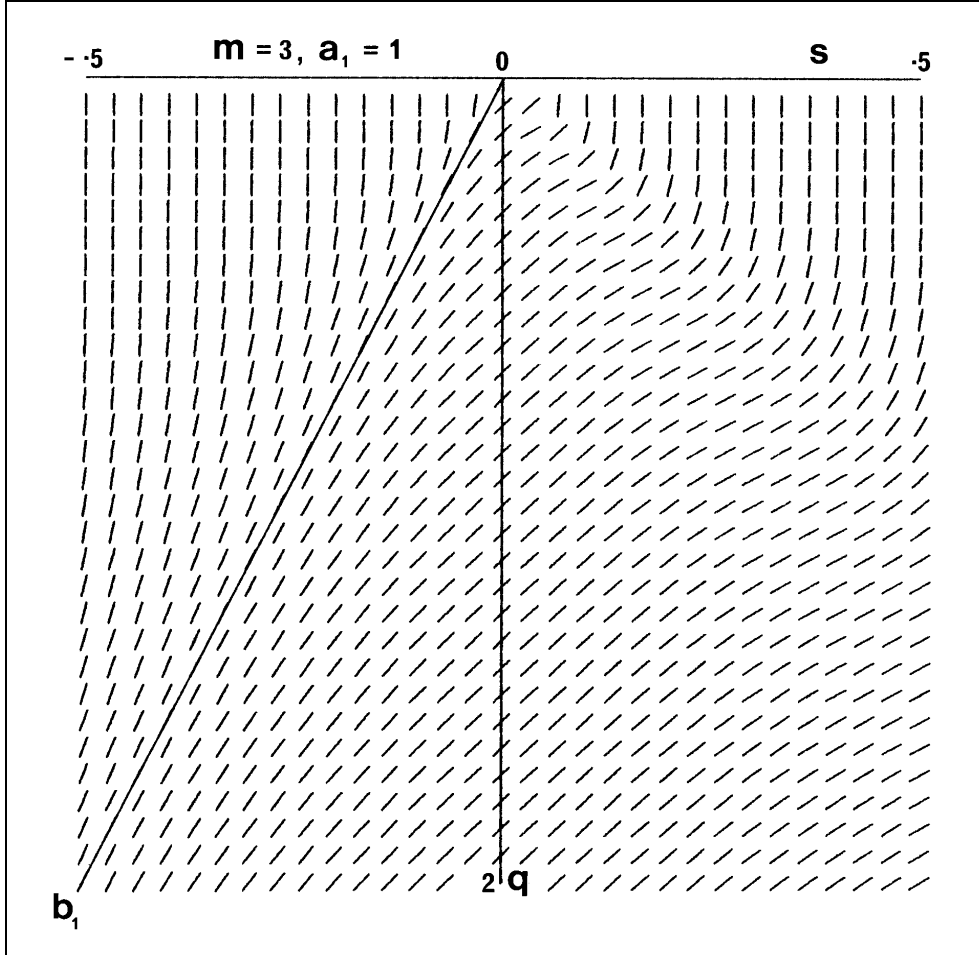


Fig. 16(a)

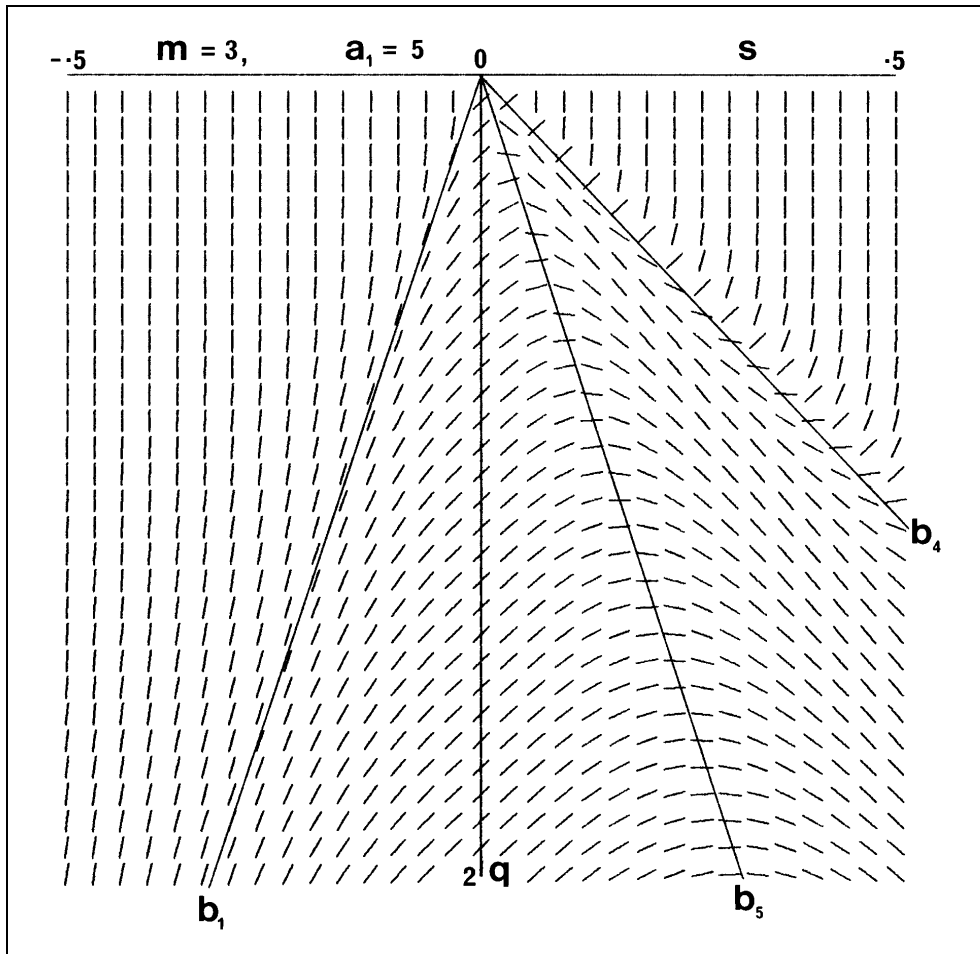


Fig. 16(b)

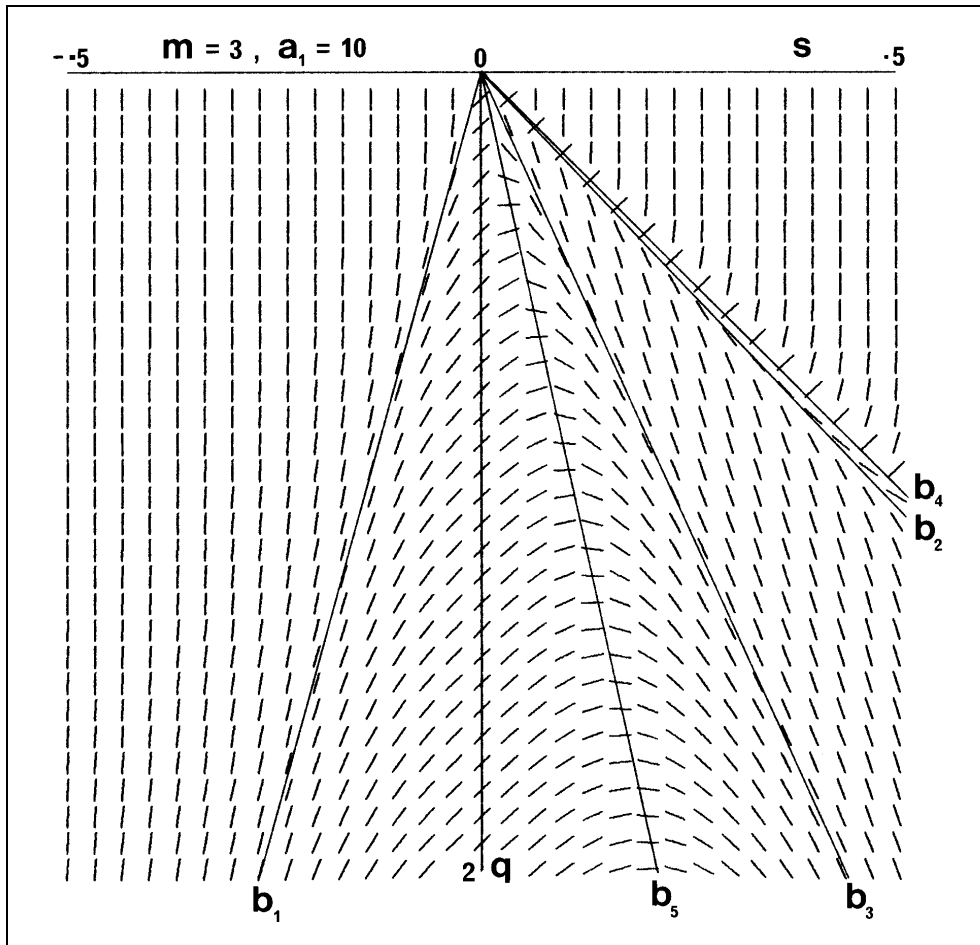


Fig. 16(c)

Chapter 8

CONCLUSIONS

The new work presented in this thesis on the Tolman model is composed of three parts: the calculation of the redshift structure of the bang surface; the derivation of the conditions for no shell crossings; and an investigation of the ESC singularity. All of them have to do with singularities in this model, and all of them have resulted in possible restrictions on the arbitrary functions of the model, depending on the physical properties that are desired.

The result of chapter ??3 is that divergent blueshifts can indeed occur along the radial direction if the bang time is not simultaneous, and that the infinite energy fluxes implied by this are physically unacceptable. This is in good agreement with Silk's (1977) view that the infinite density and curvature contrasts that occur at a non simultaneous bang are an "unattractive property". Assuming that the present universe is homogeneous on the very large scale, it is concluded that the only large scale Tolman cosmology that is stable at early times, and evolves to homogeneity is the Robertson-Walker form.

The method used to solve the geodesic equations, that of assuming a series expansion for the tangent vectors, is not completely general, since there are functions that cannot be expressed as power series near a divergence (e.g. $\ln(r)$, $e^{1/r}$). Nevertheless, it is considerably more general than assuming the existence of a conformal Killing vector in the r - t plane. Moreover, since the functions of the Tolman metric can be expressed in the same form, and since the resulting equations do solve without any problems, it is reasonable to expect these results to hold for all Tolman models. One caveat should be mentioned, though. If the model contains an ESC singularity, the factor of $e^{-1/r}$ of eq (??7.17) comes dangerously close to contradicting this assumption. Fortunately this is mitigated by the fact that this function vanishes, rather than diverging, at $R \rightarrow 0$, and that in the case of the bang surface, these rays never get very far, being absorbed by the ESC singularity itself.

The equation of state of the Tolman model, that of dust, is particularly simplistic. Again, I believe this is not an important problem, since the redshift behaviour is due to the fact that \dot{R} always diverges on Σ_0 , while R' only diverges if $a' \neq 0$. In my opinion, a different equation of state will only affect the powers of R , and not the qualitative behaviour.

The most serious problem is that the geometrical optics approximation breaks down when the spacetime curvature becomes comparable with the wavelength of the light, i.e. near Σ_0 . But, of course, a more accurate method is also more difficult to solve. These infinite blueshifts may be regarded as an indication of some kind of unphysical behaviour, for example, a divergent flux of created particles in the semiclassical approximation.

Lastly there is the question of why, when $a' \neq 0$, only the radial rays display this unphysical behaviour, or why only g_{rr} is divergent. To be sure that this is due to a real instability in $a' \neq 0$

models, and not just an artifact of spherical symmetry, it is necessary to investigate models with less symmetry, for example the Szekeres metrics (Szekeres 1975), which have no Killing vectors in general, but contain both axially symmetric and spherically symmetric models as special cases. An even more general possibility is the class of velocity dominated singularities in irrotational comoving dust, that were studied by Eardley, Liang and Sachs (1972).

In chapter 5 the necessary and sufficient conditions for no shell crossings to occur in Tolman models were found. It is apparent from the examples of chapter 6 that they are quite easy to satisfy, and they still allow a large range of physically interesting cases, so shell crossings certainly are not generic to the Tolman metrics. If one also requires a regular origin at $r = 0$ (or anywhere else), then the choice of arbitrary functions near the origin is further limited. The above conclusion, that the bang must be simultaneous everywhere, is entirely compatible with these conditions.

I agree with Zel'dovich and Grishchuk's speculation about what must physically happen when a shell crossing occurs — that separate particles no longer occupy separate points in space, and so a "three flow" develops, meaning there are three particle velocities at each point. But without a technique for dealing with such a process, one cannot say whether the subsequent spacetime expands or recollapses. However it is found that models which contain both elliptic and hyperbolic regions can be free of shell crossings, though they do contain surface layers of the kind commonly used to model inhomogeneities. That some parts continue to expand, while other parts recollapse presents no real problem as regards cosmic censorship, since the crunch surface is spacelike.

It has also been found that there is no necessary connection between the global geometry of a model (whether it is open or closed) and its time evolution. Of course, the local geometry is still related to the time evolution in the familiar manner, so the eventual fate of our part of the universe may still be determined by measuring the variation of the Hubble constant with distance. On the other hand, models that are free of surface layers as well as shell crossings, do have to be completely elliptic if they are closed, though the converse is not true. It is quite possible for such an open model to contain elliptic regions, or even be completely elliptic, as example ??6(b) shows.

The investigation of the ESC singularity has confirmed and extended the previous results of Eardley and Smarr for the existence of this singularity, while the conformal diagram calculated here differs from theirs in having the furrows where the u and v values jump from $-s_{\text{crit}}$ to 0. It has also been shown that the orientation of the crunch surface is ill defined at an ESC singularity, depending on how that point is approached, though the calculations are not in complete agreement with the numerical results here. The safest conclusion is that more work is needed to understand this phenomenon.

REFERENCES

- Bondi, H. 1947, *Mon. Not. Roy. Astron. Soc.* **107**, 410.
- Bonnor, W.B. 1974, *Mon. Not. Roy. Astron. Soc.* **167**, 55.
- Bonnor, W.B. 1984, private communication to K. Lake., also *Class. Qu. Grav.*, to appear¹ .
- Bonnor, W.B. 1985, private communication to K. Lake and preprint.
- Cahill, M.E. and McVittie, G.C. 1970, *J. Math. Phys.* **11**, 1382.
- Christodoulou, D. 1984, *Comm. Math. Phys.* **93**, 171.
- Datt, B. 1938, *Zeit. Phys.* **108**, 314.
- Dyer, C.C. 1979, *Mon. Not. Roy. Astron. Soc.* **189**, 189.
- Eardley, D.M. 1974, *Phys. Rev. Lett.* **33**, 442.
- Eardley, D.M., Liang, E., and Sachs, R. 1972, *J. Math. Phys.* **23**, 99.
- Eardley, D.M., and Smarr, L. 1979, *Phys. Rev. D* **19**, 2239.
- Hawking, S.W., and Ellis, G.F.R. 1968, *Astrophys. J.* **152**, 25.
- Hawking, S.W., and Ellis, G.F.R. 1973, *“The Large Scale Structure of Space-Time”* (Cambridge U. P.).
- Hellaby, C., and Lake, K. 1984, *Astrophys. J.* **282**, 1; and corrections in *ibid*, **294**, 702.
- Hellaby, C., and Lake, K. 1985, *Astrophys. J.* **290**, 381; and corrections in *ibid*, **300**, to appear² .
- Israel, W. 1966, *Il Nuov. Cim.* **44B**, 1; and corrections in *ibid* **48B**, 463 (1966).
- Kamke, E. 1944, *“Differential Gleichungen: Lösungsmethoden und Lösungen”*, 3rd edition (Chelsea).
- Lake, K. 1984a, *Phys. Rev. D* **29**, 771.
- Lake, K. 1984b, *Phys. Rev. D* **29**, 1861.
- Lake, K. and Pim, R. 1985, *Astrophys. J.*, Nov. 15, 1985.
- Landau, L.D., and Lifshitz, E.M., 1975, *“The Classical Theory of Fields”* (Pergamon).
- Lemaitre, G. 1933a, *Comptes Rendus* **196**, 903.
- Lemaitre, G. 1933b, *Comptes Rendus* **196**, 1085.
- Lemaitre, G. 1933c, *Ann. Soc. Scient. Bruxelles* **A53**, 51.
- Muller zum Hagen, H., Yodzis, P., and Seifert, H.J. 1974, *Comm. Math. Phys.* **37**, 29.

¹(1985) *Class. Qu. Grav.*, **2**, 781.

²(1986) *Astrophys. J.* **300**, 461.

- Novikov, I.D. 1963, Doctoral thesis, Shternberg State Astronomical Institute, Moscow.
- Papapetrou, A., and Hamoui, A. 1967, *Ann. Inst. Henri Poincare* **6**, 343.
- Penrose, R. 1969, *Riv. Nuov. Cim.* **1**, 252.
- Penrose, R. 1979, in “*General Relativity, An Einstein Centenary Survey*”, ed. S.W. Hawking and W. Israel (Cambridge U. P.).
- Raychaudhuri, A. 1955, *Phys. Rev.* **98**, 1123.
- Raychaudhuri, A. 1957, *Phys. Rev.* **106**, 172.
- Seifert, H.J. 1979, *Gen. Rel. Grav.* **10**, 1065.
- Silk, J. 1977, *Astron. Astrophys.* **59**, 53.
- Szekeres, P. 1975, *Comm. Math. Phys.* **41**, 55.
- Szekeres, P. 1980, in “*Gravitational Radiation, Collapsed Objects and Exact Solutions*”, ed. C. Edwards (Lecture Notes in Physics, Vol **124**; Springer-Verlag).
- Tipler, F.J., Clarke, C.J.S., and Ellis, G.F.R. 1980, in “*General Relativity and Gravitation*”, ed. A. Held (Plenum).
- Tolman, R.C. 1934, *Proc. Nat Acad. Sci.* **20**, 169.
- Zel’dovich, Y.B., and Grishchuk, L.P. 1984, *Mon. Not. Roy. Astron. Soc.* **207**, 23p.

Appendix

FORTRAN program listings omitted. (6 programs in 27 pages plus 1 page of introduction.)